Master's thesis

NTNU
Norwegian University of Science and Technology
Department of Marine Technology

Truls Wanvik Krogstadmo

Reduction of trawl impact loads on pipelines resting exposed on the seabed

Master's thesis in MTMART
Supervisor: Svein Sævik
June 2019

NTNU
Norwegian University of
Science and Technology

Truls Wanvik Krogstadmo

Reduction of trawl impact loads on pipelines resting exposed on the seabed

Master's thesis in MTMART
Supervisor: Svein Sævik
June 2019

Norwegian University of Science and Technology
Department of Marine Technology

NTNU
Norwegian University of
Science and Technology

MASTER THESIS SPRING 2019

for

Stud. Tech. Truls Wanvik Krogstadmo

Reduction of trawl impact loads on pipelines resting exposed on the seabed

Reduksjon av trållaster på offshore rørledninger

Pipelines with OD > 16 inches are normally left exposed on the seabed during the operation phase. In the Norwegian and Barent Seas there are a lot of fishing activity including the use of trawl boards that are pulled along the seabed. The trawl board/pipeline interaction loads is often the limiting factor with respect to the size and height of free spans that can be allowed. As this might cause several hundreds of million Norwegian Kroner in extra costs of a pipeline project there is a huge potential with respect to optimising the seabed correction with respect to height, width and slope of each rock dump. The present work deals with investigating different options for correcting the seabed geometry in order to protect the pipeline in a cost effective way. The work is to be carried out as a continuation of the project conducted in fall 2018 and as follows:

- A literature review into the rules and standards and literatures addressing trawl loads, the methods related to pipeline structural analysis of such loads. Also familiarize with the computer programs SIMLA and the modelling procedures related to analysing the global response from trawl loads.
- Establish load cases in terms of pipeline cross-sections, mechanical properties, seabed geometries, soil data, fishing gear details, tow velocities and directions. A load case matrix is to be established..
- Establish a global analysis models in SIMLA that can be used for parametric studies related to the above.
- Perform global analyses focusing on the global response of the pipeline in terms of the pull-over load in horizontal and vertical direction.
- Perform sensitivity analysis with respect to varying parameters related to: rockdum slope, width and height, pipe diameter, tow velocity and clumpweight mass
- Conclusions and recommendations for further work

The work scope may prove to be larger than initially anticipated. Subject to approval from the supervisors, topics may be deleted from the list above or reduced in extent.

In the project report, the candidate shall present his personal contribution to the resolution of problems within the scope of the project work

Theories and conclusions should be based on mathematical derivations and/or logic reasoning identifying the various steps in the deduction.

The candidate should utilise the existing possibilities for obtaining relevant literature.

Project report format
The project report should be organised in a rational manner to give a clear exposition of results, assessments, and conclusions. The text should be brief and to the point, with a clear language. Telegraphic language should be avoided.

The report shall contain the following elements: A text defining the scope, preface, list of contents, summary, main body of thesis, conclusions with recommendations for further work, list of symbols and acronyms, references and (optional) appendices. All figures, tables and equations shall be numerated.

The supervisors may require that the candidate, in an early stage of the work, presents a written plan for the completion of the work.

The original contribution of the candidate and material taken from other sources shall be clearly defined. Work from other sources shall be properly referenced using an acknowledged referencing system.

The report shall be submitted in electronic format (.pdf):
- Signed by the candidate
- The text defining the scope shall be included (this document)
- Drawings and/or computer models that are not suited to be part of the report in terms of appendices shall be provided on separate (.zip) files.

Ownership
NTNU has according to the present rules the ownership of the project reports. Any use of the report has to be approved by NTNU (or external partner when this applies). The department has the right to use the report as if the work was carried out by a NTNU employee, if nothing else has been agreed in advance.

Thesis supervisors:

Prof. Svein Sævik, NTNU
Dr. Erik Levold, Equinor
Dr. Vegard Longva, Sintef Ocean
Harald Wathne, DNVGL

Deadline: June 11th , 2019

Trondheim, January 15th , 2019

Svein Sævik

Candidate – date and signature:

Preface

The master thesis is written in guidance with Svein Sævik and is based on his master description formulated in January 2019 at the department of Marine Technology, Norwegian University of Science and Technology. The master thesis is written during the spring semester of 2019 and is a continuation of the work I did while writing my project thesis during the fall of 2018. The master counts as 30 credits and encloses 5 years of studying at the institute of Marine Technology.

I would like to thank my supervisor Professor Svein Sævik for excellent guidance and involvement during weekly follow-up meetings throughout the semester. I would also like to thank doctor Vegard Longva for excellent support regarding SIMLA input files, which was handed out at the start of the thesis along with the licence file and a python script for post-processing purpose. Their guidance and facilitation has been brilliant. SINTEF Ocean should also be acknowledged for lending out the licence file.

Truls W. Krogstadmo
Trondheim, June 24, 2019

Abstract

Today subsea installations are commonly found across the Norwegian and Barent sea with pipelines spanning approximately 8800 kilometres across the Norwegian continental shelf. Large networks of pipelines exist around the offshore installation and are connected to onshore terminals via long export pipelines. Between installations and onshore terminals the pipelines are subjected to trawl gear impact loads. Due to an increasing amount of pipeline trawl gear interactions, DNVGL has published a recommended practice (DNV-GL, 2014), which has been reworked several times, 2014 being the latest. This practice covers the aspect of trawl gear pipeline interference and seeks to maintain the integrity of pipelines resting on the seabed.

The present project deals with investigating options for correcting the seabed geometry in order to ensure pipeline integrity in a cost effective way. A global analysis model in SIMLA is established for sensitivity studies related to seabed geometries, soil data, pipeline dimensions and trawl velocity. The pull-over loads in horizontal and vertical direction are compared towards equivalent cases with a flat seabed.

Initial tests with updated interaction curves for the proposed rockdumping have been performed. Results with a stiffer seabed correction indicates that pull-over loads are larger for stiffer soil properties. By increasing the rock dump up to ten times the original stiffness, pull-over loads are approximately doubled. Observations from result files indicate that the clump weight behaviour gets excessive and unrealistic as contact is made with the updated soil property, and the original interaction curve is kept for further simulations.

The overlying focus has been made towards a sensitivity study in regards of altering a seabed correction beneath pipeline sections and investigating the associated pull-over loads in both transverse and vertical direction. Simulations with rockdumping indicates that the largest pull-over loads comes from clump weight roller pipe collision and are worst for large rock dump widths. For small rock dump widths large pull-over loads are most prominent for lower heights, whereas for larger widths they are prominent for the steepest slopes.

The effect of increasing pipe dimensions were investigated for a selection of rockdump geometries. Comparison of pull-over loads from simulations with a 16” pipe indicates no positive effect from rock dumps with a small width compared to a flat seabed. The pull-over loads are however reduced by approximately 50 % for cases where the width is large. For a 24” pipe no distinct change in pull-over loads are observed but pull-over duration is both increased and reduced.

Pull-over loads have been investigated with reduced towing velocity for both the 12.75” and 16” pipe. The same trawl gear has been used for all simulations. The pull-over loads are slightly reduced from rockdumping effects. For a 16” pipe the build-up in transverse pull-over load is considerable for a case with flat seabed whereas it is cancelled at earlier stages with active rockdumping.

Sammendrag

I dag finnes havbunnsinstallasjoner rundt omkring i Nordsjøen og Barentshavet med rørledninger som strekker seg totalt over 8800 kilometer på norsk sokkel. Rørledninger eksisterer rundt offshore-anlegget og er koblet til landbaserte terminaler via lange eksportrørledninger. Mellom offshore installasjoner og landbaserte terminaler blir rørledninger utsatt for støtlaster fra trålingutstyr. På grunn av en økende mengde interaksjoner mellom trålutstyr og rørledninger har DNVGL publisert en anbefalt praksis (DNV-GL, 2014), som har blitt revidert flere ganger, senest i 2014. Denne praksisen dekker flere aspekter rundt interaksjonen mellom tråleutstyr og rørledninger på havbunnen og søker å opprettholde integriteten til rørledninger.

Dette prosjektet handler om å undersøke muligheter rundt korrigering av havbunnsgeometrien under rørledningen for å sikre rørledningens integritet på en kostnadseffektiv måte. En global analysemodell i SIMLA er etablert for sensitivitetsstudier relatert til havbunnsgeometri, sjøbunnsdata, rørledningsdimensjoner og trålhastighet. Kontaktkrefter i horisontal og vertikal retning er sammenlignet med tilsvarende tilfeller for en flat havbunn.

Initielle tester med oppdaterte interaksjonskurver for den foreslåtte steindumpingen har blitt gjennomført. Resultat fra en hardere havbunn indikerer at kontaktkreftene er større for stivere sjøbunnsegenskaper. Ved å øke stivheten på steindumpen med opptil ti ganger så mye som den opprinnelige stivheten blir det omtrent en fordobling i størrelsen på kontaktkreftene. Observasjoner fra resultatfilene indikerer at klumpvektens adferd blir overdreven og urealistisk ettersom den treffer den oppdaterte steindumpen, og den opprinnelige interaksjonskurven beholdes derfor for videre simuleringer.

Det overliggende fokuset har vært en sensitivitetsstudie med hensyn på å korrigere havbunnstopografien under rørledningsseksjoner og sammenligne kontaktkrefter mellom tråd og rørledning i alle tilfellene. Simuleringer med steindumping indikerer at de største kontaktkreftene kommer fra kollisjon mellom klumpvektens rulle og rørledningen, og er verst for steindumper med store bredder. For små bredder på steindumpene er store kontaktkrefter mest fremtredende for lave høyder, mens for større bredder er de fremtredende for sjøbunns-korreksjoner med de bratteste bakkene.

Effekten av økende rørdimensjoner ble undersøkt for et utvalg av steindump-geometrier. Sammenligning av kontaktkrefter fra simuleringer med 16-tommers rør indikerer ingen positiv effekt fra steindumper med liten bredde sammenlignet med en flat havbunn. Kontaktkreftene reduseres imidlertid med ca. 50 % for tilfeller hvor bredden er stor. For en 24-tommers rørledning er det ikke observert noen tydelig endring i kontakreftene, men overtrekksvarigheten er både økt og redusert.

Kontaktkrefter har også blitt undersøkt på 12.75-tommers og 16-tommers rørledninger der tråleren er simulert med redusert hastighet. Det samme trålutstyret har blitt brukt for alle simuleringer. Kontaktkreftene blir delvis redusert med steindumping. For et 16-tommers rør er oppbygningen av kontaktkraften i tverrgående retning betydelig i tilfeller med flat havbunn mens den avbrytes på et tidligere tidspunkt hvis steindumping innføres.

Table of Contents

List of Tables

List of Figures

Nomenclature

Abbreviations

DNVGL Det Norske Veritas

DOF degrees of freedom

NTNU Norwegian University of Science and Technology

OD outer diameter

RD rock dump

Symbols

$\ddot{\boldsymbol{u}}$ acceleration field

$\hat{\boldsymbol{K}}$ effective stiffness matrix

$\hat{\boldsymbol{R}}$ effective load vector

$\boldsymbol{\sigma}$ Cauchy stress tensor

$\boldsymbol{C}_e$ elasticity tensor

$\boldsymbol{C}$ system damping matrix

$\boldsymbol{f}$ volume force vector

$\boldsymbol{K}$ system stiffness matrix

$\boldsymbol{k}_m$ local material stiffness matrix

$\boldsymbol{K}_T$ global tangential stiffness matrix

$\boldsymbol{k}_T$ local tangential stiffness matrix

$\boldsymbol{k}_\sigma$ local initial stress stiffness matrix

$\boldsymbol{M}$	system mass matrix
$\boldsymbol{n}$	outward surface vector
$\boldsymbol{R^E}$	external load vector
$\boldsymbol{R^I}$	internal load vector
$\boldsymbol{R}$	load vector
$\boldsymbol{r}$	displacement vector
$\boldsymbol{S}$	2nd Piola-Kirchoff stress tensor
$\boldsymbol{t}$	surface traction
$\boldsymbol{u}$	displacement vector
$\boldsymbol{x}$	coordinates
Δ	increment
δ	virtual quantity
δ_p	pipe displacement at point of interaction
$\dot{\boldsymbol{E}}^{(p)}$	plastic part of the rate of Green's strain tensor
$\dot{\lambda}$	scalar function depending on the current stress and strain
ϵ	natural strain tensor
γ, β, α	integration parameters
κ	strain-hardening parameter
ν	Poisson's ratio
ψ	warp angle
ρ	material density
θ	sweep angle
C_D	radial drag coefficient
C_M	radial added mass coefficient
$C_{D,t}$	tangential drag coefficient
$C_{M,f}$	clump weight frame added mass coefficient

$C_{M,r}$ clump weight roller added mass coefficient

$C_{M,t}$ tangential added mass coefficient

D diameter

d water depth

D_f clump weight frame diameter

d_g contact condition

D_r clump weight roller diameter

E Young's modulus

E_{xx} longitudinal Green strain

EA axial stiffness

EI bending stiffness

F_p maximum horizontal pull-over force

F_{z1} downward maximum pull-over force

F_{z2} upward maximum pull-over force

g_0 initial gap

H rock dump height

k_w warp line stiffness

L pipeline length

L_1 length of pipe zone 1

L_2 length of pipe zone 2

L_3 length of pipe zone 3

L_lower lower warp line

L_r clump weight roller length

L_w warp line length

L_{clump} distance from reaction point to clump weight center of gravity

m dry mass

m_f clump weight frame dry mass

m_r	clump weight roller dry mass
m_s	submerged mass
m_t	steel mass
$m_{s,f}$	clump weight frame submerged mass
$m_{s,r}$	clump weight roller submerged mass
p_i	internal pressure
r	mean structural radius
S	slope of rock dump
t	structural thickness
T_p	pull-over duration
V	trawling velocity
W	rock dump width

Chapter 1

Introduction

1.1 Motivation

Since the offshore industry had its manifestation at the start of 1980 the demand for safe and cost effective solutions has been pursued. Today the Norwegian continental shelf is decorated with pipelines at the seabed transporting oil and gas from the drilling sites back to onshore terminals. The seabed topography is naturally varying between the offshore installations and onshore terminals, so pipelines must be designed with dimensions able to withstand e.g. current forces and potential long free spanning sections. They must also be able to withstand pull-over loads from trawl gear used in conjunction with bottom trawl fishing, which is assumed to be the most hazardous risk jeopardizing the integrity of pipelines resting on the seabed.

Multiple studies have been performed in order to investigate pull-over loads for free-spanning pipelines. The studies are usually compared with current regulations for trawl gear impact loads in order to predict any potential over-conservatism in the regulations. What seem to be missing are studies investigating the effect of altering the seabed topography beneath pipeline sections in order to protect the pipeline in a cost effective way.

1.2 Scope of work

The proposed solution for handling this risk is by introducing seabed corrections in order to fill potential gaps creating large spanning sections. The proposed solution does also include altering the seabed geometry beneath pipeline sections resting at the seabed, thus creating a negative slope surrounding the pipeline. This elevation of pipeline sections are simulated and discussed in the thesis with the overlying goal of protecting the pipeline in a cost effective way.

The seabed alteration is further investigated for varying pipeline dimensions and trawl speed. All results are compared with pull-over loads taken from a case with flat seabed in order to document the underlying effect a correction in seabed geometry beneath pipe sections has for larger pipe dimensions and reduced trawl velocity.

1.3 Chapter overview

Chapter 2: The chapter describes typical trawl gear used in Norwegian waters and discusses the recommended practice (DNV-GL, 2014) and its calculation methods related to estimation of pull-over loads and impact energy. Lastly relevant literature is discussed in terms of conference, journal papers and earlier master theses that addresses the subject of trawl pull-over loads.
Chapter 3: Presents the general FE principles as applied to non-linear analysis followed by addressing the solution method and finite elements used in SIMLA.
Chapter 4: The case matrix is described in this chapter. All input variables regarding the rock dump are addressed and followed by a description of all simulations with different pipeline dimension and trawl speed.
Chapter 5: The chapter includes a description of the numerical model and all input parameters used with relevant contact elements. The analysis procedure and a description of how the data is post-processed is included at the end.
Chapter 6: All simulations with corresponding results are presented and discussed along the way with an overall summary at the end. Results are presented as force-time histories with a running average of 0.05 s. The chapter also includes a brief description of the clump weight pipe interaction for each simulation.
Chapter 7: Conclusions and recommendations based on the simulated results are presented with further work addressed at the end.

Chapter 2

Background

This chapter contains a brief description of the trawling gear used in Norwegian waters. Interference between pipeline and trawl gear is further categorized in order to illustrate the impact this loading effect has on the pipelines exposed on the seabed. The current regulation (DNV-GL, 2014) is then described in order to address current design loads and regulations.

The chapter continues by addressing previous work done regarding interference between pipeline and trawl gear. This section gives a brief introduction to journals, research papers and master theses and the difference between earlier work and the proposed scope of work for this thesis.

2.1 Pipelines

Today, the total length of the Norwegian gas pipeline network is about 8800 kilometres, which is roughly the distance from Oslo to Bangkok (Directorate et al., 2018). These networks are mainly located around the offshore production sites but they are also connected to long export pipelines to onshore terminals. The dimensions vary in size, all dependent on the capacity they are designed for. As a result of the increase in demand, huge areas of seabed on the Norwegian continental shelf are covered with pipelines. The pipeline is to be protected against impact loads that can jeopardize the structural integrity and in worst case scenario, result in major spillage, causing negative environmental effects and potential loss of lives . The export pipelines on the Norwegian continental shelf are illustrated in figure 2.1.

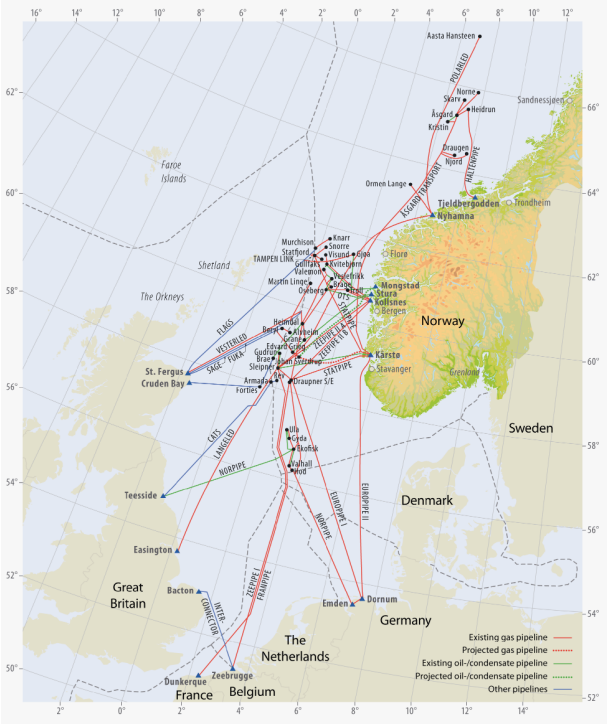

Figure 2.1: Pipelines covering the Norwegian Continental Shelf

2.2 Trawl gear

Trawling is a fishing activity that is continually used in and around Norwegian waters and is considered one of the most hazardous risks regarding impact loads on sub sea pipelines. Trawl velocity and pattern is mainly governed by fish movement pattern, the respective swimming speed of the desired catch and economic speed of the trawl vessels. Prawn trawling is typically performed at 2-3 knots, whereas trawling for fish is performed at up to 5-6 knots (DNV-GL, 2014). The type of trawl is mainly dependent on how the net is kept open and whereas the trawling is performed mid water or at the seabed bottom (Maalø, 2011). Fishing activities such as bottom trawling shall be considered for offshore pipelines (DNV-GL, 2014) and it can be further divided into beam trawls and otter trawls.

2.2.1 Beam trawl

In beam trawling a beam is used to keep the net open. Beam shoes are mounted at each end which indicates a substantial hazard to pipelines due to their sharp edges and large kinetic energy (DNV-GL, 2014). Figure 2.2 illustrates the most common configuration where a vessel is operating one beam trawl from each side. Because of the transverse beam, the trawl net will be kept open regardless of the vessel speed. The disadvantage is however the net, which is supposed to not surpass a spreading height of 1 m. It is therefore not the most common trawl setup at the Norwegian continental shelf.

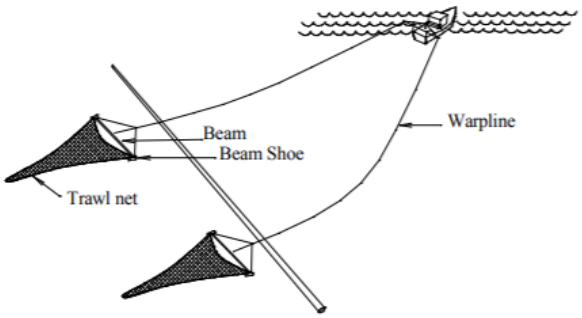

Figure 2.2: Beam trawl gear crossing a pipeline (DNV-GL, 2014)

2.2.2 Otter trawl

The otter trawl is the most common trawl gear in Norwegian waters, and consist of two sweep lines and warp lines, only separated by a respective trawl board. The trawl board holds the net open by a hydrodynamic spreading force (DNV-GL, 2014). A typical otter trawl is illustrated in figure 2.3 and is dragged along the seabed. As shown in figure 2.3, the sweep lines connect the trawl net with the trawl board, and the warp line connects the trawl board with the vessel. The weight of the trawl board has to be considerably large in order to keep the trawl net from drifting upwards from the seabed.

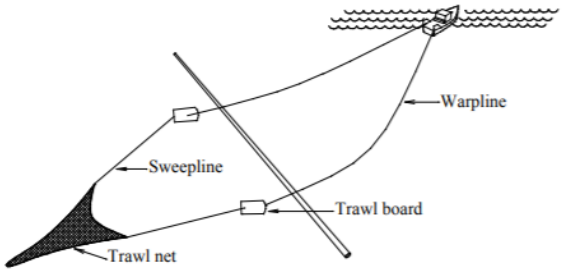

Figure 2.3: Otter trawl gear crossing a pipeline (DNV-GL, 2014)

2.2.3 Twin trawl

Twin trawling is typically used in consumption trawling (DNV-GL, 2014) and is shown in figure 2.4. Twin trawling increase the efficiency by connecting one warp line at each side of the vessel. In twin trawling a clump weight is introduced, as shown in figure 2.4, connected by the sweep lines from each respective trawl net and a third warp line connected directly to the vessel. The center warp line will take most of the towing resistance, lowering the tension in the outer warp lines and increasing the spreading height of the trawl nets. The clump weight is thus introduced, as heavier trawl equipment is needed for the increasing upward pull at the center warp line.

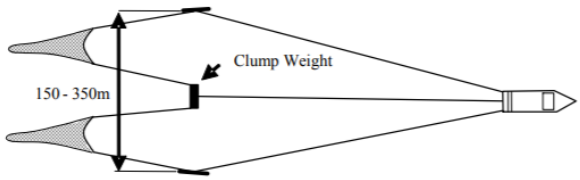

Figure 2.4: Twin trawling with clump-weight (DNV-GL, 2014)

The clump weight has a mass typically in the range of 2 to 9 tonnes, and can cause larger impact energy and pull-over loads than trawl boards (DNV-GL, 2014). Different types of clump weights are used, and is typically dependent on the seabed configuration and size of the vessel and equipment used. In figure 2.5 and 2.6 typical clump weights are shown.

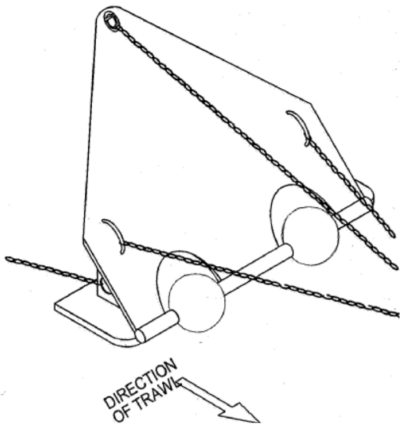

Figure 2.5: Typical clump weight (Bobbin type) (DNV-GL, 2014)

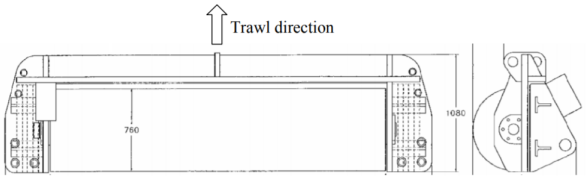

Figure 2.6: Typical clump weight (Roller type) (DNV-GL, 2014)

2.3 Interaction between trawl equipment and pipeline

Since clump weights are towed regularly across the seabed, interference with pipelines are unavoidable and could expose the pipeline to substantial loads that may damage it. The interaction is usually divided into two phases, the initial impact and the subsequent pull-over phase.

The initial impact is a short phase where the specific mass (clump weight for twin trawling) hits the pipeline. The energy transfer generally lasts some hundredths of a second and most of it will be absorbed as local deformation. The local resistance of the pipeline including any protective coating and/or attached electric cable protection structure are mobilized to resist the impact force (DNV-GL, 2014). The magnitude of the impact force depend in general on the shape of the front of the clump weight, pipe

diameter, span height and on the direction of travel relative to the pipelines (DNV-GL, 2014).

The pull-over phase describes the second phase where the trawl board is pulled over the pipeline. The pull-over usually last from around 1 second to some 10 seconds, dependent on span height, water depth and other factors (DNV-GL, 2014). During the pull-over phase the pipeline is subjected to global deformation and it will experience large horizontal and vertical forces. If the warp line tension is not enough to pull the trawl gear over the pipeline, a special case, named hooking is experienced. This is a rare occurring accidental situation where the trawl equipment is stuck under the pipeline. The pipeline may experience forces as large as the breaking strength of the warp during hooking in extreme cases (DNV-GL, 2014).

2.4 DNV-RP-F111

In the Norwegian sector, trawl gear design loads are generally implemented by the recommended practice under the name of DNV-RP-F111 - *Interference between Trawl Gear and Pipelines* (DNV-GL, 2014). The recommended practice supersedes DNV-RP-F111, October 2010 by changes made in September 2014. It aims to provide guidance and risk management for pipeline integrity due to loads from trawl gear.

The recommended practice provide criteria and calculation methods for trawl gear interference with pipelines during impact, pull-over and hooking phases described in section 2.3. The design criterion and methods are based on experimental model tests done by Sintef Ocean and are edible for rigid steel pipelines with outer diameter larger than 10" (DNV-GL, 2014). Design loads during pull-over phase are described in this section due to its ability to initiate global deformations and impact loads are described because they are relevance to the scope of the thesis.

2.4.1 Pull-over loads for clump weights

The recommended practice claims that a structural dynamic analysis should be carried out in order to estimate the structural behaviour of the pipeline. Further, a large part of the pipeline and the surrounding seabed is needed in order to get sufficient results. The clump weight should be applied as a point force as long as it is of the sphere/bobbin or roller type, described in section 2.2.3. The estimate for maximum horizontal pull-over force is then given as

$$F_p = 3.9 \cdot m_t \cdot g \cdot (1 - e^{-1.7 \cdot h^{'}}) \cdot (\frac{OD}{L_{clump}})^{-0.65} \tag{2.1}$$

$$h^{'} = (H_{sp} + OD)/L_{clump} \tag{2.2}$$

where m_t is the steel mass, g is the gravitational acceleration, OD is the outer diameter of the pipe and L_{clump} is the distance from reaction point to center of gravity of the clump weight as shown in figure 2.7.

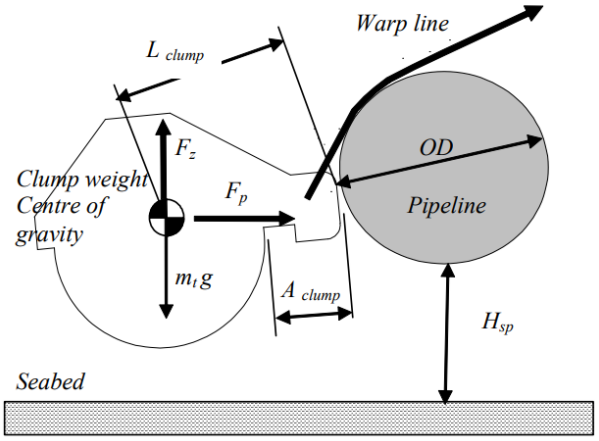

Figure 2.7: Clump weight interaction with pipeline (DNV-GL, 2014)

Further, the maximum vertical design load is important in order to consider the most critical load combination. Downward and upward maximum force is dependent on the maximum lateral load and is shown in equation 2.3 and 2.4.

$$F_{z1} = 0.3F_p - 0.4 \cdot m_t \cdot g \tag{2.3}$$

$$F_{z2} = 0.1F_p - 1.1 \cdot m_t \cdot g \tag{2.4}$$

2.4.2 Pull-over duration for clump-weights

From the model tests done by Sintef Ocean it is shown that the clump weight can be represented as a quasi-static load, neglecting dynamic effects during the pull-over (DNV-GL, 2014). The clump weight will stop after the impact with the pipeline, and the warp line will tighten before the clump weight is rotated along the surface and eventually released from the pipeline. This process is described in figure 2.8. The first 0.2 seconds describe the clump weight impact with the pipeline which is approximately half the lateral maximum load. Then the load increases linearly as the warp line tightens until clump weight is released at maximum lateral load.

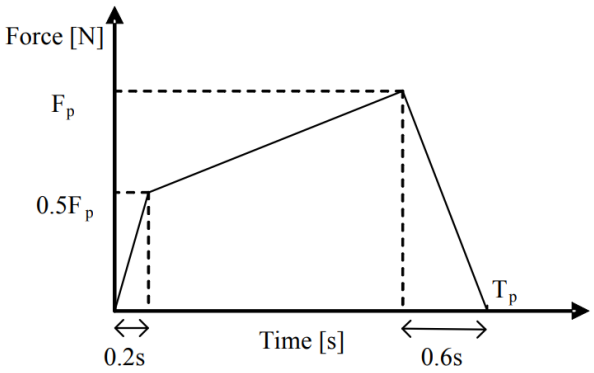

Figure 2.8: Sketch of force-time history for clump weight pull-over force (DNV-GL, 2014)

The pull-over duration for a clump weight can be calculated as

$$T_p = F_p/(k_w \cdot V) + \delta_p/V \tag{2.5}$$

where k_w is the warp line stiffness, V is the trawling velocity and δ_p is the displacement of the pipe at the point of interaction. This is however unknown before a response simulation, and it needs to be assumed and corrected by iterative approach (DNV-GL, 2014).

2.4.3 Impact loads for clump weights

In order to measure trawl gear impact loads the recommended practice states that they are associated with the transfer of kinetic energy. The energy transfer usually finds place on a small enough interval such that all energy is absorbed as local deformation (DNV-GL, 2014). However, if the pipeline diameter is small enough the energy absorption could result in global deformation of the pipe and soil. The impact energy is generally depending on the shape of the incoming object, its speed and direction relative to the pipeline, constituting an effective mass and an effective velocity (DNV-GL, 2014). The total absorbed energy can be calculated as

$$E_{loc} = R_{fs} \cdot \frac{1}{2}(m_t + m_a) \cdot V^2 \tag{2.6}$$

and is a simple way of calculating the energy absorbed locally. Here R_{fs} is a correction factor for energy absorbed by global pipeline deformation and in the soil, m_t and m_a is the dry mass and added mass for the clump weight respectively, constituting an effective mass, and V is trawling speed.

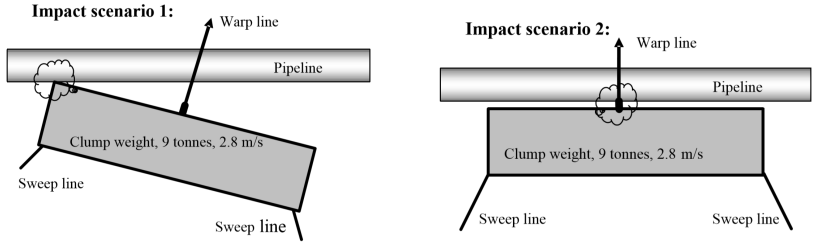

(a) Clump weight corner hitting the pipeline

(b) Clump weight hitting perpendicular on pipeline

Figure 2.9: Main impact scenarios for clump weight energy absorption (DNV-GL, 2014)

The impact loads is generally divided into two different scenarios shown in figure 2.9. Figure 2.9 a) shows the clump weight corner hitting the pipeline, while figure 2.9 b) shows the clump weight with a trawling direction normal to the pipeline. at the center warp line bracket. The first impact scenario typically reduces the effective mass by approximately 50 %, hence giving a reduced impact energy because of the rotation needed in order to pull the clump weight over the pipeline. The second impact scenario is generally the most critical one as clump weights are installed with a warp line bracket protruding in front of the clump weight roller. As the warp line bracket hits the pipeline all weight is transferred to the middle of the clump weight causing a larger impact load. Clump weight bracket frame impact is shown in figure 2.10 (b).

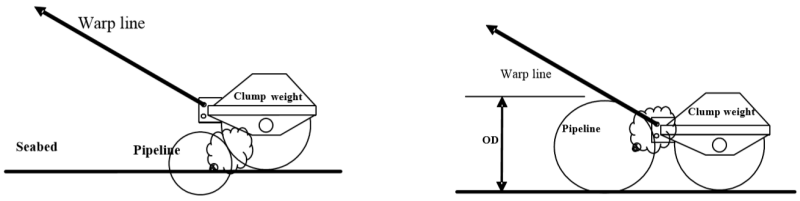

(a) Concept **(b)** Model

Figure 2.10: Clump weight impact configurations (DNV-GL, 2014)

Figure 2.10 a) illustrates clump weight roller hit partly penetrated into soil and/or small diameter pipeline. This configuration reduces the impact load significantly since the weight is spread over the width of the clump weight. This thesis covers different seabed configurations where the pipeline is resting on top of a rock dump surrounded by a decreasing incline acting as a ramp for objects dragged along the soil. By varying the rock dump parameters, both impact configurations shown in figure 2.10 may appear relevant. This will be discussed later in chapter 6.

2.5 Literature review

There is only a limited amount of research papers regarding trawl gear pipeline interaction. The simulations are usually carried out by the computer software SIMLA, which runs both static and dynamic analyses and are designed for sub sea pipeline simulations. Some conference papers addresses simulations run by conducting a FE-model into OrcaFlex, and any remarks or conclusions are generally extracted from the software. From the 25th International Conference on Offshore Mechanics and Arctic Engineering it is stated that clump weight pipeline interference increases the efficiency of the trawlers and that this type of trawling is expected to become more commonly used in the future (Fyrileiv et al., 2006). In the following years multiple conference papers address the clump weight pipeline interference and development of more accurate representations and advanced numerical models. This section will address relevant conference papers, science journals and master theses in order to give a brief introduction to previous research on clump weight pipeline interference and the related FE-models.

2.5.1 Pipeline trawl interaction

In 2010 Vegard Longva investigated the effect of oblique trawl board crossings, increased trawl board added mass due to seabed proximity and the effect of a more rectangular trawl board geometry (Longva, 2010). During the thesis, Longva examined a new hydrodynamic load model which handles the seabed proximity and forward speed in a more consistent way. By application of a polyvalent trawl board, Longva found out that increasing trawl board added mass due to seabed proximity did not have any influence on neither pull-over loading nor pipeline response. The application of the advanced hydrodynamic model did however predict the DNV-RP-F111 to be non-conservative when simulating a span height of 0 m, and it showed good agreement with the DNV-RP-F111 recommendations for a span height of 1 m, thus suggesting the new hydrodynamic load model for further simulations. One of the major findings was that a perpendicular angle of impact did not predict the largest pull-over load, and that a rectangular trawl board predicted a larger pull-over load compared to a polyvalent board (Longva, 2010).

From the 30th International Conference on Ocean, Offshore and Arctic Engineering, Longva et al. (2011) published a study on a trawl board represented by a 6-DOF hydrodynamic load model. In the study both

mass and drag coefficients are expressed as functions of seabed gap, seabed inclination angle and heading angle, thus including both effects from seabed proximity and trawl board forward speed. The effects are examined in application with finite element software in order to predict pipeline pull-over loads. The applied drag coefficients were established by model testing, while the hydrodynamic mass was found by potential theory, resulting in a more consistent hydrodynamic load model compared to previous efforts. Observations based on the study shows that numerical simulations gives a more realistic description of the pull-over loading than the DNV-RP-F111 recommendation. The simulations did however include problems regarding unexpected pipeline penetration, and the problem was solved by increasing the contact stiffness in a step-wise manner. A method in order to detect abnormal penetrations was suggested in order to improve the contact element stiffness, and the report also suggests that the contact problem might be related to the geometrical description of the contact surfaces, hence a better contact formulation should be investigated (Longva et al., 2011).

In september 2013, Longva et al. (2013) published a paper in the journal of Marine Structures representing the strategy for predicting fishing gear interference loads on subsea pipelines. The study involves 34 model test-runs carried out for three different trawl boards in order to validate the numerical model. The simulations predicted a pull-over load within 10 % of model test measurements and a sensitivity study of nearly 250 simulations was then conducted based on the validated results from the previous runs. The paper aims to apply a contact model for board-pipe interaction (Longva and Sævik, 2013), presenting a FE formulation for frictional contact between pipelines and rigid three-dimensional bodies (Longva and Sævik, 2012), (Longva and Sævik, 2013). Figure 2.11 shows the kinematics and body geometry in order to describe the trawl board and pipe interaction. The SIMLA model and the contact elements applied in the thesis is further discussed in chapter 5.

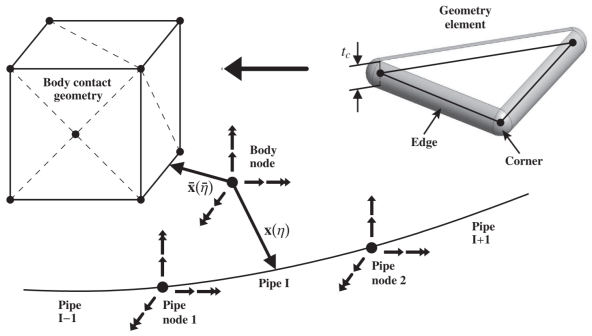

Figure 2.11: Contact kinematics and representation of body geometry

2.5.2 Pipeline clump weight interaction

In 2011 Kristian Maalø investigated pull-over loads from clump weights on free spanning pipelines using the computer software SIMLA. Maalø performed six small scale tests in order to verify the numerical model and continued the work by looking at the effect of increasing pipeline flexibility. The major finding was that pull-over loads increase for decreasing pipeline flexibility and increased warp line length, and that the pull-over loads was reduced by moving the clump weight center of gravity forward.

Ingrid Berg Johnsen continued working on the numerical model established by Maalø in 2012, and investigated the effect of changing pipe diameter, free span height and pipe end conditions with several sensitivity studies regarding warp line alteration and clump weight wobbling. One of her findings was that full scale simulations predicted lower pull-over loads compared to rigid pipeline model simulations. The sensitivity study also indicated a connection between the span height and pull-over load for small

diameter pipelines, whereas the pull-over load would decrease for lower span heights and increase for higher span heights.

At the 31st International Conference on Ocean, Offshore and Arctic Engineering, Maalø et al. (2012) recommended further investigation on clump weight type, mass, size and trawling velocity with varying pipeline diameter. They compared results from numerical simulations with scaled down pull-over tests and found little to no deviation.

In the proceedings of the 25th International Ocean and Polar Engineering Conference, Lyngsaunet et al. (2015) presented a Detailed Simulation of Interference Between Clump Weight and Subsea Pipelines (Lyngsaunet et al., 2015). The simulations were performed in SIMLA using a full scale replica of model tests done by MARINTEK on behalf of Equinor for the Kristin field development in 2004. The model captured the interaction between clump weight and pipeline successfully by confirmation from the model tests performed in a scale of 1:10. The simulations carried out interaction between a pipeline and a clump weight of the bobbin type, as shown in figure 2.5. The results showed a much smaller pull-over loading from the numerical model compared to the recommended practice (DNV-GL, 2014), indicating a conservatism in the recommended practice and a possible safety margin.

There are no previous studies regarding alteration in seabed profile beneath the pipeline in clump weight pipeline interference. A lot of studies regarding clump weight pipeline interference investigates pull-over loads and potential hooking scenarios compared with today's regulations in order to predict whether or not current regulations are conservative. Although there have been performed model tests in regards of covering the pipeline in order to reduce the impact loads, no previous investigations regarding rockdumping effects beneath the pipeline have been done.

Chapter 3

Nonlinear Finite Element Analysis

SIMLA is a computer program that has been used in order to solve the trawling gear pipeline interference. SIMLA is FEM based and is made primarily for non-linear static and dynamic analysis of pipelines. In addition to general features regarding pipe and cable structures, SIMLA includes powerful contact elements able to solve the governing interactions. This chapter discusses the basic principles of finite element analysis and the theory applied in SIMLA with its solution methods. The finite elements used in the modelling is also discussed with regard to the kinematics and the material law.

3.1 Finite element principles

Three basic principles must be dealt with in non-linear finite element analysis:

- Equilibrium by virtual work on total and incremental form
- Kinematic compatibility
- Constitutive behaviour

3.1.1 Equilibrium by virtual work on total and incremental form

The Principle of Virtual Displacement, also known as the Principle of Virtual Work, obtains equilibrium between the internal and external forces in an average sense. However, the stresses and strains do not need to be the actual distribution in the deformed body, but could be independently chosen (Sævik, 2017). This is because in many cases the exact solution is almost impossible to find, and introducing statically admissible stresses and strains makes it possible to solve the differential equation for the problem by weight function multiplication and volume integration. From equilibrium the error in the weight function for internal stresses must be equal to the error in the weight function for external work. If then the virtual displacement satisfies the boundary condition the error in the equation is eliminated and *integrated equilibrium* is obtained (Sævik, 2017). This is a special case where the average error is zero, but e.g. the differential equation might not be fulfilled at an arbitrary point in the volume. SIMLA excludes volume forces, so the principle in equilibrium state is written as

$$\int_V (\rho \ddot{\boldsymbol{u}} - \boldsymbol{f}) \cdot \delta \boldsymbol{u} dV + \int_V \boldsymbol{\sigma} : \delta \epsilon dV - \int_S \boldsymbol{t} \cdot \delta \boldsymbol{u} dS = 0 \tag{3.1}$$

where ρ is the material density, $\ddot{\boldsymbol{u}}$ is the acceleration field, $\mathbf{f}$ is the volume force vector, $\boldsymbol{\sigma}$ is the Cauchy stress tensor, δ is a virtual quantity, ϵ is the natural strain tensor, $\boldsymbol{t}$ is the surface traction and $\boldsymbol{u}$ is the displacement vector. V and S are respectively deformed volume and surface.

In SIMLA most quantities are referred to the initial C_0 configuration where Green strain and 2nd Piola Kirchoff stress are energy conjugated quantities (Sævik, 2017). For these cases the strain measure is significantly small, such that the difference between stress measures and choice of reference configuration will be small. The 2nd Piola Kirchoff stress tensor $\boldsymbol{S}$ and $\boldsymbol{\sigma}$ will be handled as equal quantities (Sævik, 2017), hence equation 3.1 needs to be modified:

$$\int_V (\rho \ddot{\boldsymbol{u}} - \boldsymbol{f}) \cdot \delta \boldsymbol{u} dV_0 + \int_V \boldsymbol{S} : \delta \epsilon dV_0 - \int_S \boldsymbol{t} \cdot \delta \boldsymbol{u} dS_0 \int_S \boldsymbol{p} \cdot \delta \boldsymbol{u} (1 + \epsilon_{11} + \epsilon_{22}) dS_0 = 0 \tag{3.2}$$

where ϵ_{11} and ϵ_{22} are the principal strains of the surface plane (Sævik, 2017).

3.1.2 Kinematic compatibility

Strains should be compatible with deformations, i.e. kinematic compatibility requires that the approximated deformations are continuous over the element boundary and compatible with the strains. By introducing continuous interpolation functions for the displacement and finite strains, the criteria is fulfilled. In SIMLA the kinematic relation contribution to the equilibrium equation is established by applying Bernoulli-Euler and Navier hypothesis (Sævik, 2017). Here Green strain tensor is used as strain measure, but neglecting the second order longitudinal strain term according to von Karman (Sævik, 2017). The longitudinal Green strain is given by:

$$E_{xx} = u_{x_0,x} - y u_{y_0,xx} - z u_{z_0,xx} + \frac{1}{2}(u_{y_0,x}^2 + u_{z_0,x}^2) + \theta_{,x}(y u_{z_0,x} - z u_{y_0,x}) + \frac{1}{2}\theta_{,x}^2 (y^2 + z^2) \tag{3.3}$$

where the displacements are expressed as

$$\begin{aligned} u_x(x,y,z) &= u_{x_0} - y u_{y_0,x} - z u_{z_0,x} \\ u_y(x,y,x) &= u_{y_0} - z\theta_x \\ u_z(x,y,z) &= u_{z_0} - y\theta_x \end{aligned} \tag{3.4}$$

3.1.3 Stress-strain behaviour

From Hook's law we know that the elastic stress-strain relationship applies:

$$\begin{bmatrix} \sigma_{11} \\ \sigma_{22} \\ \tau \end{bmatrix} = \frac{E}{1-\nu^2} \begin{bmatrix} 1 & \nu & 0 \\ \nu & 1 & 0 \\ 0 & 0 & \frac{1-\nu^2}{2(1+\nu)} \end{bmatrix} \begin{bmatrix} \epsilon_{11} \\ \epsilon_{22} \\ \gamma \end{bmatrix} \tag{3.5}$$

If the stresses exceed the elastic limit, an elasto-plastic formulation is needed in order to account for the non-linear effects. Some of these effects are likely to happen in pipeline clump weight interference and will be discussed later in section 3.2.2.

3.2 Non-linear effects

When the ultimate strength of structures that buckle and collapse are calculated, the assumption about small displacements and linear material properties is not enough (Moan, 2003). A collapsed structure is likely to have been exposed to non-linear effects, and in pipeline clump weight interaction that is likely to happen. Non-linearities exist in three sub-categories: Geometrical, material and boundary conditions.

3.2.1 Geometrical non-linearity

Geometrical non-linearities occur when structures undergo large deformations. This has to be accounted for in the equilibrium equation by calculating strains from the displacement (Moan, 2003). In a pipeline clump weight interaction, the pipeline could experience large horizontal deformations, hence geometric non-linearity has to be accounted for. Due to large deformations, a suitable reference formulation is needed in order to describe the geometry and the deformations precisely. This will be further explained in section 3.4.

3.2.2 Material non-linearity

Material non-linearity is present when the stress-strain relationship is non-linear, i.e. when the material experiences plasticity. For non-linear material behaviour we have three major features:

- An yield condition
- A flow rule
- A hardening rule

Yield condition

The yield condition defines the stress intensity where plastic deformation occurs at first, and can generally be expressed as

$$f(\boldsymbol{S}, \kappa) = 0 \tag{3.6}$$

where f is a scalar function and κ is a strain-hardening parameter which depends upon the loading history in the plastic range and $\boldsymbol{S}$ is the stress tensor of 2nd Piola-Kirchoff stress (Sævik, 2017).

Flow rule

The flow rule relates the rate of plastic strain to the history of the stress and strain and the stress rate. The material is then assumed to follow Drucker's postulate for a stable material (Sævik, 2017):

- The yield surface is convex,
- The plastic strain increment is normal to the yield surface,
- The plastic strain increment is a linear function of the stress increment,

This is shown in

$$\dot{\boldsymbol{E}}^{(p)} = \dot{\lambda}\frac{\partial f}{\partial \boldsymbol{S}} \tag{3.7}$$

where $\dot{\boldsymbol{E}}^{(p)}$ is the plastic part of the rate of Green's strain tensor, and $\dot{\lambda}$ is a scalar function depending on the current stress and strain, and on the stress rate (Sævik, 2017).

Hardening rule

The hardening rule describes how the yield criterion changes as loading is reversed. This modification of the yield criterion is shown in figure 3.1 and illustrates isotropic and kinematic hardening. If the material yields in position B as illustrated in figure 3.1, the hardening is said to be kinematic if yielding reappears when reversing the load to a stress of magnitude $\sigma_B - 2\sigma_Y$.

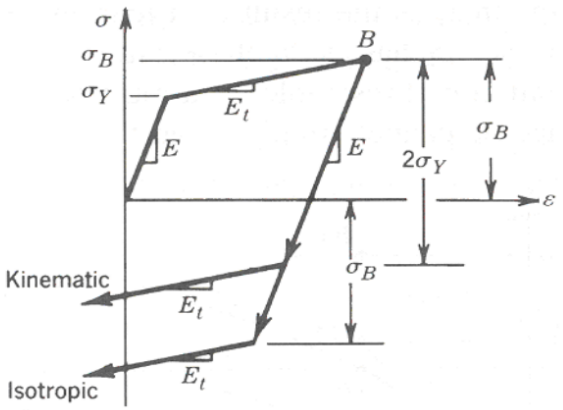

Figure 3.1: Kinematic and Isotropic hardening rules

3.2.3 Boundary conditions

Non-linearity may also be associated with boundary conditions. This type of non-linearity occurs in most contact problems due to the stresses and strains of the contacting bodies not being linearly dependent to the applied loads (Moan, 2003). Friction could also cause another non-linear effect. A contact problem is shown in figure 3.2.

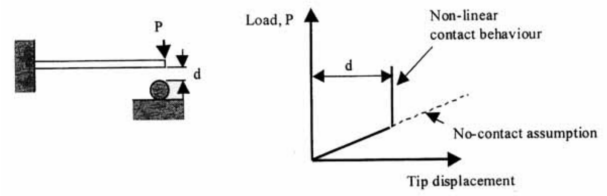

Figure 3.2: Tip of cantilever in contact with a rigid surface (Moan, 2003)

3.3 Incremental solution procedure

In order to solve the nonlinear problem, SIMLA solves the equilibrium equation on incremental form, thus an incremental stiffness matrix has to be established. By taking a look at equation **??** within an infinitesimal increment Δ we get

$$\int_V \boldsymbol{C_e} : (\epsilon + \Delta \boldsymbol{E}) : \delta(\epsilon + \Delta \boldsymbol{E}) dV_0 - \int_S (\boldsymbol{t} + \Delta \boldsymbol{t}) \cdot \delta \boldsymbol{u} dS_0 = 0 \tag{3.8}$$

where $\boldsymbol{C_e}$ is the elasticity tensor, $\boldsymbol{S}$ is the 2nd Piola Kirchhoff stress tensor, $\boldsymbol{E}$ is the Green strain tensor and Δ is the increment between two configurations. Equation 3.8 represents the incremental equilibrium equation where the first term represents the material stiffness matrix and the second terms represents the initial stress stiffness matrix, also known as the geometric stiffness (Sævik, 2017). By introducing kinematic compatibility and a stress-strain relationship, discussed in section 3.1.2 and 3.1.3 respectively, with selected displacement interpolation functions, the incremental stiffness equation can be established in order to further calculate the tangential stiffness matrix

$$\boldsymbol{k}_T = \boldsymbol{k}_m + \boldsymbol{k}_\sigma \tag{3.9}$$

where $\boldsymbol{k}_m$ is the local material stiffness matrix and $\boldsymbol{k}_\sigma$ is the local initial stress stiffness matrix. The co-rotated coordinate system is usually different from the global, thus local displacements and forces has to be transformed from local reference frame to global coordinates (Longva, 2010). The system equation can then be established by collecting the local load vectors and incremental stiffness matrices into a global matrix system. For a static system the global incremental relation is

$$\boldsymbol{K}_T \Delta \boldsymbol{r} = \Delta \boldsymbol{R} \tag{3.10}$$

where $\boldsymbol{K}_T$ is the global tangential stiffness matrix, $\Delta \boldsymbol{r}$ is the incremental displacement and $\Delta \boldsymbol{R}$ the load increment. The equation system is typically solved by performing load increments until a satisfactory level and solving for equilibrium in each step.

3.4 Co-rotated formulation

Total Lagrangian (TL) and Updated Lagrangian (UL) are mostly used in large deformation problems. In a TL formulation the virtual work is calculated with respect to the initial configuration. From figure 3.3, TL uses C_0 as reference configuration. TL refers stresses and strains to the initial configuration with 2nd Piola Kirchoff stress and Green strain. The UL formulation use the deformed configuration, i.e. the last obtained equilibrium configuration. This is visualized as C_n in figure 3.3.

Several variations of TL and UL have been developed for computational efficiency. The basic idea is to separate the rigid body motion from the local element deformation, hence separating non-linearities related to global deformation from non-linearities within the element (Sævik, 2017). SIMLA uses the Co-rotational formulation referring all variables to the C_{0n} configuration shown in figure 3.3.

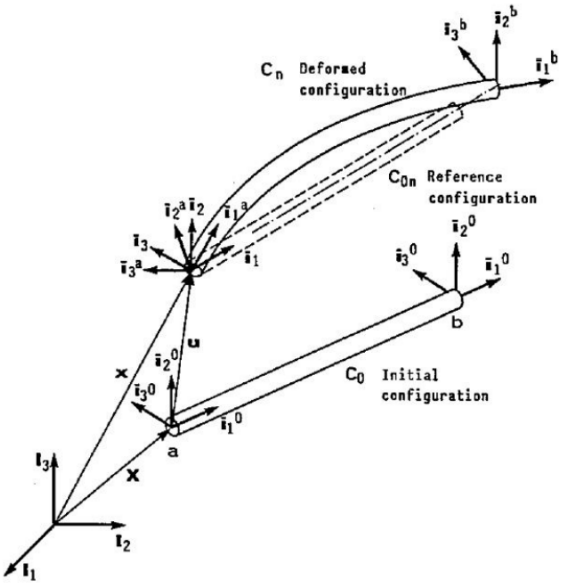

Figure 3.3: Motion of beam nodes (Sævik, 2017)

3.5 Solution method

In order to solve the incremental system equations, SIMLA can use both static and dynamic procedures. The static procedure is however not relevant in this project since its focus is on a dynamic analysis between trawl gear and pipeline interference. Dynamic solution methods will therefore be focused in this section.

3.5.1 Dynamic solution method

A nonlinear dynamic problem cannot be solved by modal superposition. The equation of motion is therefore solved by use of direct time integration, which can be split into explicit or implicit methods.

Explicit method

Explicit methods are usually formulated as in equation 3.11 where the displacement at the next time step is a function of the current displacement and from previous steps. Here subscript k refers to the current time step. Explicit methods are conditionally stable and small time steps must be used. Explicit methods are therefore often used in impulse type response problems where short time steps are needed in order to capture the response (Sævik, 2017).

$$\boldsymbol{r}_{k+1} = \boldsymbol{f}(\ddot{\boldsymbol{r}}_k, \dot{\boldsymbol{r}}_k, \boldsymbol{r}_k, \boldsymbol{r}_{k-1}, ...) \tag{3.11}$$

Implicit method

Implicit methods are usually formulated as in equation 3.12 where the displacement at the next time step is a function of quantities at the next time step and from the current step. This method will have better numerical stability than the explicit methods as it enforces equilibrium at the next time step. The various implicit methods differs in the way the acceleration is assumed to vary between the time steps. Assuming a constant acceleration between the time steps will result in an unconditionally stable method, and numerical stability is provided regardless of the time step size. When these methods are used it is necessary to solve a coupled equation system at every time step, making it uneconomical to apply for situations where short time steps are needed (Sævik, 2017). An implicit method is therefore beneficial for analysis of long time series.

$$\boldsymbol{r}_{k+1} = \boldsymbol{f}(\ddot{\boldsymbol{r}}_{k+1}, \ddot{\boldsymbol{r}}_k, \dot{\boldsymbol{r}}_{+1}k, \dot{\boldsymbol{r}}_k\boldsymbol{r}_k, ...) \tag{3.12}$$

In a dynamic simulation the response from high frequency modes are generally not of big importance. Removing the high frequency modes and ensure good accuracy for the lower frequency modes are therefore of interest. By increasing the damping ratio, or introducing Rayleigh-damping in the Newmark-β method, it can be shown that the result will have zero contribution from the middle modes. The higher modes can further be removed by numerical damping, which introduced to the Newmark-β method, will reduce the accuracy from 2nd to 1st order. The drawback from 2nd to 1st order accuracy is then again eliminated by introducing the HHT-α method, which will damp out high frequency modes while retaining 2nd order accuracy (Sævik, 2017).

Incremental time integration

In the HHT-α method the modified equilibrium equation for the system is given as

$$\boldsymbol{M}\ddot{\boldsymbol{r}}_{k+1} + (1+\alpha)\boldsymbol{C}\dot{\boldsymbol{r}}_{k+1} - \alpha\boldsymbol{C}\dot{\boldsymbol{r}}_k + (1+\alpha)\boldsymbol{R^I}_{k+1} - \alpha\boldsymbol{R^I}_k = \tag{3.13}$$

where $\boldsymbol{M}$ is the mass matrix, $\boldsymbol{C}$ is the damping matrix which includes both Rayleigh damping and a diagonal damping matrix $\boldsymbol{C}_0$, given by equation 3.14, $\boldsymbol{R^I}$ the internal force vector and $\boldsymbol{R^E}$ the external force vector (Sævik, 2017).

$$\boldsymbol{C} = \boldsymbol{C}_0 + \alpha_1 \boldsymbol{M} + \alpha_2 \boldsymbol{K}_T \tag{3.14}$$

The HHT-α method uses the same approach as the Newmark-β method when calculating the acceleration and velocities at the next time step:

$$\Delta \ddot{\boldsymbol{r}}_{k+1} = \Delta \ddot{\boldsymbol{r}}_{k+1} - \Delta \ddot{\boldsymbol{r}}_k = \frac{1}{\Delta t^2 \beta} \Delta \boldsymbol{r}_{k+1} - \frac{1}{\Delta t \beta} \dot{\boldsymbol{r}}_k - \frac{1}{2\beta} \ddot{\boldsymbol{r}}_k \tag{3.15}$$

$$\Delta \dot{\boldsymbol{r}}_{k+1} = \Delta \dot{\boldsymbol{r}}_{k+1} - \Delta \dot{\boldsymbol{r}}_k = \frac{\gamma}{\Delta t \beta} \Delta \boldsymbol{r}_{k+1} - \frac{\gamma}{\beta} \dot{\boldsymbol{r}}_k - \Delta t (\frac{\gamma}{2\beta} - 1) \ddot{\boldsymbol{r}}_k \tag{3.16}$$

If α = 0 the method will correspond the the Newton-β method, and for a linear undamped free oscillating system, the method will be unconditionally stable when (Sævik, 2017):

$$-\frac{1}{3} < \alpha < 0 \tag{3.17}$$

$$\gamma = \frac{1}{2}(1 - \alpha) \tag{3.18}$$

$$\beta = \frac{1}{4}(1 - \alpha)^2 \tag{3.19}$$

If we subtract all current time steps k from equation 3.13 we get

$$\hat{\boldsymbol{K}}_k \Delta \boldsymbol{r}_{k+1} = \Delta \hat{\boldsymbol{R}}_{k+1} \tag{3.20}$$

where $\hat{\boldsymbol{K}}_k$ is the effective stiffness matrix for time step k and $\Delta \hat{\boldsymbol{R}}_{k+1}$ is the effective load vector at time step k+1 (Sævik, 2017). From solving equation 3.20 we get the displacement which then again is needed for solving the acceleration and velocity, respectively in equation 3.15 and 3.16. The effective load vector, $\Delta \hat{\boldsymbol{R}}_{k+1}$, adjusts for any potential unbalance at the time step k, eliminating a potential unbalance propagating through the equilibrium equation 3.13.

Iteration method

In general the solution obtained in the incremental time integration does not sufficiently fulfill the equilibrium equation. SIMLA then uses Newton-Raphson iteration for each time step until sufficient accuracy is obtained (Sævik, 2017).

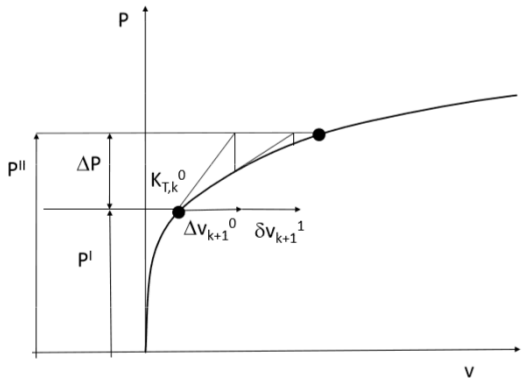

Figure 3.4: Illustration of Newton Raphson iteration

In figure 3.4 the Newton-Raphson iteration method is illustrated. By introducing a load increment, the internal load vector and the stiffness matrix is updated and the iterations are repeated until convergence is obtained. If the tangent stiffness is not updated the method is known as modified Newton-Raphson. We have a Newton-Raphson formulation on equation 3.20 (Sævik, 2017):

$$\hat{\boldsymbol{K}}_k^i \delta \boldsymbol{r}_{k+1}^{i+1} = \Delta \tag{3.21}$$

and the increment in the acceleration and velocity vectors are found from the contributing terms in equation 3.15 and 3.16 defining the updating process as follows (Sævik, 2017):

$$\Delta \boldsymbol{r}_{k+1}^{i+1} = \tag{3.22}$$

$$\Delta \dot{\boldsymbol{r}}_{k+1}^{i+1} = \tag{3.23}$$

$$\Delta \ddot{\boldsymbol{r}}_{k+1}^{i+1} = \Delta \ddot{\boldsymbol{r}}_{k+1}^{i} + \frac{\gamma}{\Delta t^2 \beta} \delta \boldsymbol{r}_{k+1}^{i+1} \tag{3.24}$$

3.6 Finite elements in SIMLA

In SIMLA nodal coordinates are defined by the NOCOOR command by attaching nodes to geometrical positions along the structure. Elements are then defined by attaching them to specific nodes via the ELCON command. The numerical model consist of the trawl gear and a pipeline where both parts are being modelled by pipe elements. Pipe elements are generally beam elements with thin walled tubular cross-section characteristics. The element is based on linear interpolation for torsion and axial displacement whereas cubic interpolation is used in transverse directions. The degrees of freedom can be seen in figure 3.5. Incremental equilibrium equation is obtained by applying equation 3.2 in combination with the material law and the respective interpolation function. Hydrodynamic loads are found using Morison's equation and lumped and Rayleigh damping are included in the element (Sævik, 2017).

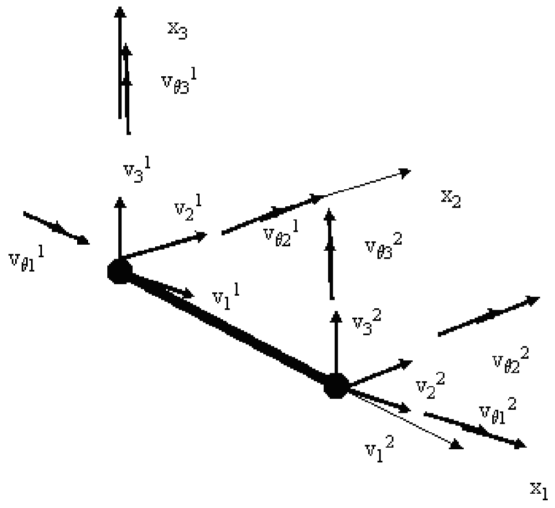

Figure 3.5: DOFs for PIPE elements (Sævik, 2017)

3.6.1 PIPE31

PIPE31 is the elastic version of the pipe element and is described by a displacement pattern showed in equation 3.4. According to von Karman the second order longitudinal Green strain term is neglected along with the coupling terms between strain and torsion (Sævik, 2017). The longitudinal Green strain is then found by:

$$E_{xx} = u_{x_0,x} - yu_{y_0,xx} - zu_{z_0,xx} + \frac{1}{2}(u_{y_0,x}^2 + u_{z_0,x}^2) \tag{3.25}$$

The element assumes a stress-strain relationship based on Hook's law in eq. 3.5.

3.6.2 PIPE33

PIPE33 is the elastoplastic version of the pipe element described by the displacements and longitudinal Green strain in eq. 3.4 and 3.3 respectively. The element accounts for material non-linearity, described in section 3.2.2.

Chapter 4

Case study

The study deals with simulating a trawl gear pipeline impact for a corrected seabed. The scope of the thesis is to establish a load case matrix with seabed geometries, soil data, pipeline cross-sections and tow velocities and perform a parametric study. This chapter describes the case matrix and all input variables regarding the rock dump, which is further investigated with different pipeline dimensions and trawl speed. Rock dump is abbreviated RD from now on. All simulations from the parameter study is addressed with a naming system. Any remarks experienced during the performance of all simulations in order to increase the performance of the parameter study are addressed.

4.1 Parameter study

The naming system is illustrated in figure 4.1. The equivalent slope for the example shown in figure 4.1 is 1 in 3, hence the underscore is interpreted as the ratio between the displaced length in z- and y-direction. All further simulations are named as the example in figure 4.1 and figure 4.2 illustrates all the parameters.

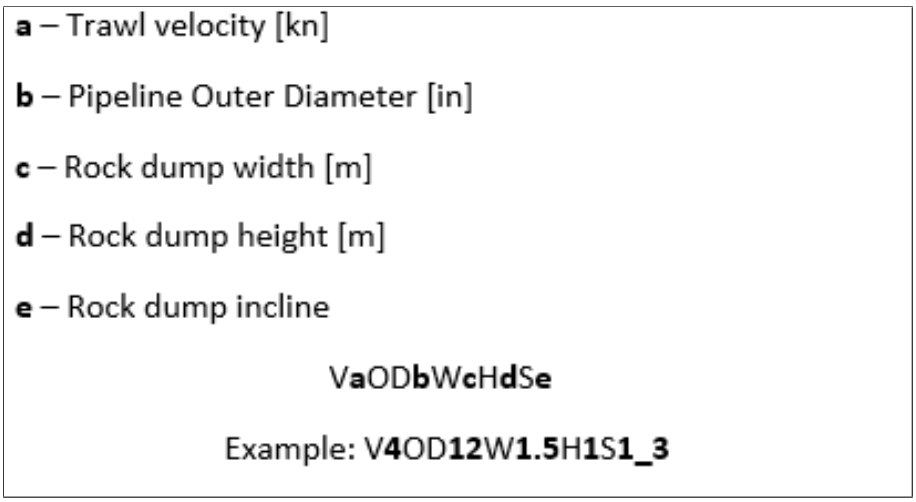

Figure 4.1: Naming system.

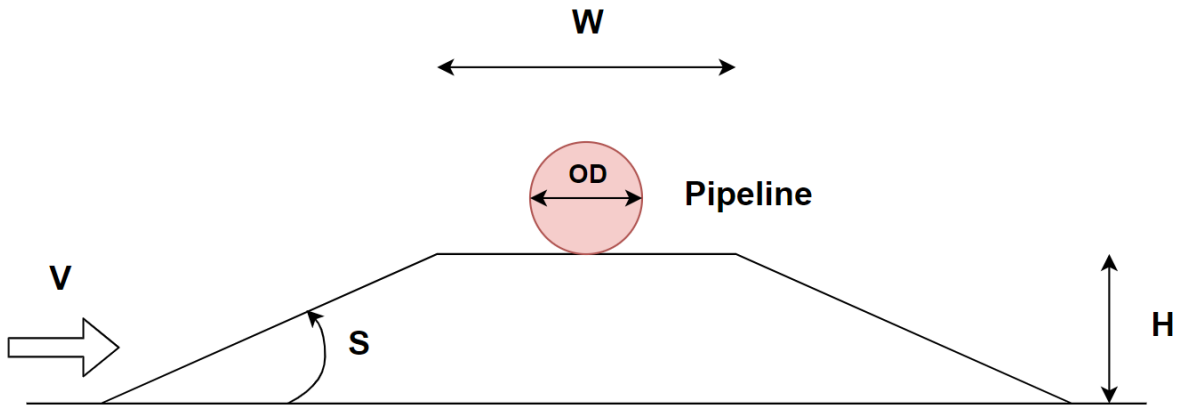

Figure 4.2: Concept of all governing parameters.

4.1.1 Seabed geometry alteration

In order to cover a wide range of seabed geometries each height is simulated with four different widths in order to capture the effect with both small and large values. Each height and width configuration is then simulated with seven different slopes, ranging from 1 in 1.5 up to 1 in 5, or 33.69 ° to 11.31 ° respectively. By introducing these parameters the idea is to get a representation of the values between the extremes, i.e. a representation between a flat seabed and a steep RD, enough to make the clump weight jump over the pipeline. This results in a set of four different RD widths for each individual RD height, whereas for each individual width a set of seven different slopes are analyzed. This results in 12 different combinations of RD height and width, and combined with all slope configurations, a total of 84 simulations.

The original 84 simulations are carried out with a pipeline structural radius of 154 mm and a structural thickness of 15.9 mm, equivalent to an outer diameter of 12.75 inches. Chapter 5 goes further in depth describing pipeline and trawl gear data. These simulations are however performed with fixed pipeline dimensions and trawl speed, and since the seabed geometry is changing for each simulation, the naming system described in figure 4.1 is applied in order to differentiate between the analyses. Each respective simulation is shown in table 4.1, 4.2 and 4.3. For the sake of simplicity the simulations are named with an outer diameter of 12 inches, ”OD12”, while they in reality are 12.75 inches. Since all the original 84 simulations are performed with a trawl speed of 5 knots, the ”V” term in the naming system is not included for this trawl speed in order to better fit the tables.

	RD width, W			
RD slope, S [°]	1.5 m	2.0 m	4.0 m	6.0 m
33.7	OD12W1.5H0.5S1_1.5	OD12W2H0.5S1_1.5	OD12W4H0.5S1_1.5	OD12W6H0.5S1_1.5
26.6	OD12W1.5H0.5S1_2	OD12W2H0.5S1_2	OD12W4H0.5S1_2	OD12W6H0.5S1_2
21.8	OD12W1.5H0.5S1_2.5	OD12W2H0.5S1_2.5	OD12W4H0.5S1_2.5	OD12W6H0.5S1_2.5
18.4	OD12W1.5H0.5S1_3	OD12W2H0.5S1_3	OD12W4H0.5S1_3	OD12W6H0.5S1_3
15.9	OD12W1.5H0.5S1_3.5	OD12W2H0.5S1_3.5	OD12W4H0.5S1_3.5	OD12W6H0.5S1_3.5
14.0	OD12W1.5H0.5S1_4	OD12W2H0.5S1_4	OD12W4H0.5S1_4	OD12W6H0.5S1_4
11.3	OD12W1.5H0.5S1_5	OD12W2H0.5S1_5	OD12W4H0.5S1_5	OD12W6H0.5S1_5

Table 4.1: RD sensitivity study with height, H = 0.5 m and trawl speed V = 2.6 m/s = 5 knots.

	RD width, W			
RD slope, S [°]	1.5 m	2.0 m	4.0 m	6.0 m
33.7	OD12W1.5H1S1_1.5	OD12W2H1S1_1.5	OD12W4H1S1_1.5	OD12W6H1S1_1.5
26.6	OD12W1.5H1S1_2	OD12W2H1S1_2	OD12W4H1S1_2	OD12W6H1S1_2
21.8	OD12W1.5H1S1_2.5	OD12W2H1S1_2.5	OD12W4H1S1_2.5	OD12W6H1S1_2.5
18.4	OD12W1.5H1S1_3	OD12W2H1S1_3	OD12W4H1S1_3	OD12W6H1S1_3
15.9	OD12W1.5H1S1_3.5	OD12W2H1S1_3.5	OD12W4H1S1_3.5	OD12W6H1S1_3.5
14.0	OD12W1.5H1S1_4	OD12W2H1S1_4	OD12W4H1S1_4	OD12W6H1S1_4
11.3	OD12W1.5H1S1_5	OD12W2H1S1_5	OD12W4H1S1_5	OD12W6H1S1_5

Table 4.2: RD sensitivity study with height, H = 1.0 m and trawl speed V = 2.6 m/s = 5 knots.

	RD width, W			
RD slope, S [°]	1.5 m	2.0 m	4.0 m	6.0 m
33.7	OD12W1.5H2S1_1.5	OD12W2H2S1_1.5	OD12W4H2S1_1.5	OD12W6H2S1_1.5
26.6	OD12W1.5H2S1_2	OD12W2H2S1_2	OD12W4H2S1_2	OD12W6H2S1_2
21.8	OD12W1.5H2S1_2.5	OD12W2H2S1_2.5	OD12W4H2S1_2.5	OD12W6H2S1_2.5
18.4	OD12W1.5H2S1_3	OD12W2H2S1_3	OD12W4H2S1_3	OD12W6H2S1_3
15.9	OD12W1.5H2S1_3.5	OD12W2H2S1_3.5	OD12W4H2S1_3.5	OD12W6H2S1_3.5
14.0	OD12W1.5H2S1_4	OD12W2H2S1_4	OD12W4H2S1_4	OD12W6H2S1_4
11.3	OD12W1.5H2S1_5	OD12W2H2S1_5	OD12W4H2S1_5	OD12W6H2S1_5

Table 4.3: RD sensitivity study with height, H = 2.0 m and trawl speed V = 2.6 m/s = 5 knots.

The numerical model consists of a global pipeline spanning a total of 1 km on the seabed, thus consuming an unfavorable amount of time and large CPU usage. In order to minimize the time needed in order to complete all simulations they are performed on a separate computer through a remote desktop application. This way the personal computer is not affected by heavy numerical calculations and multiple simulations can be run at once. The remote computer has enough cores in order to complete a batch of more than 10 simulations, thus minimizing the time needed in order to complete the study. 40 GB of disk space was made available in order to manage the result files from SIMLA and post-processing files from both simpost and dynpost.

4.1.2 Pipeline dimension alteration

In order to adjust the pipeline dimensions and investigate the effects of increased outer diameter, a set of seabed configurations have to be chosen for further investigation. These configurations are, equivalent to the 12.75 inch pipe, compared to a case with flat seabed. This way any similarities or discrepancies between altering the pipe dimensions are easily reported. Interesting RD geometries are chosen for further simulations with varying pipe dimensions. The height is fixed at H = 1.0 m, while the width is tested for both 1.5 m and 6.0 m. Both an incline of 1 in 1.5, 1 in 3 and 1 in 5 are checked for each width. These values are checked for both a 16 inch and 24 inch pipe, as shown in table 4.4 and 4.5. The simulations are performed with a trawl speed of 2.6 m/s, or 5 knots, similar to the original 86 simulations. The "V" in the naming is hence not included. The structural thickness is increased to 24.5 mm for both pipes. The purpose of checking slope 1 in 1.5 and 1 in 5 and also a width of 1.5 m and 6.0 m is to look at the extreme in both ends, while slope 1 in 3 is checked in order to get a representation in between the extremes.

	RD width, W	
RD slope, S [°]	1.5 m	6.0 m
33.7	OD16W1.5H1S1_1.5	OD16W6H1S1_1.5
18.4	OD16W1.5H1S1_3	OD16W6H1S1_3
11.3	OD16W1.5H1S1_5	OD16W6H1S1_5

Table 4.4: Simulations with pipeline outer diameter of 16", RD height, H = 1.0 m and trawl speed V = 2.6 m/s = 5 knots.

	RD width, W	
RD slope, S [°]	1.5 m	6.0 m
33.7	OD24W1.5H1S1_1.5	OD24W6H1S1_1.5
18.4	OD24W1.5H1S1_3	OD24W6H1S1_3
11.3	OD24W1.5H1S1_5	OD24W6H1S1_5

Table 4.5: Simulations with pipeline outer diameter of 24", RD height, H = 1.0 m and trawl speed V = 2.6 m/s = 5 knots.

4.1.3 Trawl speed alteration

The original trawl speed for all previous simulations are 2.6 m/s, or 5 knots, and is generally considered to be fast. The recommended practice states that trawl velocity and pattern is mainly governed by fish movement pattern, the fish's swimming speed and economic speed of trawl vessels (DNV-GL, 2014). Trawling for prawns is typically performed at 2 - 3 knots, whereas trawling for fish is performed at up to 5 - 6 knots (DNV-GL, 2014), hence investigating the effect of reduced trawl speed is of interest. The pull-over effects are investigated for 2.1 m/s with both 12.75 and 16 inch pipe. This is equivalent to approximately 4 knots which is investigated with a RD width of 1.5 m and RD height of 1 m as shown in table 4.6. 2.1 m/s is for the case of simplicity denoted V4 as shown in figure 4.1.

	Pipeline outer diameter, OD	
RD slope, S [°]	12.75”	16”
18.4	V4OD12W1.5H1S1_3	V4OD16W1.5H1S1_3
11.3	V4OD12W1.5H1S1_5	V4OD16W1.5H1S1_5

Table 4.6: Simulations with trawl speed V = 2.1 m/s = 4 knots.

Chapter 5

Modeling

The SIMLA input files was received from Vegard Longva at the start of the project thesis, and further developed for this master thesis. This chapter describes the numerical model and all input parameters needed in order to simulate the clump weight pipeline interference. All input parameters are defined and relevant contact elements are addressed. The analysis procedure and a description of how the data is post-processed is also included.

No relevant information regarding the input parameters extracted from the model was given, hence this chapter will not describe any comprehensive reasoning behind the parameters and their existence. The chapter therefore refers to a short and concise description of the information interpreted from the numerical model.

5.1 Seabed input file

In order to change the seabed geometry, the seabed input file is changed. The original file consists of 3 lines along the y-axis, the first one being defined as the center line where the pipeline is located and the two last lines representing the edges of the seabed, respectively on the left and right side. When modelling the RD, four lines between the center line and each respective outer line is added to the seabed file in order to capture the slope and change in z-direction. The center line remains unchanged while an innermost pair of lines is extracted to the left and right respectively in order to describe the top of the RD slope. This pair has its normal vector perpendicular to the RD flat, while the following pair of lines have the same coordinate, but with a normal vector perpendicular to the slope of the RD. The next two set of lines defines the bottom of the RD slope whereas the normal vector is defined perpendicular for both the slope and the flat seabed for each pair of lines respectively. The final two lines marks the end of the seabed model, stretching a total of 1.5 km in both directions away from the clump weight which is assumed to be at the origin of the coordinate system.

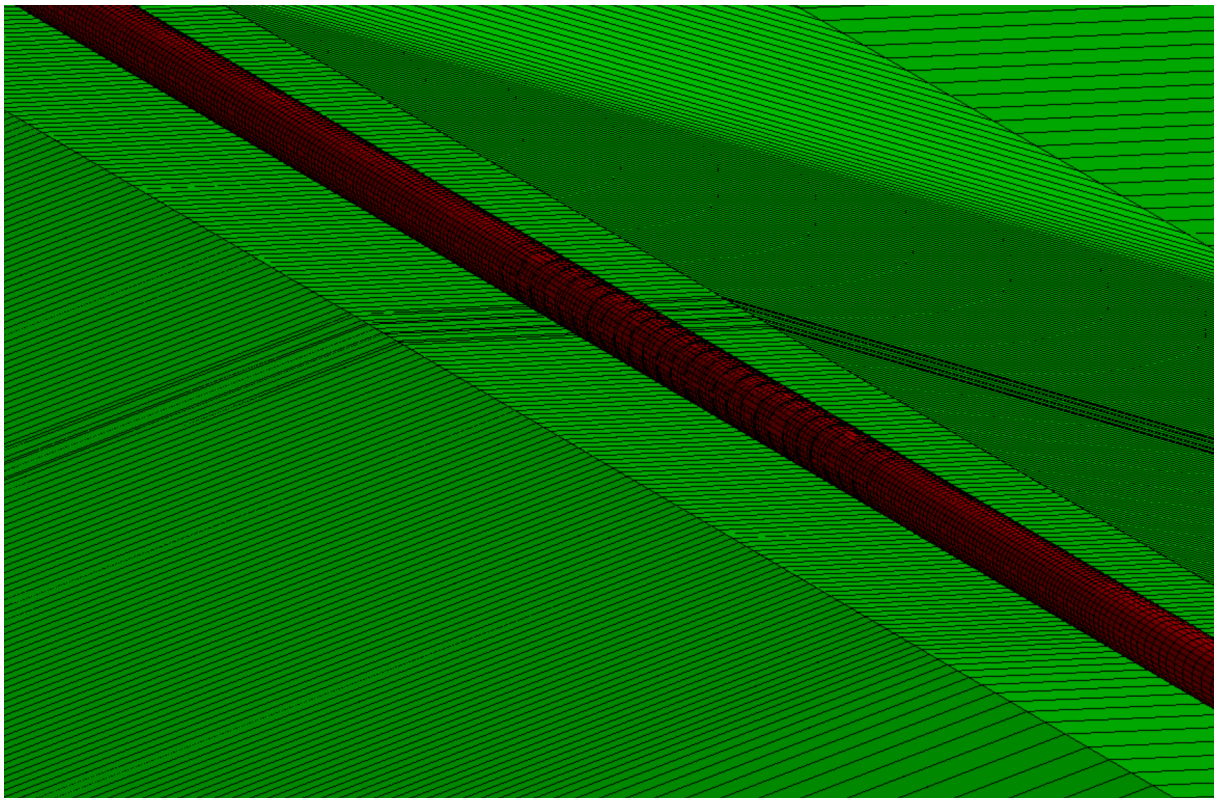

Figure 5.1: Pipeline for case OD12W2H2S1_3

5.2 Pipeline data

The pipeline is 1000 meters straight at a depth of 200 m below water surface. As the seabed is altered the pipeline coordinates are corrected in z-direction in order to keep the pipe on top of the RD. The seabed geometry study is performed with an outer diameter of 12.75", which is later increased to 16" and 24" for a limited set of RD geometries. Each respective end is equipped with springs fixing the pipe for any displacements in z-direction during interaction and a transverse stiffness of 10^{10} N/m. The pipe is modelled into three parts, where the first zone is centered at the midpoint where point of interaction is located. This zone contains a fine mesh accounting for plasticity, whereas the second zone has a coarser mesh and is present at both sides of the first zone. The third and final zone is based on the length of the previous zones and the total length of the pipe. The pipeline is modelled with pipe33-elements, a stress-strained based elastoplastic pipe element which is further described in section 3.6. The element length increases by a factor of 1.1 for each element within a specific zone. Figure 5.1 shows the clump weight point of attack for the OD12W2H2S1_3 case, where the highlighted lines across the RD are the track where the clump weight is dragged across. Relevant properties of all pipelines are given in table 5.1, 5.2 and 5.3. All pipelines follows a kinematic hardening curve when yielding.

Quantity	Symbol	Value	Unit
Pipeline length	L	1000	m
Length of zone 1	L_1	50	m
Length of zone 2	L_2	150	m
Length of zone 3	L_3	325	m
Outer diameter	OD	323.9	mm
Mean structural radius	r	154	mm
Structural thickness	t	15.9	mm
Radial drag coefficient	C_D	0.7	-
Radial added mass coefficient	C_M	2.0	-
Dry mass	m	228.25	kg/m
Submerged mass	m_s	35.69	kg/m
Internal pressure	p_i	16	MN/m^2
Young's modulus	E_p	207	GPa
Steel density	ρ	7850	kg/m^3
Poisson's ratio	ν	0.3	-

Table 5.1: Properties for 12.75" pipe

Quantity	Symbol	Value	Unit
Pipeline length	L	1000	m
Length of zone 1	L_1	50	m
Length of zone 2	L_2	150	m
Length of zone 3	L_3	325	m
Outer diameter	OD	406	mm
Mean structural radius	r	190.75	mm
Structural thickness	t	24.5	mm
Drag coefficient	C_D	0.7	-
Added mass coefficient	C_M	3.29	-
Dry mass	m	265	kg/m
Submerged mass	m_s	132.563	kg/m
Internal pressure	p_i	16	MN/m^2
Young's modulus	E_p	207	GPa
Steel density	ρ	7850	kg/m^3
Poisson's ratio	ν	0.3	-

Table 5.2: Properties for 16" pipe

Quantity	Symbol	Value	Unit
Pipeline length	L	1000	m
Length of zone 1	L_1	50	m
Length of zone 2	L_2	150	m
Length of zone 3	L_3	325	m
Outer diameter	OD	610	mm
Mean structural radius	r	292.75	mm
Structural thickness	t	24.5	mm
Drag coefficient	C_D	0.7	-
Added mass coefficient	C_M	3.29	-
Dry mass	m	503.5	kg/m
Submerged mass	m_s	203.94	kg/m
Internal pressure	p_i	16	MN/m^2
Young's modulus	E_p	207	GPa
Steel density	ρ	7850	kg/m^3
Poisson's ratio	ν	0.3	-

Table 5.3: Properties for 24" pipe

In order to capture the changes in added mass the radial added mass coefficient is increased by 1.29 due to the pipe resting on the free surface, hence giving an added mass 2.29 times the added mass for large H/R values (Faltinsen, 1990). The increase in radial added mass coefficient of 1.29 comes from equation 5.1

$$C_M = C_A + 1 \tag{5.1}$$

where C_M is the mass coefficient and C_A is the added mass coefficient, thus giving an added mass coefficient of $C_A = C_M - 1 = 2.29 - 1 = 1.29$. This value is to be added to the coefficient in SIMLA giving a radial added mass coefficient, C_M = 3.29 for 16" and 24" pipe.

5.3 Trawl gear data

The trawl gear configuration is illustrated in figure 5.2 and 5.3. The simulations are performed with a clump weight of the Roller type as described in section 2.2.3 and shown in figure 2.6 and the same trawl configuration is performed for all simulations. The clump weight is pulled by the warp line which is connected to a towing node at the sea surface. As the load acting at the towing node is gradually increased the warp line tension will start to increase and eventually pull the trawl gear towards the pipeline. The sweep lines are connecting two trawl nets to the clump weight.

The trawl nets are represented by two drag nodes with a drag coefficient of 10 in transverse direction and 37 in towing direction. The trawl nets are modelled without mass properties in order to avoid compression forces in the sweep lines during interference (Maalø, 2011). A warp angle of 19.5° and a sweep angle of 27.5° was kept the same for all simulations. The towing node is gradually accelerated up to a constant trawl velocity of 2.6 m/s by applying a load time history at the spring. In order to keep the trawl nets at a constant sweep angle they are applied the same load history pattern through an individual towing node. Both towing nodes are connected to the trawl nets with a single pipe31 element and has the

same spring configuration as the towing node at the water surface. The trawl gear data is given in table 5.4.

Quantity	Symbol	Value	Unit
Water depth	d	200	m
Warp angle	ψ	19.5	deg
Sweep angle	θ	27.5	deg
Trawl net drag coefficient in towing direction	C_d	37	-
Trawl net transverse drag coefficient	$C_{d,t}$	10	-
Trawl net mass	m	0.0	kg

Table 5.4: Trawl gear data

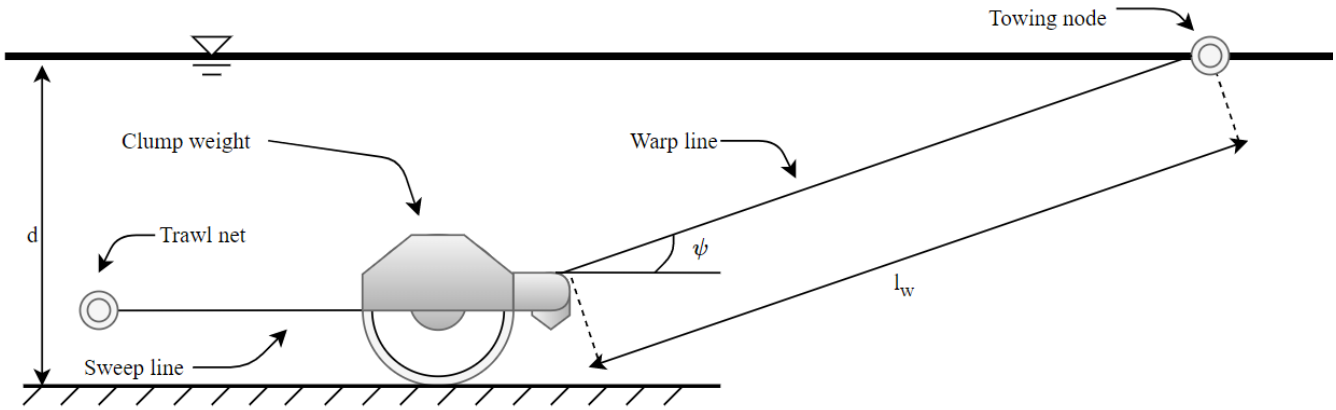

Figure 5.2: Trawl gear in the vertical plane

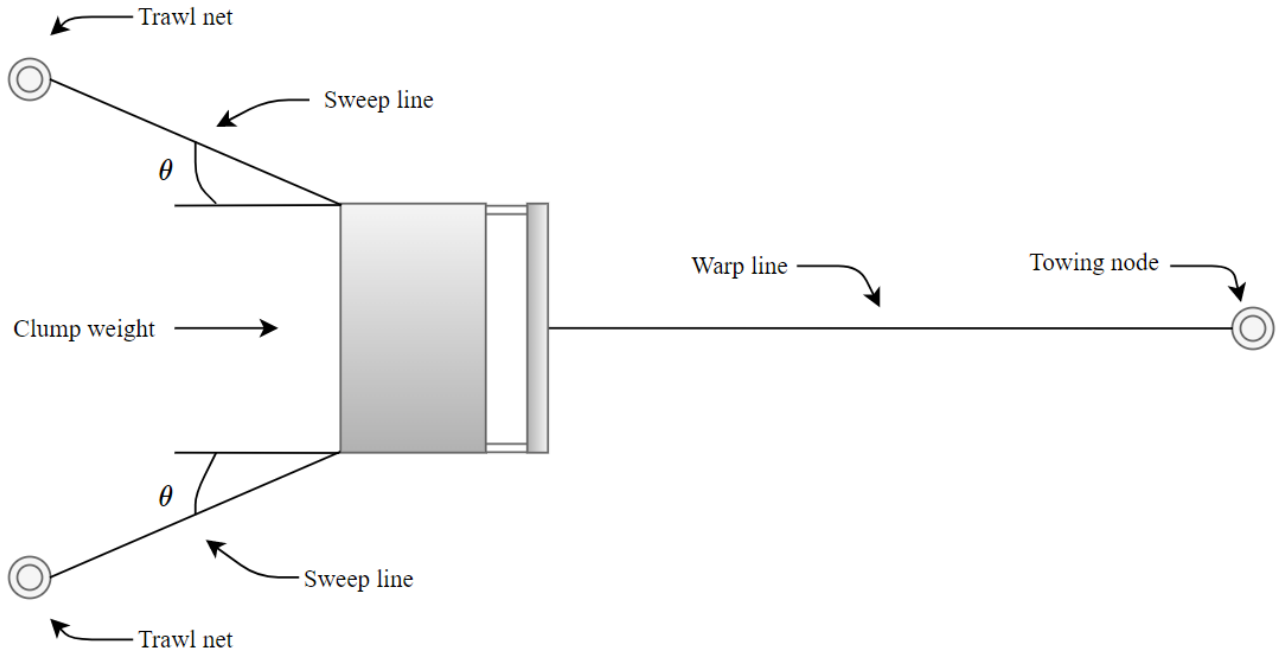

Figure 5.3: Trawl gear in the horizontal plane

5.3.1 Clump weight

The clump weight is of a Roller type discussed in section 2.2.3 and consists of a roller with a top rod omitted by a frame system and weight plates. The clump weight frame is connected to the warp line shackle and both sweep lines and is also connected to weight plates in front of the roller and to the side of the roller and top rod. A comparison between the clump weight used and a typical clump weight of the Roller type shown in section 2.2.3 is seen in figure 5.4 and 5.5. Relevant properties are described in table 5.5. The roller, top rod and the framework omitting the roller is simulated with pipe31 elements.

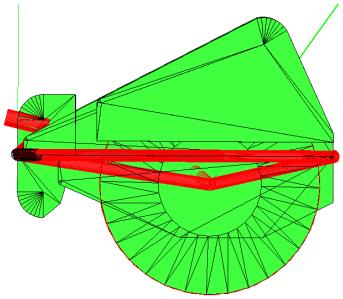

(a) Clump weight model

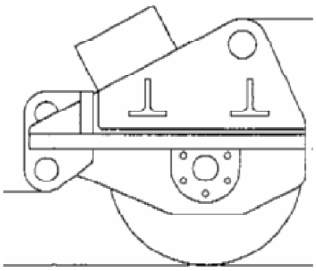

(b) Clump weight of the Roller type (DNV-GL, 2014)

Figure 5.4: Clump weight cross section geometries

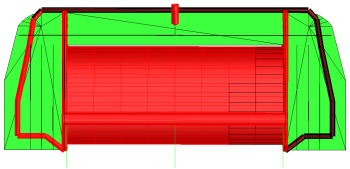

(a) Clump weight model

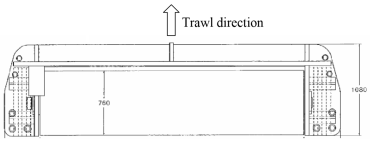

(b) Clump weight of the Roller type (DNV-GL, 2014)

Figure 5.5: Clump weight geometries in the horizontal plane

Quantity	Symbol	Value	Unit
Roller length	L_r	3.7	m
Roller diameter	D_r	760	mm
Roller added mass coefficient	$C_{M,r}$	1.0	-
Roller submerged mass	$m_{s,r}$	3524	kg
Roller dry mass	m_r	4314	kg
Framework diameter	D_f	40	mm
Framework added mass coefficient	$C_{M,f}$	1.0	-
Framework submerged mass	$m_{s,f}$	2215	kg
Framework dry mass	m_f	2400	kg

Table 5.5: Clump weight properties

5.3.2 Warp line

The warp line is connected to the clump weight via the warp line shackle and the clump weight frame and is modelled with elastic pipe31 elements. The warp line is modelled in one lower and one upper part whereas the lower part is equipped with roller contact elements in order to capture the interference between the pipeline and the warp line. The lower part is modelled with an element length of 0.05 m where the mesh is gradually increasing to 3.5 m in the upper part. The warp line shackle is modelled with one element of 0.15 m.

Quantity	Symbol	Value	Unit
Warp line length	L_w	600	m
Lower warp line length	L_lower	12.5	m
Warp line diameter	D	38	mm
Axial stiffness	EA	58.34	MN
Bending stiffness	EI	4	kNm^2
Radial drag coefficient	$C_{Dw,r}$	1.6	-
Tangential drag coefficient	$C_{Dw,t}$	0.1	-
Radial added mass coefficient	$C_{Mw,r}$	2.0	-
Tangential added mass coefficient	$C_{Mw,t}$	1.0	-
Dry mass	m	8.9	kg/m
Submerged mass	m_s	7.74	kg/m

Table 5.6: Warp line properties

5.3.3 Sweep lines

The sweep lines are 80 m long and modelled with 2 m long pipe31 elements. In order to keep the trawling nets at a constant sweep angle a single 80 m long element with equal properties is introduced. These two elements connects both trawl nets to each individual towing node with identical load history to the towing node at sea surface. The single pipe elements are constrained from all degrees of freedom except from the vertical direction and the towing direction. Sweep line properties are shown in table 5.7.

Quantity	Symbol	Value	Unit
Sweep line length	L	80	m
Sweep diameter	D	25	mm
Axial stiffness	EA	52.83	MN
Bending stiffness	EI	4	kNm^2
Radial drag coefficient	$C_{D,r}$	1.0	-
Added mass coefficient	C_M	2.0	-
Dry mass	m	3.85	kg/m
Submerged mass	m_s	0.0	kg/m

Table 5.7: Sweep line properties

5.4 Contact interaction

SIMLA includes powerful contact elements able to solve the governing interactions. Contact elements are used when modelling surfaces without attachment but in contact that transmits contact forces to each other. The contact elements are developed when considering two bodies, A and B each of which occupies a region in space with certain boundary conditions. The bodies displacement fields are denoted $\boldsymbol{u^A} = \boldsymbol{u^A}(\boldsymbol{x^A})$ and $\boldsymbol{u^B} = \boldsymbol{u^B}(\boldsymbol{x^B})$ where $\boldsymbol{x}$ represents the updated coordinates. At the beginning of a time increment the initial gap is defined as (Sævik, 2017):

$$g_0 = (\boldsymbol{u}^B - \boldsymbol{u}^A) \cdot \boldsymbol{n} \tag{5.2}$$

where $\boldsymbol{n}$ is outward surface vector of body A. After a time increment Δt the contact condition is defined as:

Gap opening:

$$d_g = (\Delta \boldsymbol{u}_B - \Delta \boldsymbol{u}_A) \cdot \boldsymbol{n} + g_0 \geq 0 \tag{5.3}$$

Contact:

$$d_g = (\Delta \boldsymbol{u}_B - \Delta \boldsymbol{u}_A) \cdot \boldsymbol{n} + g_0 < 0 \tag{5.4}$$

If contact is expected at certain structural elements, a contact group is established with master and slave elements. The slave elements are a set of structural elements and master elements are contact elements searching for slave elements. Contact search is done at each time step and as soon as a slave element is within the reach of a master element, the distance between them is calculated. The contact condition defines contact if the gap is negative and is shown in equation 5.3 and 5.4 for a time increment, Δt (Sævik, 2017). In this case body B represents the master elements and body A represents the slave elements.

5.4.1 Seabed contact

The seabed is entirely flat along the pipeline but the geometry around it is modified in the seabed input file as shown in figure 5.1. With extra lines describing the seabed, more alternatives regarding soil properties are introduced. The seabed is divided into a grid where each square can be assigned different soil properties. The interaction between physical objects and the sea floor are modelled with contact element cont126. The element is a 1-noded contact element and is linked to a predefined contact surface, which in this case is the seabed. A friction force is applied in both transverse and axial direction. Friction characteristics are decided by seabed interaction curves defining an unit friction force per meter displacement (Johnsen, 2012). The friction coefficient is 0.3 in local axial direction and 0.6 in local transverse direction.

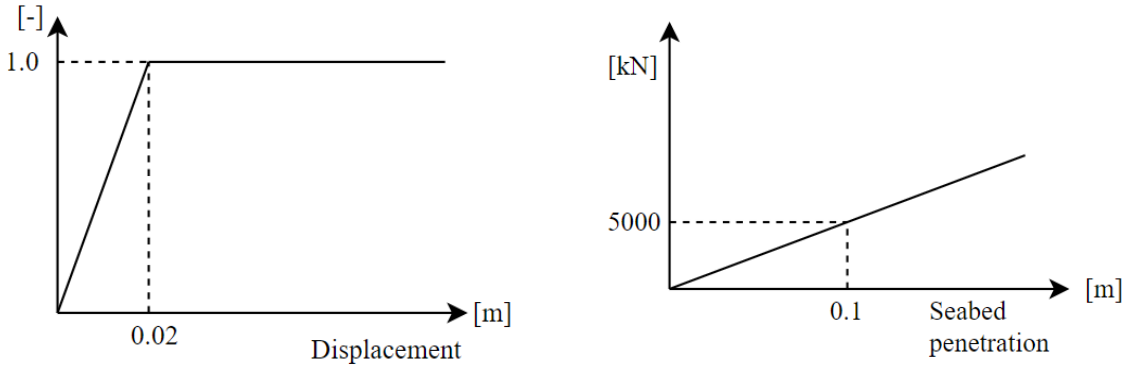

(a) Seabed lateral and axial interaction curve

(b) Seabed vertical interaction curve

Figure 5.6: Seabed interaction curves

Figure 5.6 a) shows the seabed interaction curve in both lateral and axial direction whereas figure 5.6 b) shows the vertical interaction curve. In order to simulate rockdumping with increased stiffness compared to the seabed soil initial tests are performed. The updated interaction curves for the tests are shown in figure 5.7.

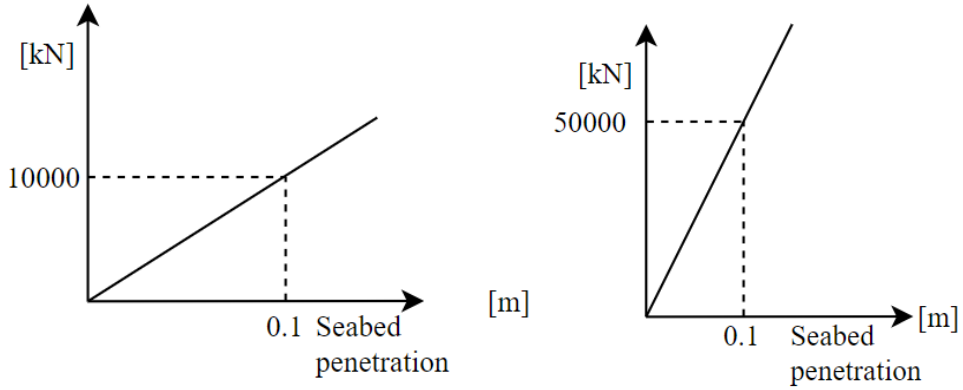

(a) Updated vertical interaction curve

(b) Updated vertical interaction curve

Figure 5.7: Tested interaction curves in vertical direction

5.4.2 Contact between warp line and pipeline

The warpline pipe interaction is modelled with cont164 contact elements. Cont164 is a three-dimensional 3-noded roller element that assume contact is obtained between an user defined cylinder attached to node 1 and an arbitrary position between two pipe nodes in our case (Svein Sævik and Gjøsteen, 2018). Figure 5.8 illustrates the geometrical relations for the roller contact element. The lower warpline and warpshackle are equipped with roller contact elements.

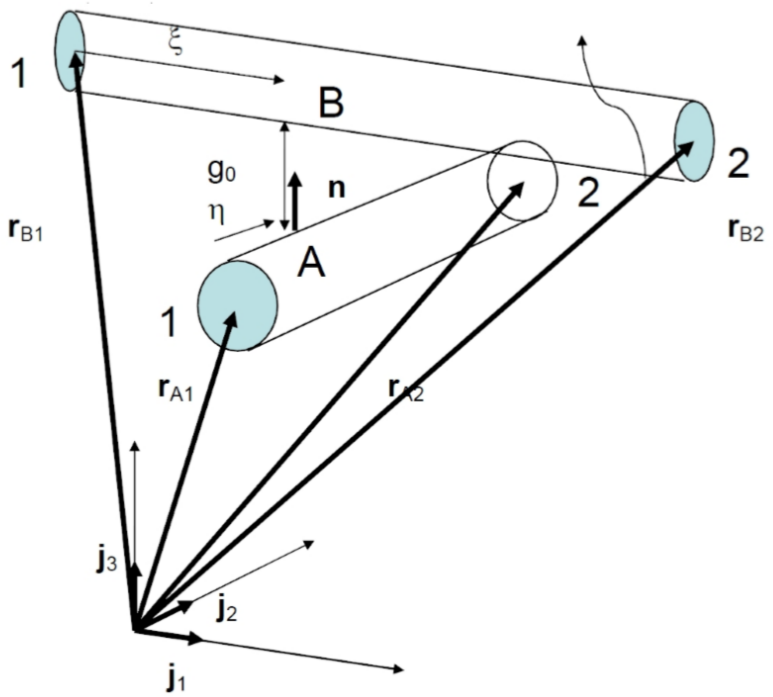

Figure 5.8: Geometrical relations for roller contact element (Sævik, 2017).

The initial gap can be expressed by:

$$g_0 = (\boldsymbol{r}^{B1} - \boldsymbol{r}^{A1}) \cdot \boldsymbol{n} R^A - R^B \tag{5.5}$$

where $\boldsymbol{r}^{l1}$, l = A or B, represents the updated coordinate positions of the roller and pipe first endpoint, R^A and R^B is the roller and pipe radii respectively (Sævik, 2017).

5.4.3 Contact between clump weight frame and pipeline

The clump weight frame and pipe interaction is handled by contact element cont153, a penalty-based contact element tailor-made for global response prediction of pipelines interacting with rigid bodies. The element was developed by Vegard Longva as part of his phd. work. Cont153 is a three noded contact element with 18 DOF's that describes contact between pipe elements and a three-dimensional body (Svein Sævik and Gjøsteen, 2018). As illustrated in figure 2.11, six of the DOF's belong to the three-dimensional body and twelve DOFs are associated with the pipe element.

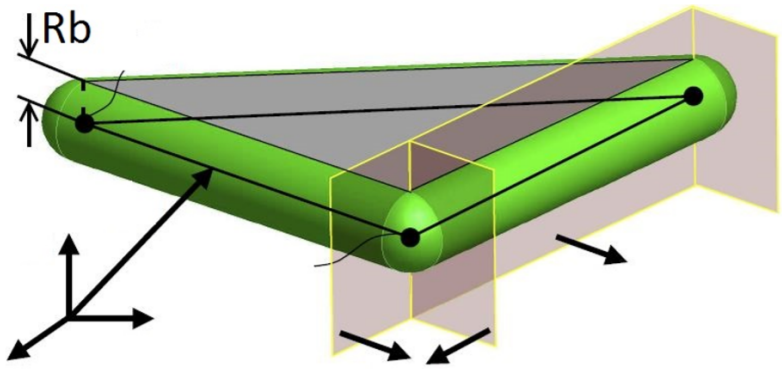

Figure 5.9: Rigid triangle with thickness Rb (Svein Sævik and Gjøsteen, 2018).

The geometry of the three dimensional body is modelled by a grid consisting of plane triangular elements with equal thickness Rb as shown in figure 5.9. The green area represents the contact surface and a continuous description of the contact geometry is obtained because of the equal thickness (Svein Sævik and Gjøsteen, 2018). The geometry is proved to be numerical robust because the contacting surfaces have a continuous description (Longva et al., 2013).

5.5 Analysis procedure

The analysis can be separated into three parts, where each part has its own input file controlled by the TIMECO command. TIMECO defines the analysis as a function of time (Svein Sævik and Gjøsteen, 2018). The clump weight is situated at the origin of the global coordinate system, 120 m from the pipeline. At analysis start all static loads are applied to the structure, such as gravity and external pressure. After one second all static loads approaches unit value and the analysis switches into dynamic mode. The clump weight boundary conditions are released and the towing node is accelerated the first 30 seconds until the velocity reaches 2.6 m/s. The towing node travels with constant speed another 20 seconds in order to damp out any transients related to the trawl gear.

The last input file ends after the clump weight pipe impact is done with a governing time increment of 1 ms during clump weight pipeline interference and 10 ms during the last 15 seconds of the acceleration phase and also during the constant towing speed. A time increment of 5 ms is used the first 15 seconds as the clump weight is accelerated from starting position. The convergence ratio for each equilibrium iteration varies between 10^{-5} and 10^{-7} for the static simulation whereas the dynamic simulation varies between 10^{-6} down to 10^{-8} during interaction between clump weight and pipeline. The simulations demanded approximately 30 minutes of CPU-time. As the trawl velocity is lowered the third input file is altered in order to account for the delayed interference between clump weight and pipeline. With a trawl speed reduced to 1.6 m/s the interference got delayed by over 20 seconds and CPU-time increased by five times at the longest.

5.6 Data post-processing

In order to retrieve simulation results simpost and dynpost are used, both post-processing extensions for results from SIMLA. Simpost extracts user specified input from the result file (.raf) and reports all output on .mpf format. The user specified input is characterized by a simpost input file (.spi). Dynpost is fed an input file extension .sdi with specifications made by the user and reports all output on .mpf format. Unlike simpost, dynpost reports results from the dynamic result file, or the .dyn file, created from user selected time histories in the DYNRES_ card. Dynpost is able to extract results from each timestep, whereas simpost only extracts results which are stored on the .raf file. The matrixplot (.mpf) format are ASCII files which could be further processed by a plotting script.

The pull-over forces are extracted from the DYNRES result file and generated into ASCII files by dynpost. All contact forces in x, y and z-direction between master and slave elements are sampled into a total of 206 files for each direction. These are further loaded into a Python script where accompanying element forces are summarized and presented as graphs of interest, usually compared with multiple other simulations. In order to get a better visualization of the pull-over forces a running average of 0.05 s are presented. The tension at middle of the lower warp line is also extracted. Time usage for dynpost did take approximately two and a half hour for each simulation due to the large amount of contact elements included in the model.

The clump weight nose angle is extracted via simpost by converting nodal displacement on the frame into angular quantity. Simpost completion time took approximately just below an hour but got excessively longer for larger .raf files.

Chapter 6

Results and discussion

This chapter contains results from simulations performed with varying seabed geometry, soil properties, pipeline dimensions and towing velocity. All simulations are performed with a global pipeline spanning 500 m in both directions from clump weight point of interaction. The same clump weighted described in section 5.3.1 are towed perpendicular to the pipe for all simulations, although wobbling are experienced in all cases after initial impact with either pipeline or rock dump.

Pull-over loads in axial, transverse and vertical direction are extracted from all contact elements and are represented as force-time histories with a running average window of 0.05 s in order to damp out any fluctuations from the history. All pull over loads extracted from cases with varying seabed geometry are compared to an equivalent simulation performed at a flat seabed. Vertical pull-over force is defined positive upwards. Clump weight nose angle and warp line tension are also post-processed with dynpost and simpost and plotted in time histories. These are however only used as tools for interpretation of contact forces and are not addressed in this thesis.

The contact force between warp line and pipe have been left out of all plots due to its small magnitude compared to load peaks for clump weight pipe interaction. The point of warp line pipe interaction is also measured multiple seconds earlier and covering this time interval on the plotted results would shrink important details regarding the clump weight pipe interaction. The maximum pull-over load for warp line pipe are measured to be approximately 50 % of the peak vertical pull-over load for a 24” pipe.

As for the flat seabed case with a 12.75” outer pipe diameter a large jump in the force curve is observed as the clump weight pipe contact is ended. This peak load is obtained from a contact error where the roller is slightly penetrated into the pipe during interference. As contact is again obtained, the clump weight and pipe is pushed heavily in opposite direction causing a peak in the load-curve. This is also observed for a few other cases and are neglected as realistic pull-over loads.

6.1 Pre-testing with extra nodes describing the normal vector of the rock dump slope and increased rock dump stiffness

Before doing the sensitivity study on seabed geometry some pre-testing is performed in order to investigate effects that is believed to influence the result. The testing involves investigating the effect of implementing extra set of nodes in the seabed input file where the existing node defines the change in incline. This way both surfaces connected to the node is represented by its respective normal vector. The effect of increased stiffness for the rock dump is also investigated and compared to the original stiffness. The updated interaction curves are shown in figure 5.7.

6.1.1 Extra nodes

With extra nodes at all points marking a change in incline the clump weight is behaves differently at the edge of the rock dump with an increased nose angle oscillation as shown in figure 6.1 for a 12.75" pipe with a rock dump width, W = 2.0 m, height, H = 1.0 m and slope, S = 18.4 °. This effect is believed to arise because of the difference in the allowed seabed penetration at the point where the slope ends. The point marking the top of the slope holds information regarding the normal vector for both the slope and the rock dump flat, allowing two different type of seabed penetrations at the node. This is also the same for the point marking the bottom of the slope where the normal vector for both seabed and slope is defined, hence indicating the sudden change in movement for the clump weight.

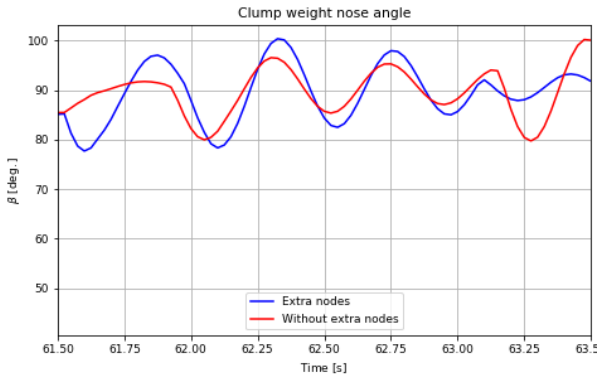

Figure 6.1: Clump weight nose angle with and without extra nodes for OD12W2H1S1_3.

The change in pull-over load along the pipe is small, but the upward and transverse pull-over load is smaller, as shown in figure 6.2. This is most likely due to the increased nose angle oscillation, whereas the longitudinal clump weight angle is effected accordingly. The extra rotational energy needed in order to pull the clump weight over the pipe reduces the pull-over load as mentioned in the recommended practice (DNV-GL, 2014). The transverse pull-over force is reduced by approximately 50% while the upward pull over force is approximately 75% of the original simulation. Appendix B.1 contains results for all tests regarding the effect of extra nodes.

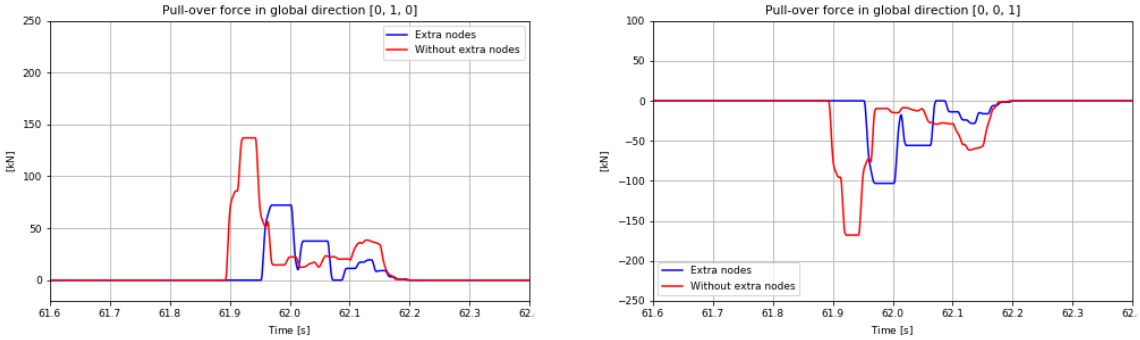

(a) Transverse pull-over load.

(b) Upward pull-over load.

Figure 6.2: Clump weight pull over loads with and without extra nodes for OD12W2H1S1_3.

6.1.2 Increased rock dump stiffness

Due to the fact that extra nodes are deemed necessary they are kept for further simulations where tests regarding the rock dump stiffness are performed. The purpose is to increase the stiffness of the rock dump compared to the seabed thus depicting the rock dump in a realistic manner, whereas the seabed usually consist of soft clay and sand compared to a potential rock dump which would typically be rocks with a much higher stiffness.

First off the stiffness was increased by a factor of 10, which led to the clump weight bouncing higher than expected. The mobility of the pipe would also increase because of the increased stiffness, hence the pipe would sometimes move over the flat of the rock dump and into the slope when exposed to large impact forces. Due to this ”unnatural” clump weight behaviour, the stiffness was reduced down to 20 %. The result seemed more applicable and realistic, and a couple batches of simulations with this stiffness were performed. Eventually the rock dump stiffness was reduced to the original seabed interaction curve due to the clump weight still bouncing excessively from the encounter with double stiffness. The original interaction curve was also known to be considerably stiff. The seabed interaction curve used in all tests are shown in figure 5.6 (b) and the updated interaction curves performed during the tests with increased stiffness are shown in figure 5.7.

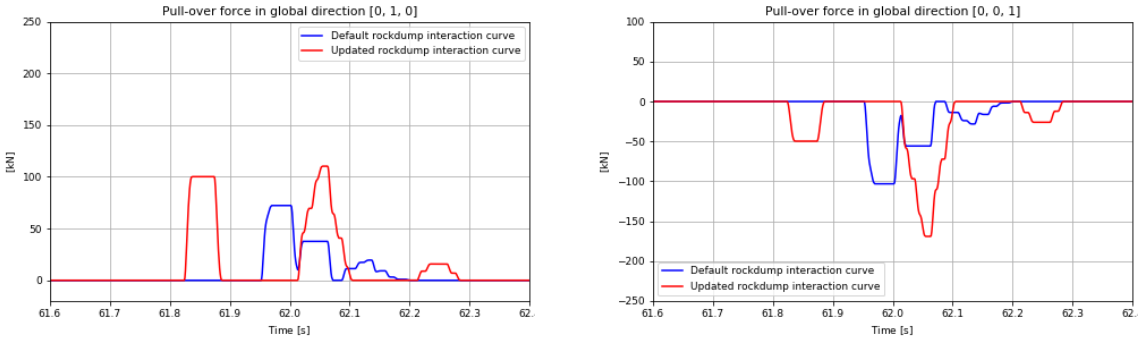

(a) Transverse pull-over load.

(b) Upward pull-over load.

Figure 6.3: Clump weight pull over loads with and w/o updated vertical soil interaction for OD12W2H1S1_3.

Figure 6.3 shows the upward and transverse pull-over loads with an updated interaction curve in ver-

tical direction applied at the rockdump. The updated interaction curve is shown in figure 5.7 (a) and the pull-over loads are compared with the default interaction curve in figure 5.6 (a). Figure 6.4 shows a comparison between the default interaction curve with the updated interaction curve from figure 5.7 (b). From testing with the updated interaction curves the general trend is that the pull-over loads increase slightly with increasing rockdump stiffness. From visual inspection it is mainly the clump weight response that changes with an updated interaction curve and the increased pull-over load could be a result from a different type of contact. Figure 6.5 illustrates the exaggerated movement of the clump weight just after hitting the rockdump with 10 times the default stiffness.

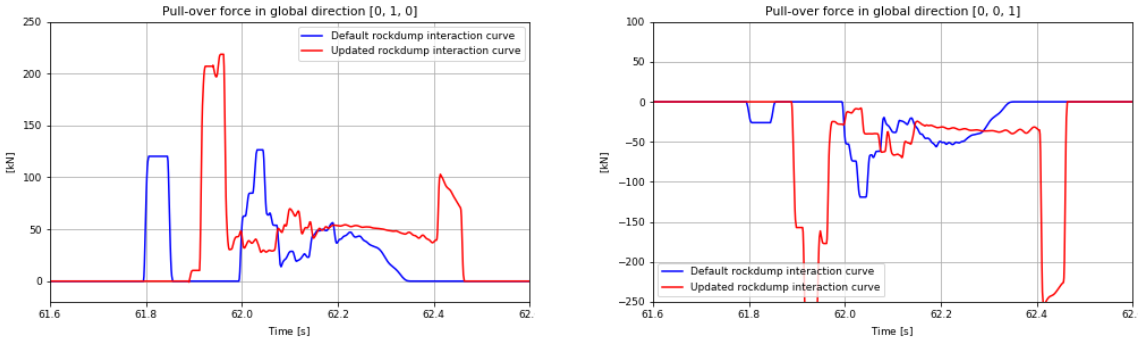

(a) Transverse pull-over load.

(b) Upward pull-over load.

Figure 6.4: Clump weight pull over loads with and w/o updated vertical soil interaction for OD12W1.5H1S1_3.

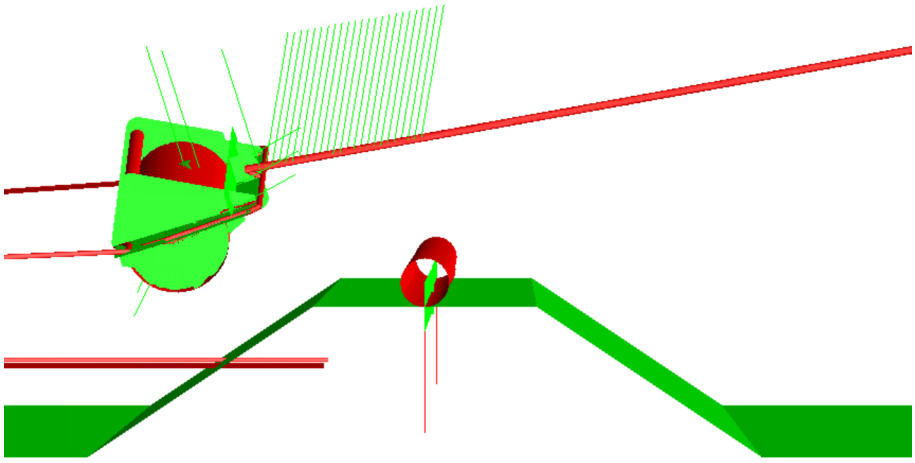

Figure 6.5: Clump weight snapshot for OD12W1.5H1S1_1.5 with updated rockdump interaction curve.

6.2 Sensitivity study

6.2.1 General clump weight pipeline interference

Interpretation of results from the sensitivity study indicates that governing pull-over loads are either induced by warp line bracket impact or clump weight roller collision with the pipe. Observations from result files reveals that roller collision is more likely to happen for small diameter pipelines whereas larger pipes are more frequently exposed to bracket impact. The sensitivity study also indicates that scenarios with bracket pipe interference are frequently more common when the trawl velocity is reduced. For a few cases the clump weight bounces over the pipeline due to large RD slope angles. This section includes tables defining type of impact for all studies performed as a measure for better visualization of the sensitivity study.

6.2.2 Seabed geometry alteration

A total of 84 simulations are completed where each single one individually represents an unique seabed geometry. Filtering of the results proved to be more difficult than expected and are hence categorized within each respective RD width and described in this section. Only the pull-over loads from a height, H = 1.0 m, are shown in this section in order to avoid large sections of plots. Remaining pull-over loads are referred in Appendix A.

RD width, W = 1.5 m

Visualizations from the result files indicates that the clump weight bounces over the pipeline for a slope S = 33.7°. With a slightly less slope, S = 21.8° and rock dump height H = 0.5 m, the clump weight roller collides with the pipe resulting in a larger upward pull-over load at impact. This is also the case for a rock dump height H = 1.0 m and slope S = 26.6° where the clump weight roller collides with the pipe, causing a larger upward and transverse pull-over load as shown in figure 6.6 and 6.7. The latter case is special for H = 1.0 m whereas the clump weight bounces over the pipe for both H = 0.5 m and H = 2.0 m. With a RD width, W = 1.5 m, the upward pull-over loads are governing which can be seen in figure 6.7 for H = 1.0 m. The transverse pull-over load is shown in figure 6.6.

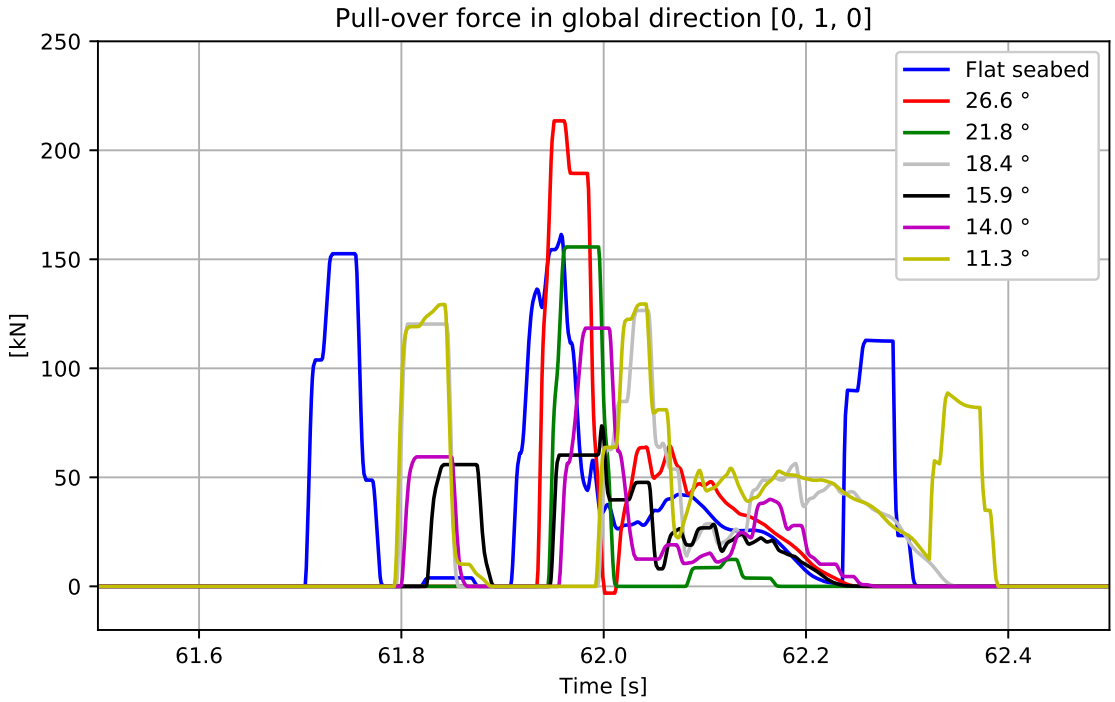

Figure 6.6: Transverse pull-over load for OD12W1.5H1 - effect of varying RD incline.

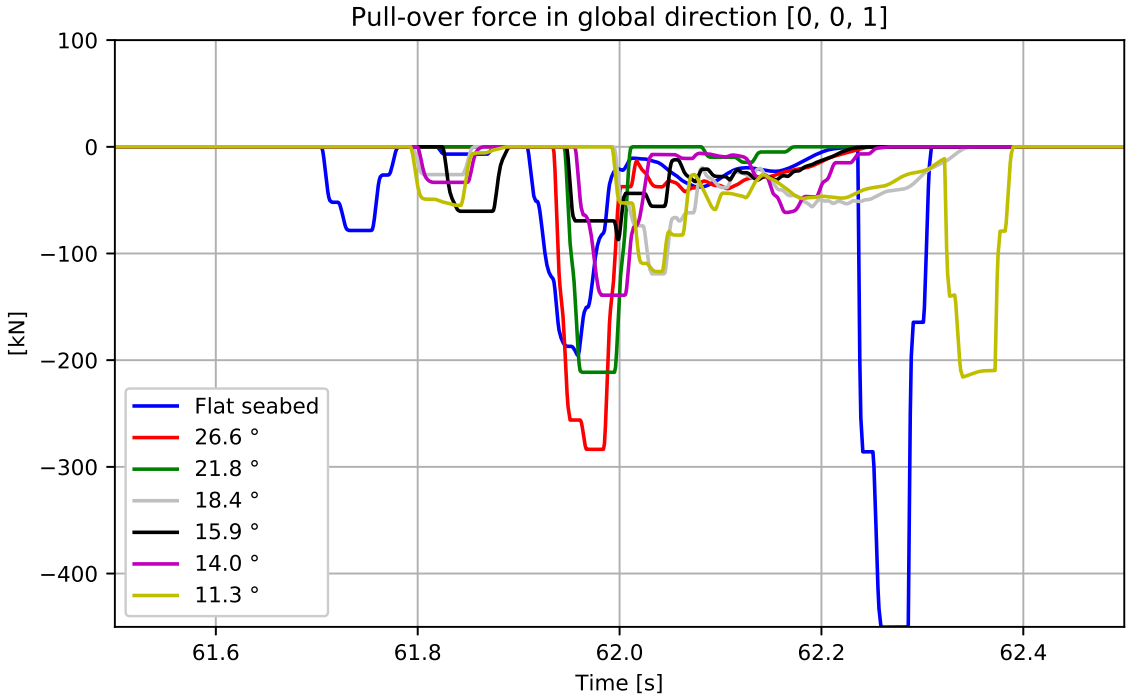

Figure 6.7: Upward pull-over load for OD12W1.5H1 - effect of varying RD incline.

Compared to a flat seabed the pull-over loads are generally smaller. Simulations with rock dumping generally results in smaller pull-over durations and the contact forces are smallest for 15.9° in this case. The pull-over loads for a slope S = 11.3° have similarities with a pipe laying at a flat seabed, although

of less magnitude. This is observed by visual inspection of the result files, where the clump weight and pipe is suddenly ejected in the vertical direction as the clump weight is about to leave contact with the pipe. This is most likely a source of error coming from the contact definition between the clump weight roller and the pipe. As the roller looks to be slightly penetrating the pipe, contact is obtained as the warp line pulls the clump weight out into the contact search region, causing a massive increase in the upward pull-over load.

	Impact scenario		
Case	Clump weight bounces over	Clump weight roller collision	Warp line bracket impact
OD12W1.5H0.5S1_1.5	X		
OD12W1.5H0.5S1_2	X		
OD12W1.5H0.5S1_2.5		X	
OD12W1.5H0.5S1_3			X
OD12W1.5H0.5S1_3.5		X	
OD12W1.5H0.5S1_4		X	
OD12W1.5H0.5S1_5			X
OD12W1.5H1S1_1.5	X		
OD12W1.5H1S1_2		X	
OD12W1.5H1S1_2.5		X	
OD12W1.5H1S1_3			X
OD12W1.5H1S1_3.5			X
OD12W1.5H1S1_4			X
OD12W1.5H1S1_5			X
OD12W1.5H2S1_1.5	X		
OD12W1.5H2S1_2	X		
OD12W1.5H2S1_2.5		X	
OD12W1.5H2S1_3		X	
OD12W1.5H2S1_3.5		X	
OD12W1.5H2S1_4			X
OD12W1.5H2S1_5			X

Table 6.1: Clump weight pipe impact scenarios for a 12” pipe with varying RD height and slope.

RD width, W = 2.0 m

The discrepancy from a width, W = 1.5 m, is almost negligible as the clump weight bounces over all height configurations with a slope, S = 33.7°. The clump weight also bounces over the pipe with slope, S = 26.6° and height, H = 0.5 m. Simulations with RD height H = 0.5 m and H = 2.0 m tend to give the lowest pull-over loads. All pull-over loads are in this case smaller compared to a flat seabed. The exception is at height H = 0.5 m where the clump weight roller collides with the pipe creating a larger contact force for slope S = 21.8° compared to the flat seabed case.

Transverse and upward pull-over loads for a RD height, H = 1.0 m, are shown in figure 6.8 and 6.9 respectively. This height has the largest amount of pull-over loads larger or equal to the flat seabed case. At a slope, S = 26.6°, the clump weight frame collides with the pipeline resulting in the large transverse pull-over load. At slope, S = 21.8°, the clump weight roller collides with the pipe while the frame is pulled over. This results in an increase of the upward pull-over load, as shown in 6.9.

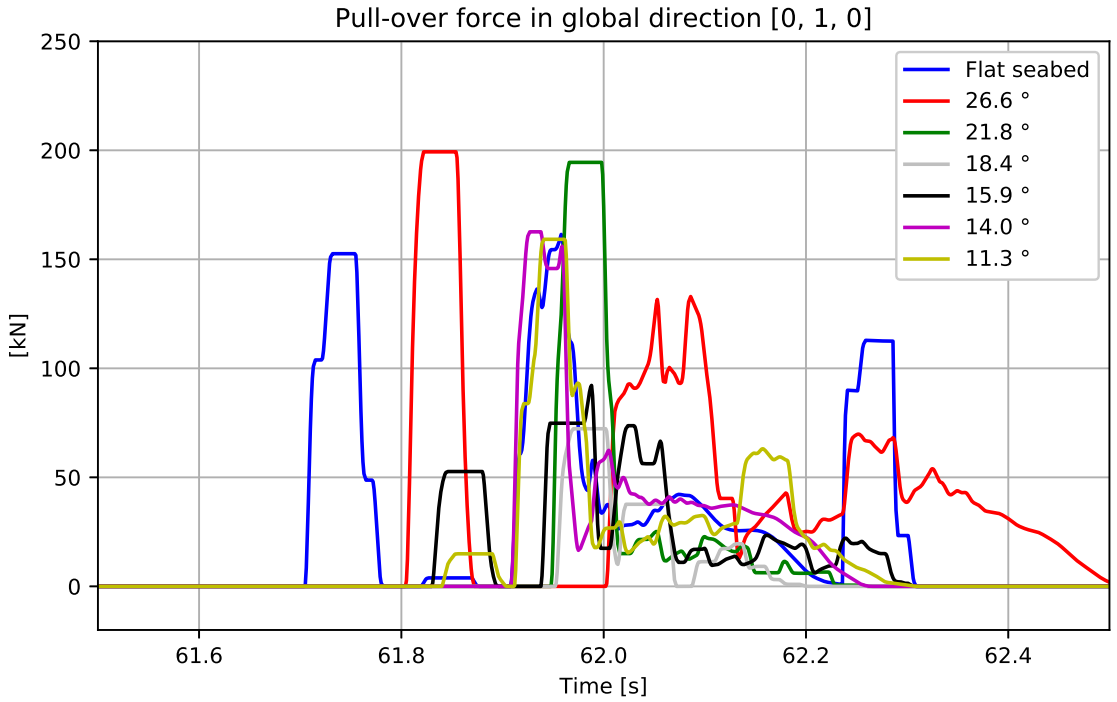

Figure 6.8: Transverse pull-over load for OD12W2H1- effect of varying RD incline.

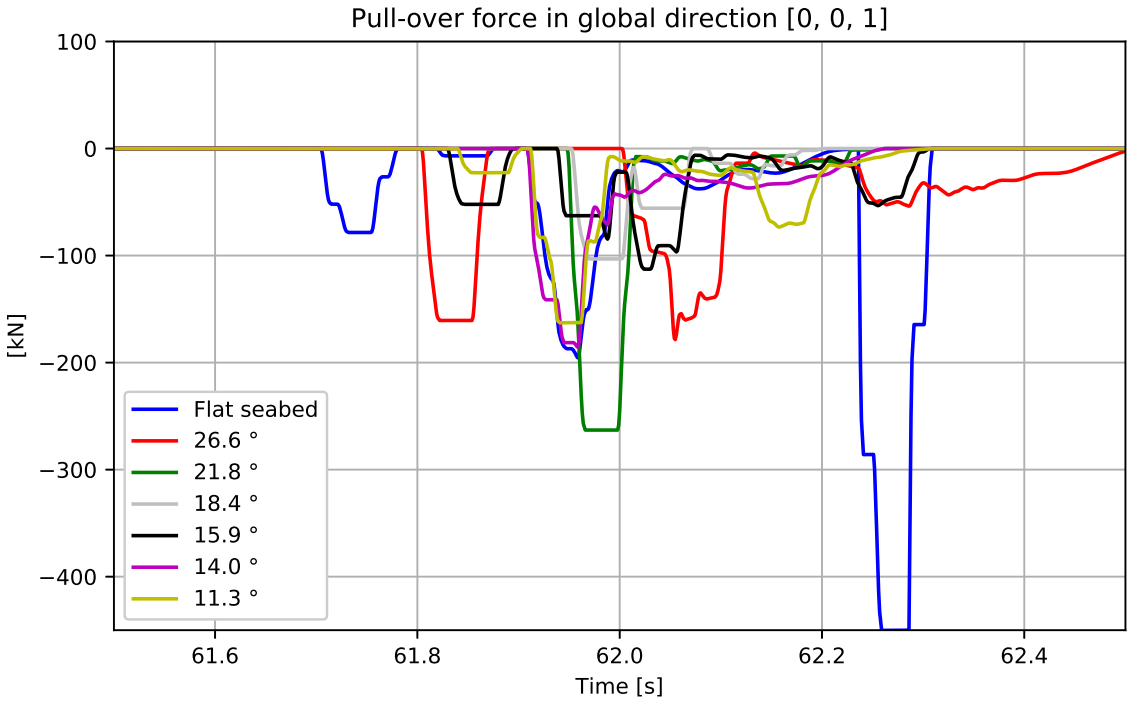

Figure 6.9: Upward pull-over load for OD12W2H1 - effect of varying RD incline.

Case	Impact scenario		
	Clump weight bounces over	Clump weight roller collision	Warp line bracket impact
OD12W2H0.5S1_1.5	X		
OD12W2H0.5S1_2	X		
OD12W2H0.5S1_2.5		X	
OD12W2H0.5S1_3			X
OD12W2H0.5S1_3.5		X	
OD12W2H0.5S1_4			X
OD12W2H0.5S1_5			X
OD12W2H1S1_1.5	X		
OD12W2H1S1_2			X
OD12W2H1S1_2.5		X	
OD12W2H1S1_3		X	
OD12W2H1S1_3.5			X
OD12W2H1S1_4		X	
OD12W2H1S1_5		X	
OD12W2H2S1_1.5	X		
OD12W2H2S1_2	X		
OD12W2H2S1_2.5		X	
OD12W2H2S1_3		X	
OD12W2H2S1_3.5		X	
OD12W2H2S1_4			X
OD12W2H2S1_5			X

Table 6.2: Clump weight pipe impact scenarios for a 12" pipe with varying RD height and slope.

RD width, W = 4.0 m

The clump weight is also pulled over the pipeline for this case but only for the case with RD height of 0.5 m. Once the height is increased to 1.0 m the clump weight roller collides with the pipe, creating a large pull-over load in both transverse and vertical direction. The large vertical pull-over load for S = 26.6° with width, W = 0.5 m, is also characterized by roller collision. By visual inspection of the result files both 33.7° and 26.6° slopes for a width, W = 2.0 m, are governed by clump weight roller collision, hence large vertical pull-over loads. Slope, S = 11.3°, with a width, W = 0.5 m, has both large transverse and upward pull-over loads as the contact between the pipe and clump weight is lost. Visual inspection from the result file indicates that the large pull-over load occurs from the contact error mentioned earlier, also indicated from the excessive clump weight and pipe motion as contact is about to end.

Small slope angles tend to have smaller upward pull-over loads compared to transverse pull-over loads since the interference is usually governed by clump weight frame collision. In clump weight frame impact the mass of the roller is evident as it governs the moment needed in order to rotate the clump weight over the pipeline. The warp line must therefore have a higher tension in order to pull the clump weight over the pipe, and as such generating a larger transverse pull-over load. In figure 6.10 and 6.11 the transverse and upward pull-over loads are shown respectively for a height, H = 1.0 m. Except for slope, S = 33.7°, the pull-over loads are generally smaller compared to a flat seabed. As shown in figure 6.10, the cases with smaller slope angle have largest transverse pull-over loads from the impact between clump weight frame and pipeline.

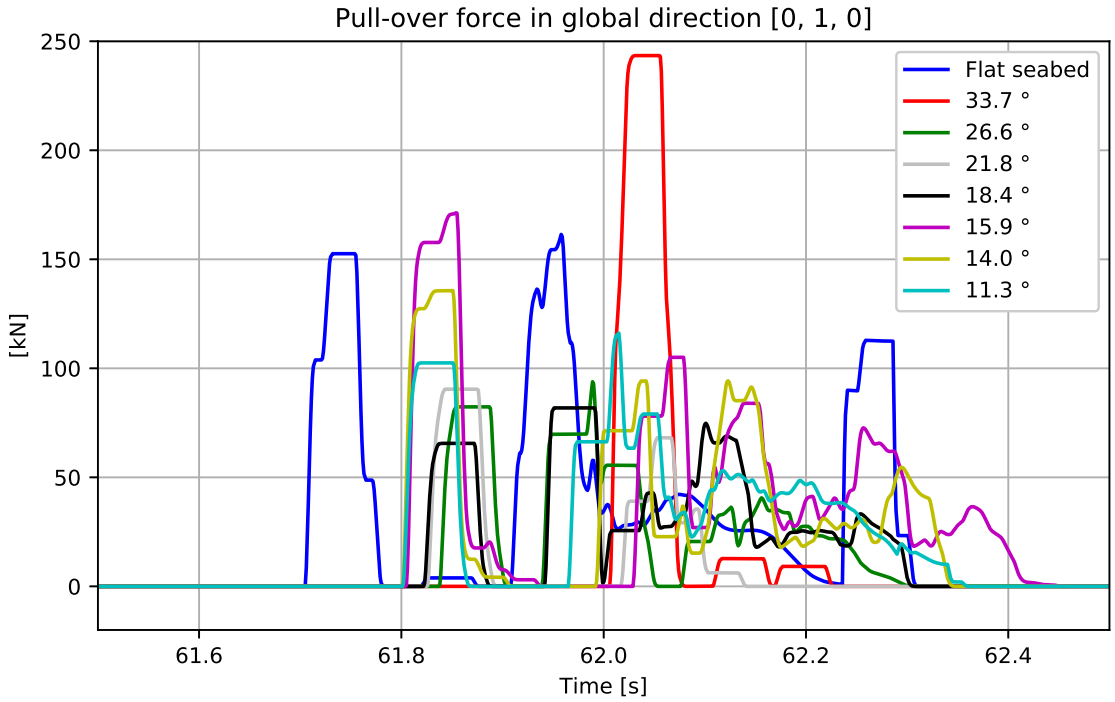

Figure 6.10: Transverse pull-over load for OD12W4H1 - effect of varying RD incline.

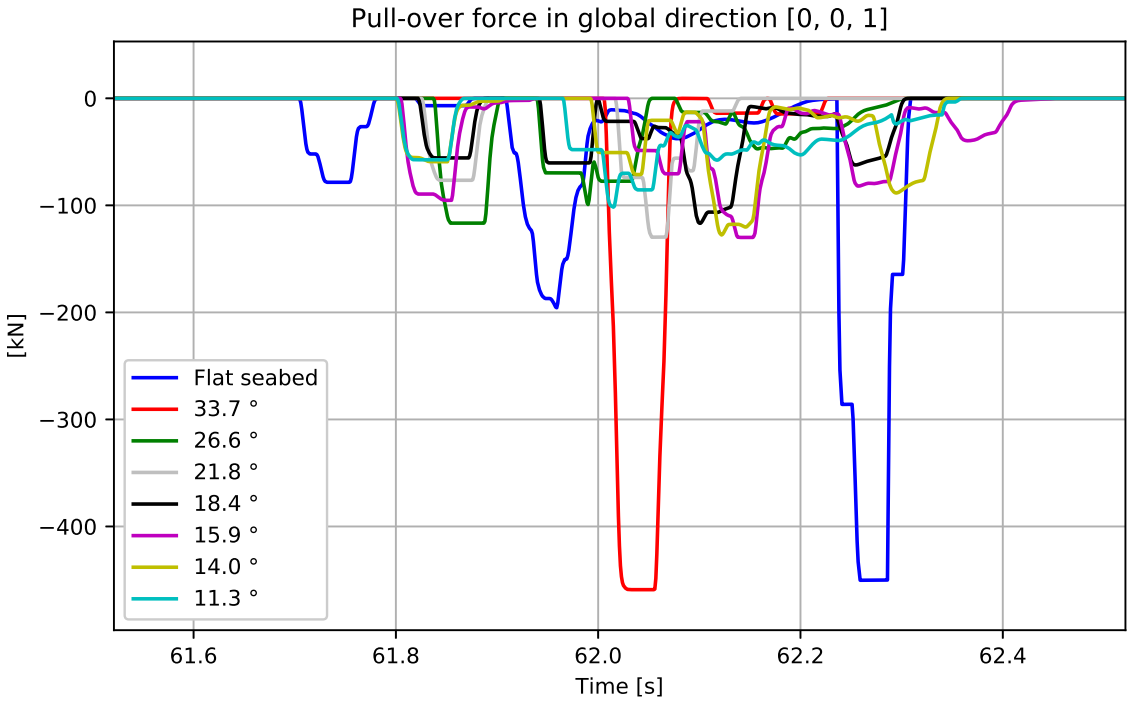

Figure 6.11: Upward pull-over load for OD12W4H1 - effect of varying RD incline.

Case	Impact scenario		
	Clump weight bounces over	Clump weight roller collision	Warp line bracket impact
OD12W4H0.5S1_1.5	X		
OD12W4H0.5S1_2		X	
OD12W4H0.5S1_2.5			X
OD12W4H0.5S1_3		X	
OD12W4H0.5S1_3.5		X	
OD12W4H0.5S1_4			X
OD12W4H0.5S1_5			X
OD12W4H1S1_1.5		X	
OD12W4H1S1_2			X
OD12W4H1S1_2.5			X
OD12W4H1S1_3			X
OD12W4H1S1_3.5			X
OD12W4H1S1_4			X
OD12W4H1S1_5			X
OD12W4H2S1_1.5		X	
OD12W4H2S1_2		X	
OD12W4H2S1_2.5		X	
OD12W4H2S1_3			X
OD12W4H2S1_3.5			X
OD12W4H2S1_4			X
OD12W4H2S1_5			X

Table 6.3: Clump weight pipe impact scenarios for a 12” pipe with varying RD height and slope.

RD width, W = 6.0 m

The clump weight is not pulled over the pipe from any simulations with this width but the clump weight roller collides with the pipe for a slope, S = 33.7°, causing a massive increase in the upward pull-over load. For all other angles, contact between the clump weight roller and the RD plateau is accomplished before interference with the pipe. This is also the case for a slope, S = 33.7° with height, H = 1.0 m and H = 2.0 m, hence the reduction in cases with extreme vertical pull-over load.

The transverse and upward pull-over loads for the case with height, H = 1.0 m, are shown in figure 6.12 and 6.13 respectively. The RD configurations shows promising results compared to a flat seabed and only the S = 21.8° case has an upward pull-over load equal to the flat seabed case. With a decreasing slope angle S the transverse pull-over force increases as the collision between the frame and pipe gets more significant. This can be seen in figure 6.12 where a 14.0° and 11.3° slope has a peak transverse pull-over load of same magnitude as the flat seabed case.

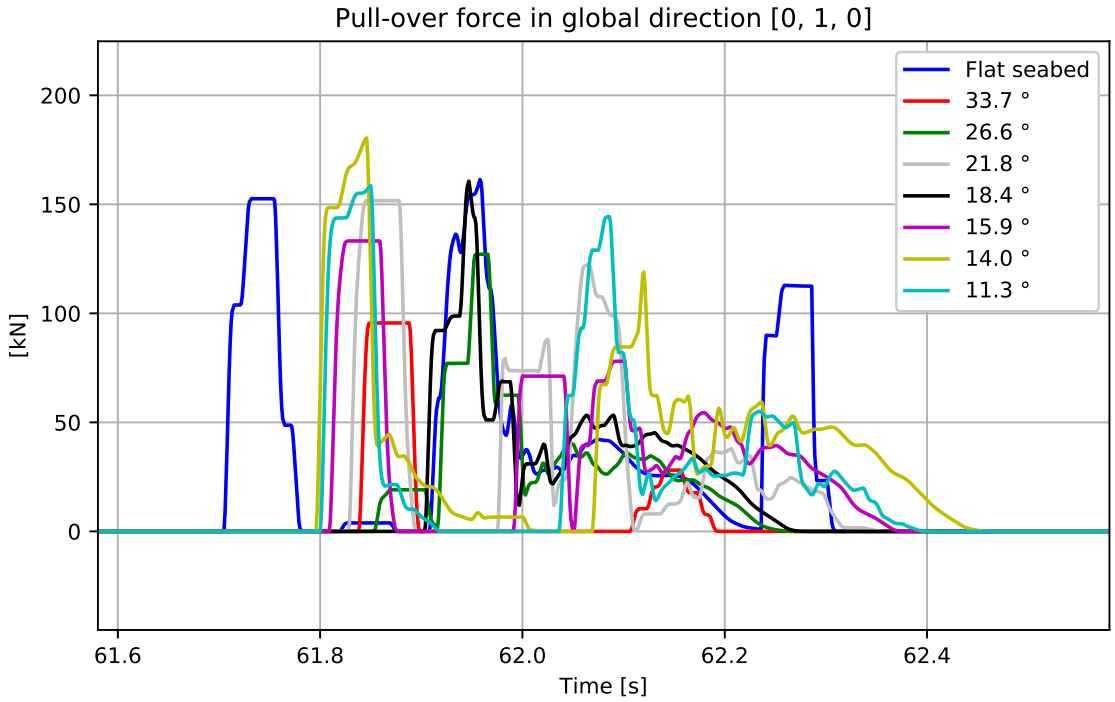

Figure 6.12: Transverse pull-over load for OD12W6H1 - effect of varying RD incline.

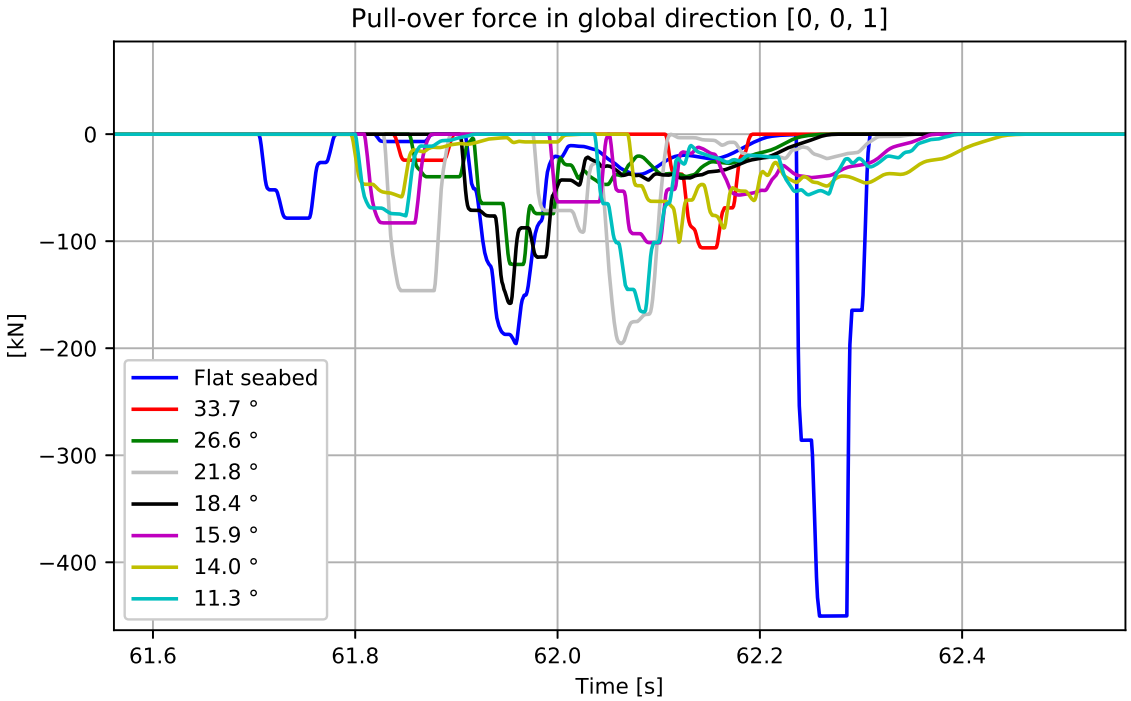

Figure 6.13: Upward pull-over load for OD12W6H1 - effect of varying RD incline.

Case	Impact scenario		
	Clump weight bounces over	Clump weight roller collision	Warp line bracket impact
OD12W6H0.5S1_1.5	X		
OD12W6H0.5S1_2			X
OD12W6H0.5S1_2.5			X
OD12W6H0.5S1_3			X
OD12W6H0.5S1_3.5		X	
OD12W6H0.5S1_4			X
OD12W6H0.5S1_5			X
OD12W6H1S1_1.5			X
OD12W6H1S1_2		X	
OD12W6H1S1_2.5			X
OD12W6H1S1_3		X	
OD12W6H1S1_3.5			X
OD12W6H1S1_4			X
OD12W6H1S1_5			X
OD12W6H2S1_1.5			X
OD12W6H2S1_2			X
OD12W6H2S1_2.5			X
OD12W6H2S1_3			X
OD12W6H2S1_3.5			X
OD12W6H2S1_4			X
OD12W6H2S1_5			X

Table 6.4: Clump weight pipe impact scenarios for a 12” pipe with varying RD height and slope.

6.2.3 Increased pipe dimensions

16” outer pipe diameter

As with a 12.75” OD pipe, the clump weight also bounces over the 16” OD pipe for a slope, S = 33.7°. This can be seen in figure 6.14 where the the transverse and vertical pull-over loads are displayed for a 16” pipe with a RD width, W = 1.5 m and height, H = 1.0 m. For both slopes the governing loads are generated from frame pipe collision which is similar to the flat seabed case. The effect of the RD is hence negligible.

Figure 6.15 shows the transverse and upward pull-over loads for the 16” pipe with an increased width, W = 6.0 m. For the 33.7° and 18.4° case the clump weight frame is pulled over the pipe avoiding frame pipe collision. This decreases the pull-over loads as seen in figure 6.15. For a 11.3° slope there is no visible change compared to a flat seabed from inspection of the clump weight pipe interaction in Xpost, and after validating the results with dynpost. Compared to a 12.75” pipe, the transverse pull-over loads are increasing, which is also reflected in the increasing warp line tension.

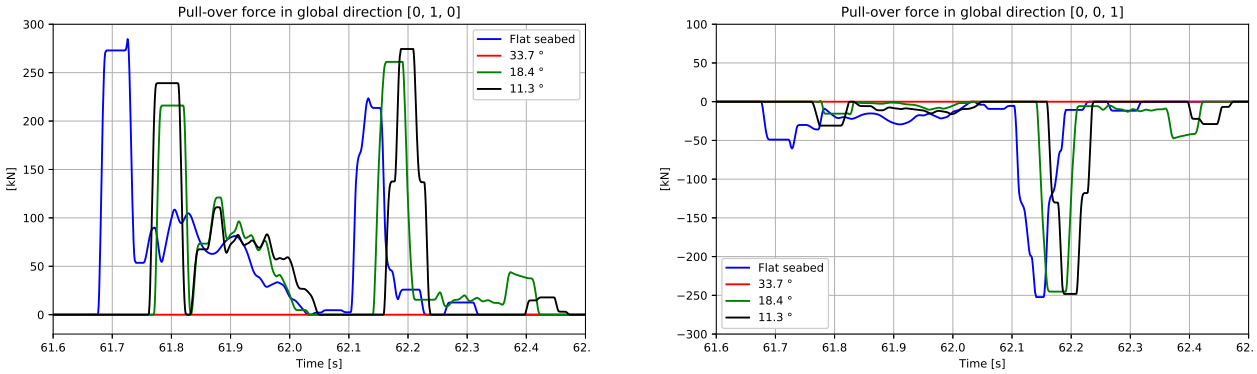

(a) Transverse pull-over load.

(b) Upward pull-over load.

Figure 6.14: Clump weight pull-over loads for OD16W1.5H1 - effect of varying RD incline.

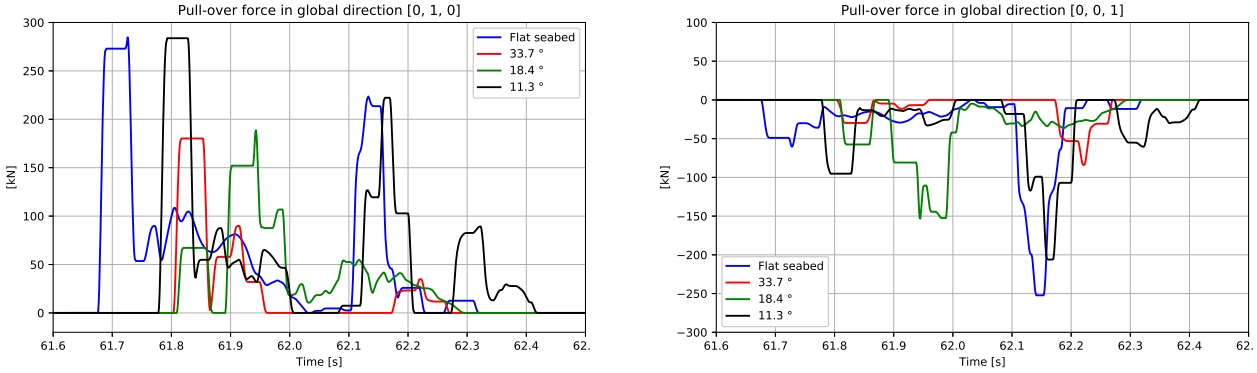

(a) Transverse pull-over load.

(b) Upward pull-over load.

Figure 6.15: Clump weight pull-over loads for OD16W6H1 - effect of varying RD incline.

24” outer pipe diameter

The warp line vertical pull-over load for a 24” pipe is approximately 50 % of the maximum pull-over load shown in figure 6.16, but since warp line pipe interaction takes place at approximately 58 seconds the loads are not visible in the plots below. As shown in figure 6.16 and figure 6.17 the pull-over duration is larger for some cases compared to a flat seabed and the warp line tension is increased simultaneously. It is clear that the transverse pull-over loads increases as pipeline dimensions are increased. The 24” pipe has large transverse pull-over loads in all cases, except for a slope, S = 33.7° at a RD width W = 1.5 m, where the clump weight bounces over the pipe. The increase in transverse pull-over load is also depicted in the warp line tension, as it is nearly doubled from the same RD configuration with a 16” pipe.

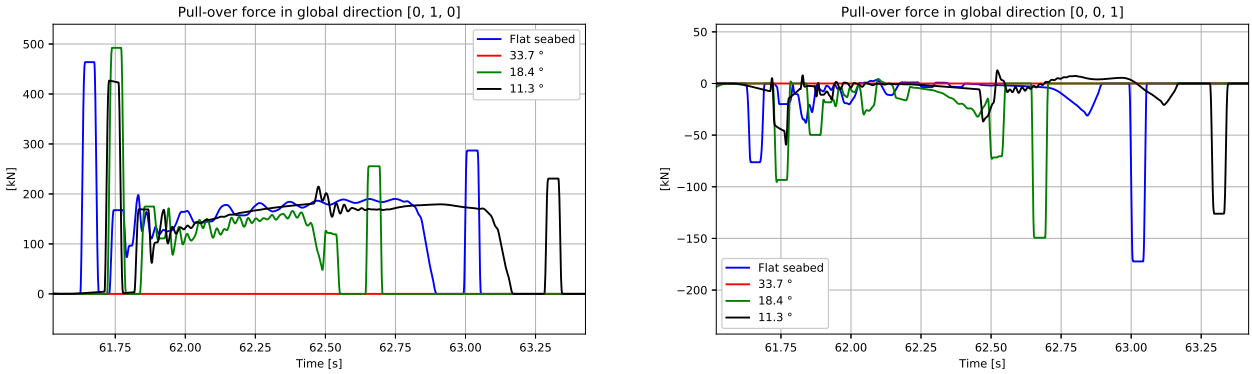

(a) Transverse pull-over load.

(b) Upward pull-over load.

Figure 6.16: Clump weight pull-over loads for OD24W1.5H1 - effect of varying RD incline.

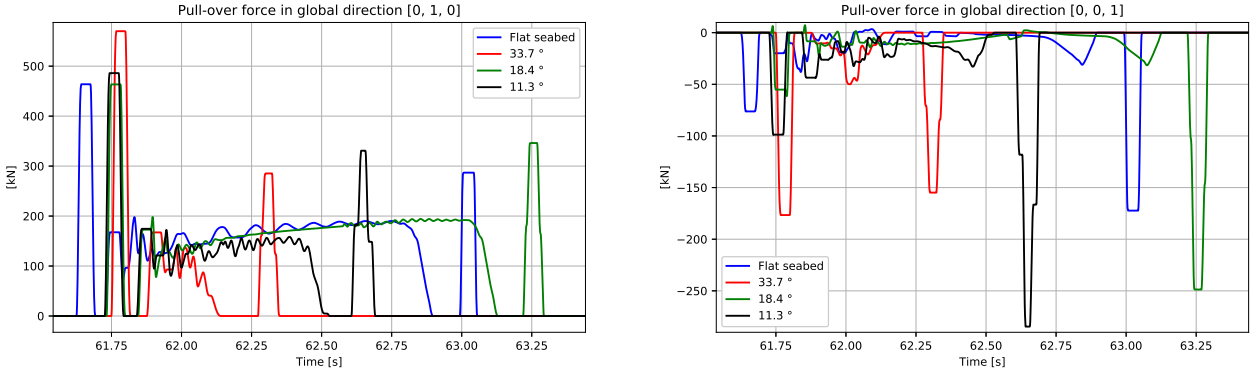

(a) Transverse pull-over load.

(b) Upward pull-over load.

Figure 6.17: Clump weight pull-over loads for OD24W6H1 - effect of varying RD incline.

Case	Impact scenario		
	Clump weight bounces over	Clump weight roller collision	Warp line bracket impact
OD16W1.5H1S1_1.5	X		
OD16W1.5H1S1_3			X
OD16W1.5H1S1_5			X
OD16W6H1S1_1.5		X	
OD16W6H1S1_3		X	
OD16W6H1S1_5			X
OD24W1.5H1S1_1.5	X		
OD24W1.5H1S1_3			X
OD24W1.5H1S1_5			X
OD24W6H1S1_1.5			X
OD24W6H1S1_3			X
OD24W6H1S1_5			X

Table 6.5: Clump weight pipe impact scenarios for a 16” and 24” pipe with varying RD height and slope.

6.2.4 Reduced trawl velocity

The original parameter study is performed with a trawl speed of 2.6 m/s, where the speed is represented by a load with a certain amplitude applied to a spring located at the warp line towing node and both trawl board nodes. The load is gradually increased the first 30 seconds in order to avoid numerical errors as loads are applied. In order to decrease the velocity, the load amplitude is scaled down for the warp line towing node and both trawl net towing nodes.

With a reduced trawl velocity the pull-over duration is reduced for both the 12.75" and 16" pipe as shown in figure 6.18 and 6.19. The contact error where the the roller is partly penetrating the pipe is observed during the 18.4° case shown in figure 6.18 where the vertical pull-over load is at a maximum of 840 kN.

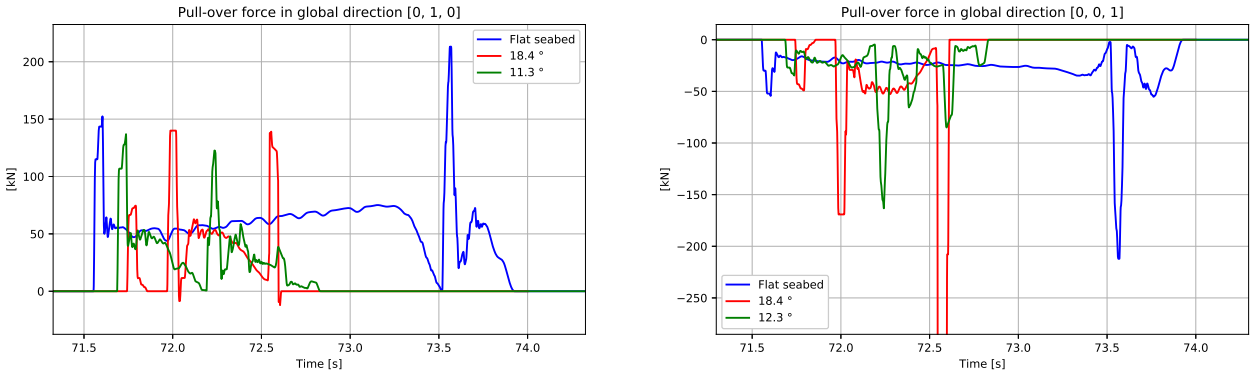

(a) Transverse pull-over load.

(b) Upward pull-over load.

Figure 6.18: Clump weight pull-over loads for V4OD12W1.5H1 - effect of varying RD incline.

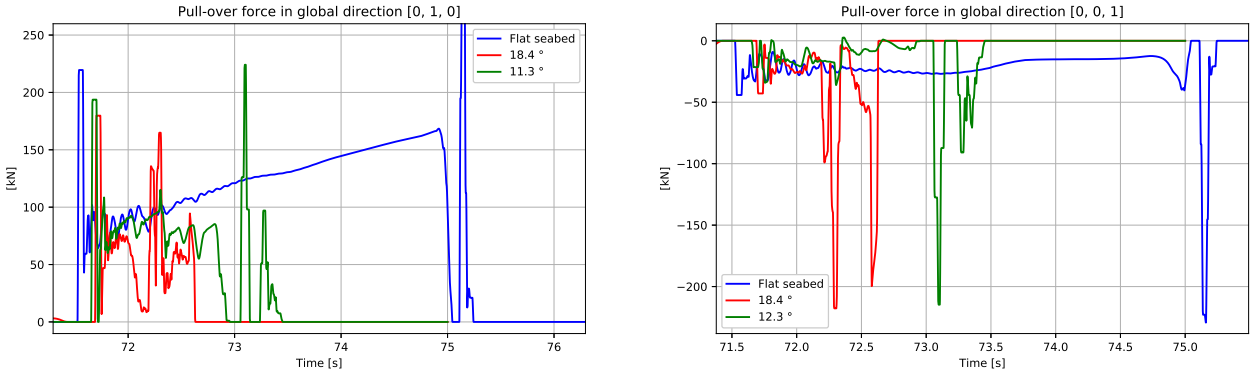

(a) Transverse pull-over load.

(b) Upward pull-over load.

Figure 6.19: Clump weight pull-over loads for V4OD16W1.5H1 - effect of varying RD incline.

Figure 6.20 shows the pull-over loads with a towing velocity, V = 1.6 m/s = 4 knots, at a flat seabed. Further simulations observing effects with rock dumping was not completed. The low trawl speed lowers the tension in the warp line which results in the warp line getting pulled lower than previous simulations by its self weight. This causes the upper part of the warp line to pass through the pipeline, and the lower warp line with cont164 rollers would have to be extended in order to capture the warp line pipeline interference which occur at a point located at the upper warp line in this case. It is noteworthy that imple-

mentation of a RD in this case could possibly reduce the pull-over time as experienced with simulations at 4 knots.

Case	Impact scenario		
	Clump weight bounces over	Clump weight roller collision	Warp line bracket impact
V4OD12W1.5H1S1_3			X
V4OD12W1.5H1S1_5			X
V4OD16W1.5H1S1_3			X
V4OD16W1.5H1S1_5			X

Table 6.6: Clump weight pipe impact scenarios for a 12.75" and 16" pipe with reduced towing velocity.

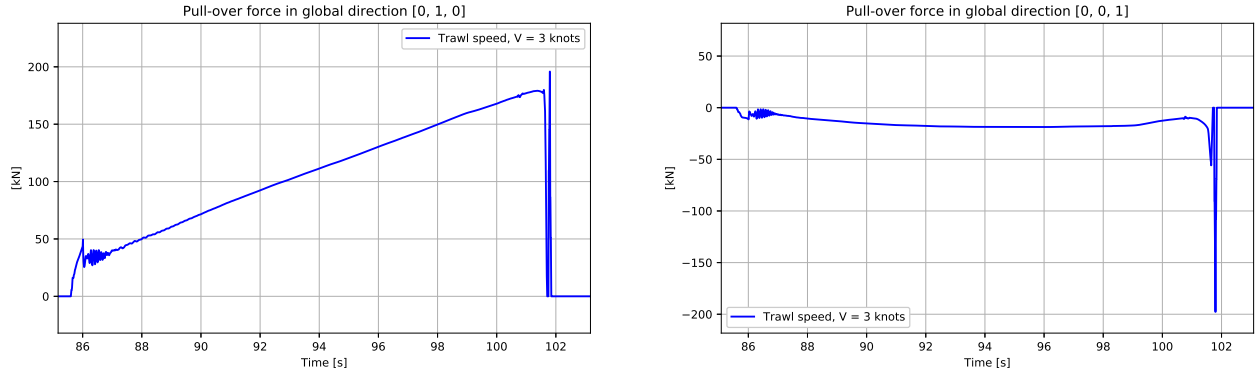

(a) Transverse pull-over load.

(b) Upward pull-over load.

Figure 6.20: Clump weight pull-over loads for a flat seabed with 12.75" outer pipe diameter and trawl speed, V = 3 knots.

6.2.5 Summary

Except the contact error related to the cont164 rollers observed in a few cases, all simulations showed realistic behaviour. The seabed geometry alteration proved to be effective for most cases, although a few individual cases exist where the pull-over loads are increased compared to a flat seabed. Warp line contact forces are maximum 50% of peak transverse or vertical contact forces, hence so small that they are not included in the plots.

For small RD widths the pull-over loads tend to decrease for high or low RD profiles whereas height, H = 1.0 m, has the overall largest pull-over loads. For both widths, W = 1.5 m and W = 2.0 m, the lowest pull-over loads comes from either the clump weight jumping over the pipe for steep slopes or the warp line bracket getting pulled over the pipe, resulting in a lower pull-over load as only the clump weight roller is pulled over the pipe after impact. The latter case is especially significant for larger RD heights as the clump weight manages to stabilize on its way up the slope. As the slope flattens out the self weight of the clump weight frame and warp line bracket pulls the clump weight nose down, whereas the warp line tension increases to the point where it pulls the frame and bracket back up over the pipeline, avoiding bracket pipe contact.

For RD width, W = 4.0 m, the lowest pull-over loads are measured at a height, H = 1.0 m, whereas smaller and bigger heights results in overall increasing loads. This is in contradiction to smaller widths

where measurements from small and big heights indicates lower pull-over loads. For the case with RD width, W = 6.0 m, all heights are pretty equal in terms of maximum load peaks and for H = 2.0 m the loads are pretty equal in terms of time of impact and pull-over duration.

A general observation is that large slope angles in combination with large RD widths tend to result in lower pull-over loads provided the clump weight initiate contact with the RD plateau before interfering with the pipe. With the right RD dimension the clump weight will collide directly with the pipe without bouncing on the plateau which could ultimately lead to large pull-over loads. The small loads are often also a result of the clump weight almost bouncing over the pipeline after initial contact with the RD plateau which might not be the case in a realistic setting where the rough surface of the plateau could lead to the clump weight behaving differently.

Results with increased pipe dimensions indicate that RD's with small widths have no huge impact on pull-over loads compared to a flat seabed. As expected, the transverse pull-over loads are increasing for larger pipe dimensions. This is due to the increased moment needed in order to pull the clump weight over a larger pipe, which can also be deducted from the increased warp line tension. The results indicate however that a RD with large width will reduce governing transverse pull-over loads by up to approximately 50% for a 16" pipe. Due to longer pull-over rates the 24" pipe is pulled over the edge of the RD and into the slope for cases where the width is small. The risk of jeopardizing the pipe is hence increased if the next clump weight is pulled into contact with the pipe from the opposite direction as the impact would be uphill. Figure 6.21 represents a snapshot at 62.8 s visualizing the difference in clump weight pipe interaction between a 16" and 24" pipe with an identical RD width, W = 1.5 m.

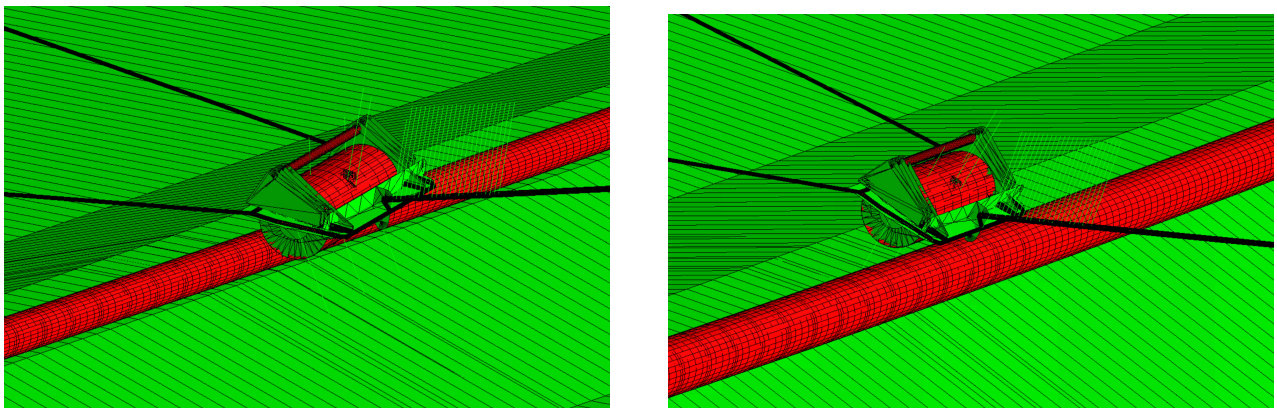

(a) 16" outer pipe diameter.

(b) 24" outer pipe diameter.

Figure 6.21: Snapshot at 62.8s showing clump weight pull-over behaviour for various pipe dimensions.

With reduced towing velocity the pull-over loads are slightly reduced. For a 16" pipe the build-up in transverse pull-over load is considerable for a case with flat seabed whereas it is cancelled at earlier stages with seabed alteration. By introducing RD designs for reduced trawl speed the pull-over duration is reduced by approximately 200 % for both the 12.75" and 16" pipe and the build-up in transverse pull-over loads are hence reduced.

A steep RD angle causes typically a larger clump weight nose angle and increasing warp line tension as the clump weight collides with the slope. Nose angle oscillations could lead to an initial tilt between the pipeline and clump weight relative to the horizontal direction, creating a momentum causing a shorter pull-over duration and lowering the pull-over loads (DNV-GL, 2014). Results indicate no relation between smaller pull-over loads with larger nose angles for the smaller RD widths as the steepest slopes

creating large nose angle oscillations tend to give the largest pull-over loads. This is however the case for larger W = 6.0 m where the pull-over loads are smaller for steep slope angles.

Globally, the direct roller impact and the subsequent pull-over phase tends to give the largest pull-over loads, whereas the frame impact is of less magnitude. However, the direction of the velocity vector is also important. If the impact takes place with a velocity vector pointing upwards in the transverse plane, the contact force is usually small. With a clump weight velocity vector pointing downward, the result is usually the opposite and could result in large contact forces shown for OD12W1.5H0.5S1_2.5 and OD12W2H0.5S1_2.5 with a slope, S = $21.8°$. For these cases the clump weight is stuck behind the pipeline for a slightly longer period of time and contact forces increase. From general observations the contact forces tend to increase with a velocity vector facing downwards, i.e. when the clump weight hits the pipeline on its way down after the initial bounce of the edge of the RD. The risk is i.e. increased when the pipe is placed on top of a wider RD where the possibility of a clump weight pipe collision with a negative velocity component in the vertical direction is present.

Pull-over loads with RD height, H = 2.0 m, seem to be less random, i.e. easier to predict time of interference and pull-over time for different slope angles. There is less correlation between contact forces with RD heights, H = 0.5 m and H = 1.0 m. H = 2.0 m could therefore prove to be more consistent in regards of predicting pull-over loads for pipelines as the clump weight manages to stabilize on its way up the slope.

Chapter 7

Conclusion

The present work deals with investigating different options for correcting the seabed geometry in order to protect the pipeline in a cost effective way. A global analysis model in SIMLA is established for parametric studies related to seabed geometries, soil data, pipeline dimensions and trawl velocity. The pull-over load in horizontal and vertical direction is compared towards the equivalent case with a flat seabed.

Results from simulations with updated seabed interaction curves indicates that the pull-over loads increase as stiffness is increased. With a soil property 10 times stiffer than the original seabed stiffness assigned at the RD, the pull-over loads are approximately of twice the magnitude. From visual inspection of the result files the clump weight response is deemed too excessive and unrealistic for further simulations. The original interaction curve is kept for further simulations.

The sensitivity study with altering seabed geometry indicates that the largest pull-over loads comes from clump weight roller collision with the pipe and are worst for large RD widths. For small RD widths large pull-over loads are most prominent for lower heights, whereas for larger widths they are prominent for the steepest slopes. It would therefore be beneficial to design the seabed incline slight or steep enough to make the clump weight jump over the pipe. For small widths one should avoid rock dump designs with low height.

Comparison of pull-over loads from simulations with a 16” pipe indicates no positive effect from rock dumps with a small width compared to a flat seabed. The pull-over loads are however reduced by approximately 50 % for cases where the RD width is large. For a 24” pipe no distinct change in pull-over loads are observed but only the pull-over duration.

With reduced towing velocity the pull-over loads are slightly reduced by introducing seabed alteration. For a 16” pipe the build-up in transverse pull-over load is considerable for a case with flat seabed whereas it is cancelled at earlier stages with seabed alteration. Rock dump design should hence be considered for future clump weight pipe interactions as it reduces pull-over duration and transverse pull-over loads.

7.1 Further work

This is the first investigation done regarding the effect of leaving a RD beneath the pipeline measuring pull-over loads compared to an unaltered seabed. Although there have been performed model tests in regards of covering the pipeline in order to reduce the impact loads, no previous investigation regarding the effects of leaving a RD beneath the pipeline have been performed. Further investigation should focus on performing experimental model tests in order to compare simulated results with experimental test results obtained.

A trawl velocity of 3 knots was only tested for a flat seabed because cont164 rollers were only implemented at the lower warp line, restricting further tests with rock dumping as the upper warp line without contact elements would penetrate the pipeline. For further simulations a larger portion of the warp line should be equipped with contact elements in order to investigate trawl velocities where the self weight of the warp line causes the warp line to move vertically causing warp line pipe contact at different warp line lengths.

The rock-dumping effect could be simulated with cont127/128 contact elements instead of cont126. Cont127/128 are 1-noded contact elements which will work according to the spring characteristics given using seabed geometry as a reference in the local y-direction only. In the local x- and z-direction the reaction forces are calculated according to the equilibrium state at which they were activated. This is to enable modelling of burial and rock-dumping effects according to Svein Sævik and Gjøsteen (2018).

Penetration of the pipeline has been a consistent problem in some of the simulations as contact is sometimes lost during interference between the pipe and clump weight roller, causing the roller to slightly penetrate the pipe. As contact is again obtained, both pipe and clump weight are pushed excessively in the opposite direction. To avoid this, a contact element providing a consistent contact search during interference should be define between the pipe and clump weight roller when simulating perpendicular trawling.

The sensitivity study was performed manually for each simulation. Instead a proposed solution could be based on extracting maximum pull-over loads from SIMLA into optimisation algorithms where all parameters are checked in order to predict the best combination. However, singularities and numerical errors would be a problem as algorithms would not account for such calculations done in SIMLA.

Bibliography

Directorate, N. P., of Petroleum, N. M., Energy, 05 2018. The oil and gas pipeline systems. https://www.norskpetroleum.no/en/production-and-exports/the-oil-and-gas-pipeline-system/.

DNV-GL, 09 2014. Recommended Practice DNV-RP-F111, Interference between Trawl Gear and Pipelines.

Faltinsen, O., 01 1990. Sea Loads on Ships and Offshore Structures.

Fyrileiv, O., Askheim Ø, D., Verley, R., Rolsdorph, H., 06 2006. Dynamic simulation of free-spanning pipeline trawl board pull-over. pp. 561–568.

Johnsen, I. B., 12 2012. Clump-weight trawl gear interaction with submarine pipelines. Master's thesis, NTNU.

Longva, V., 06 2010. Simulation of trawl loads on subsea pipelines. Master's thesis, NTNU.

Longva, V., Sævik, S., 07 2012. A penalty-based body-pipeline contact element for simulation of pull-over events. Vol. 3.

Longva, V., Sævik, S., 11 2013. A penalty-based contact element for pipe and 3d rigid body interaction. Engineering Structures 56, 1580–1592.

Longva, V., Sævik, S., Levold, E., Ilstad, H., 12 2013. Dynamic simulation of subsea pipeline and trawl board pull-over interaction. Marine Structures 34, 156184.

Longva, V., Sævik, S., Levold, E., Ilstad, H., Teigen, P., 01 2011. Dynamic simulation of free-spanning pipeline trawl board pull-over. pp. 561–568.

Lyngsaunet, O. M., Foss, P., Sævik, S., 07 2015. Detailed simulation of interference between clump weight and subsea pipelines. p. 7.

Maaløe, K., 07 2011. Clump-weight trawl gear interaction with submarine pipelines. Master's thesis, NTNU, Department of Marine Technology.

Maaløe, K., Alsos, H., Sævik, S., 07 2012. Detailed analysis of clump-weight interference with subsea pipelines.

Moan, T., 09 2003. TMR4190 - Finite Element Modelling and Analysis of Marine Structures. Faculty of Engineering Science and Technology.

Sævik, S., 02 2017. SIMLA Theory Manual. SINTEF Ocean.

Svein Sævik, Ole David Økland, G. S. B., Gjøsteen, J. K., 09 2018. SIMLA Version 3.16.0 - User Manual. SINTEF Ocean.

Appendix A

Results from seabed geometry alteration

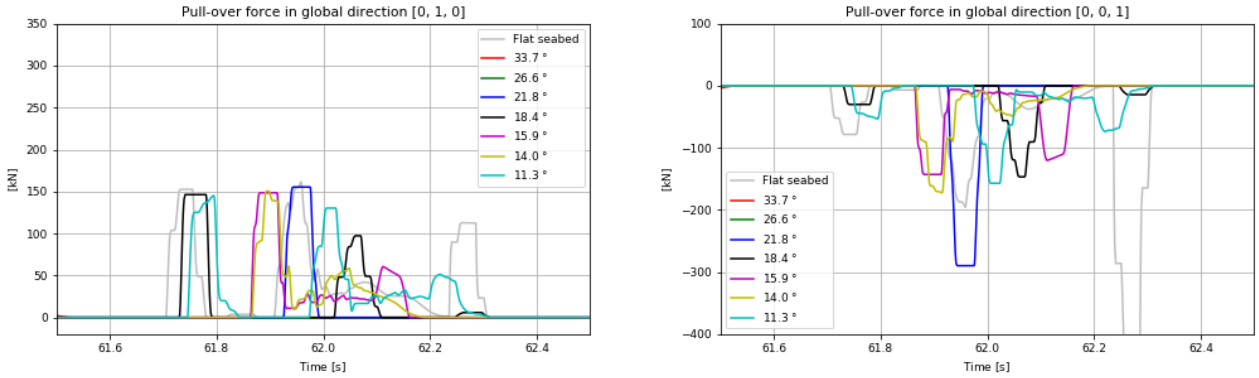

(a) Transverse pull-over load

(b) Upward pull-over load

Figure A.1: Clump weight pull-over loads for OD12W1.5H0.5

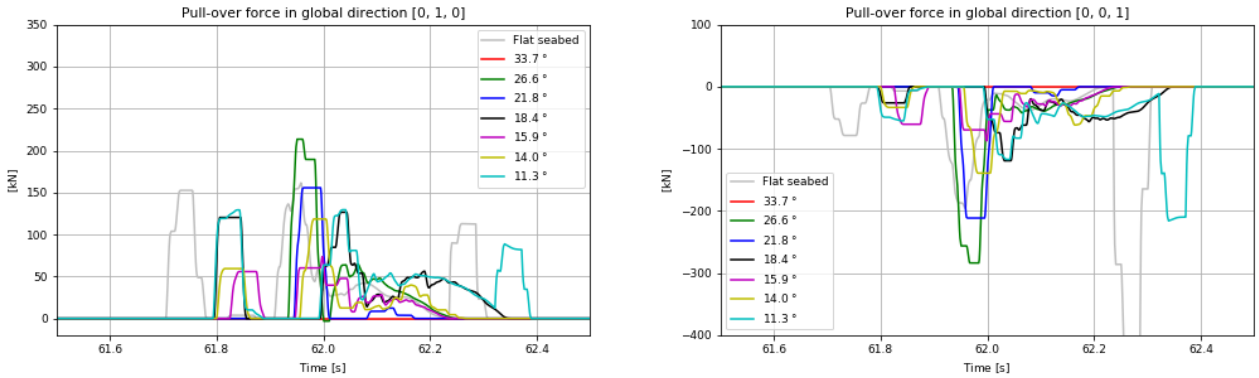

(a) Transverse pull-over load

(b) Upward pull-over load

Figure A.2: Clump weight pull-over loads for OD12W1.5H1

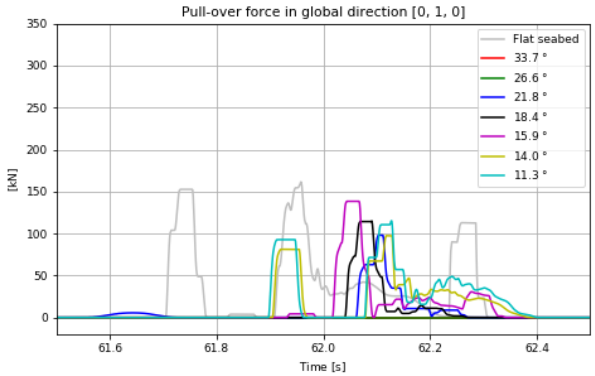

(a) Transverse pull-over load

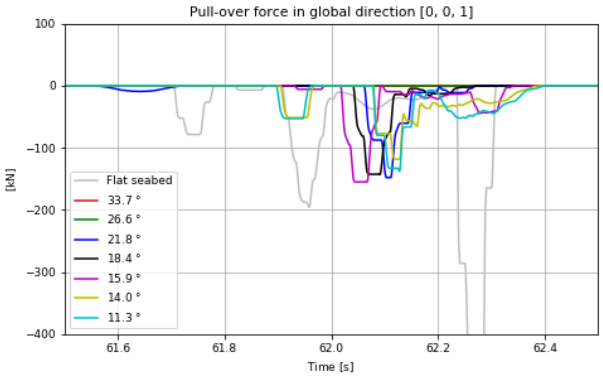

(b) Upward pull-over load

Figure A.3: Clump weight pull-over loads for OD12W1.5H2

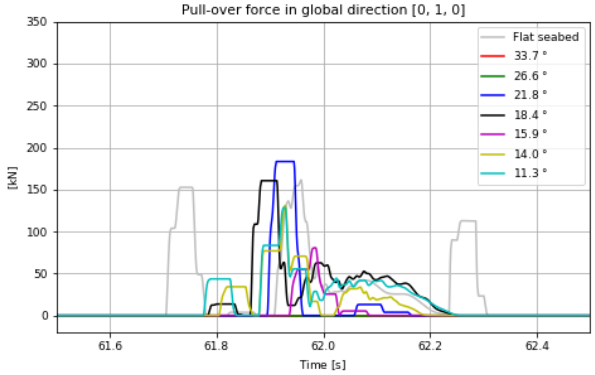

(a) Transverse pull-over load

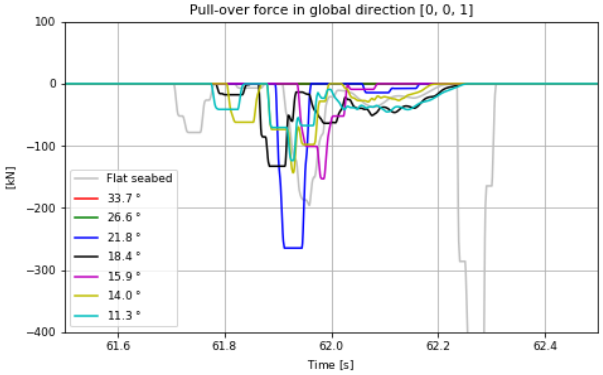

(b) Upward pull-over load

Figure A.4: Clump weight pull-over loads for OD12W2H0.5

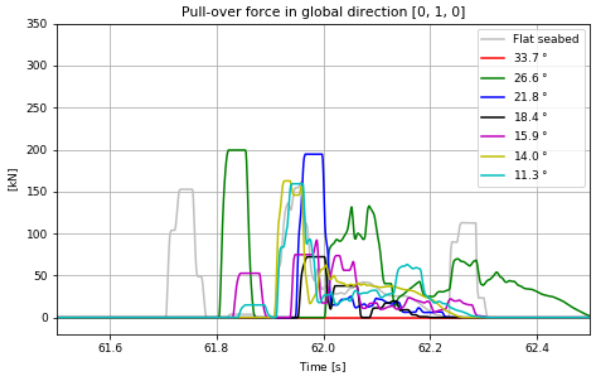

(a) Transverse pull-over load

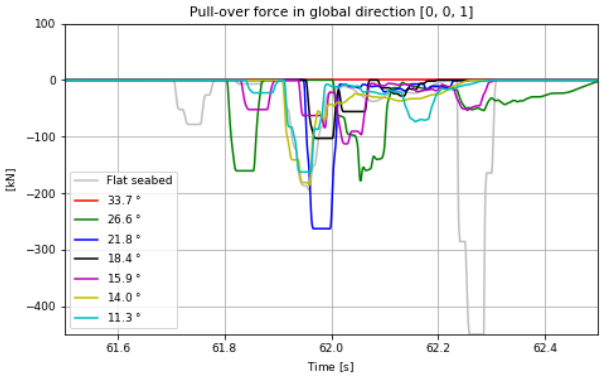

(b) Upward pull-over load

Figure A.5: Clump weight pull-over loads for OD12W2H1

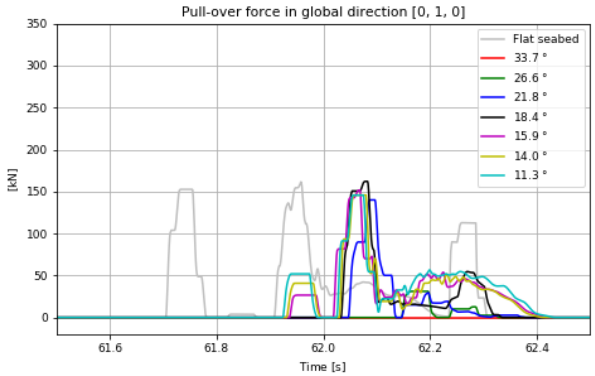

(a) Transverse pull-over load

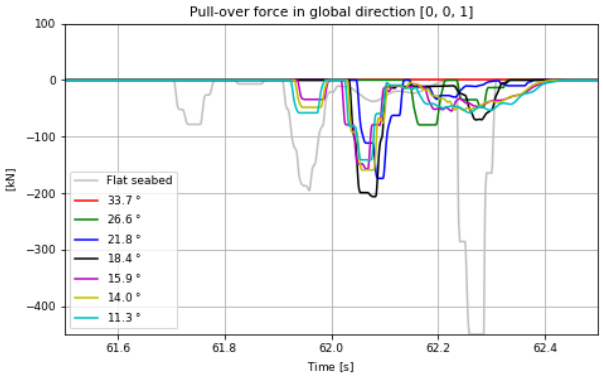

(b) Upward pull-over load

Figure A.6: Clump weight pull-over loads for OD12W2H2

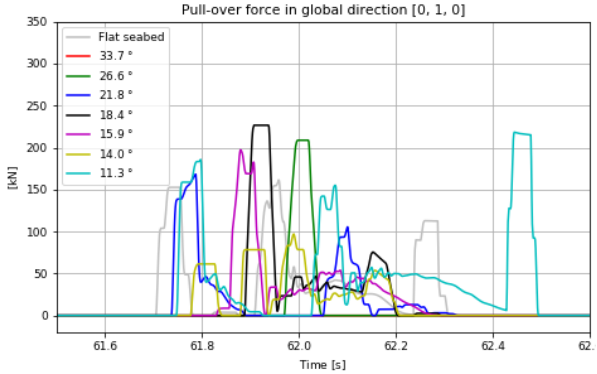

(a) Transverse pull-over load

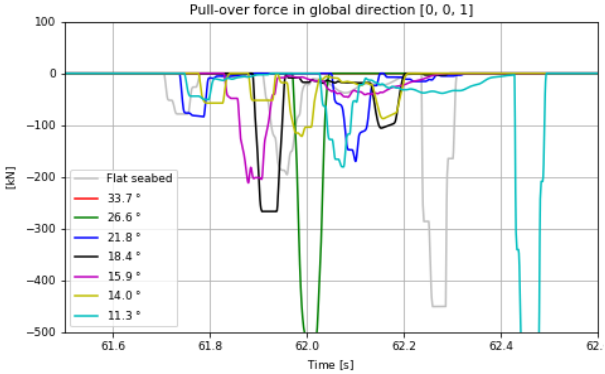

(b) Upward pull-over load

Figure A.7: Clump weight pull-over loads for OD12W4H0.5

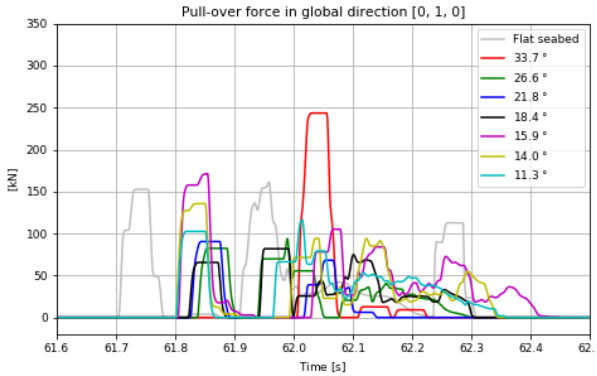

(a) Transverse pull-over load

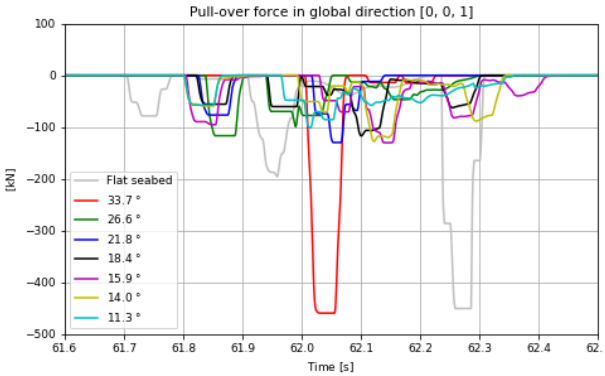

(b) Upward pull-over load

Figure A.8: Clump weight pull-over loads for OD12W4H1

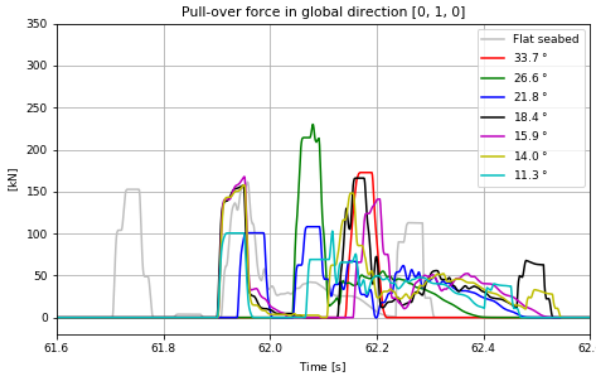

(a) Transverse pull-over load

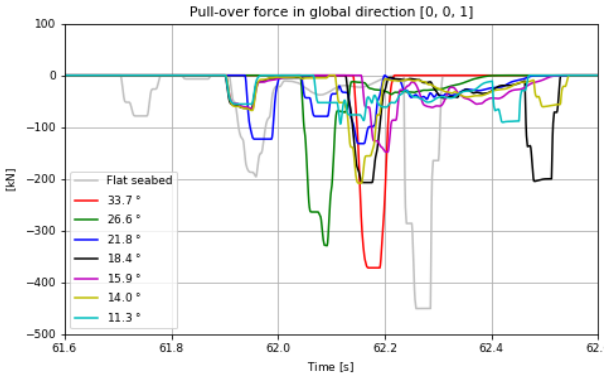

(b) Upward pull-over load

Figure A.9: Clump weight pull-over loads for OD12W4H2

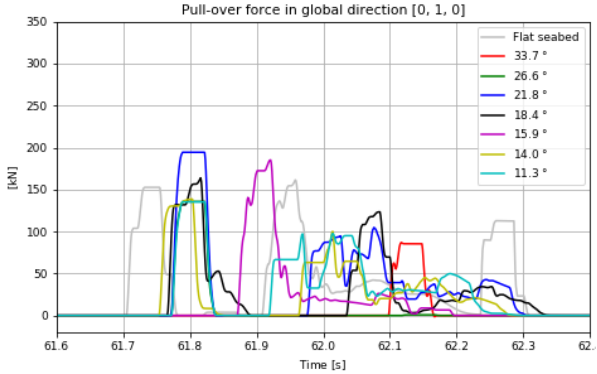

(a) Transverse pull-over load

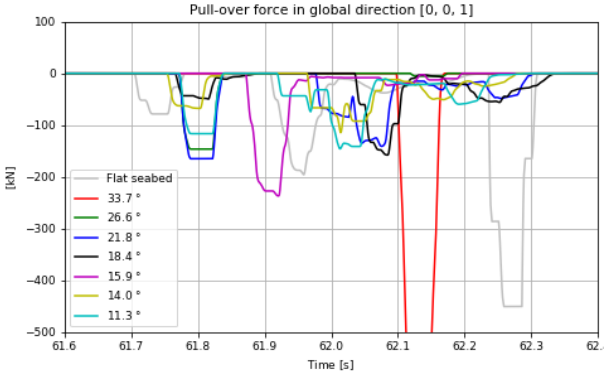

(b) Upward pull-over load

Figure A.10: Clump weight pull-over loads for OD12W6H0.5

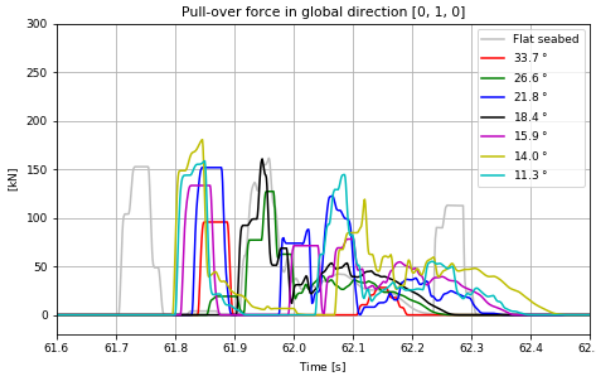

(a) Transverse pull-over load

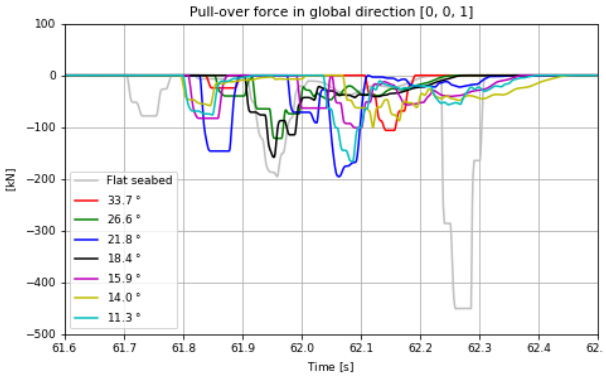

(b) Upward pull-over load

Figure A.11: Clump weight pull-over loads for OD12W6H1

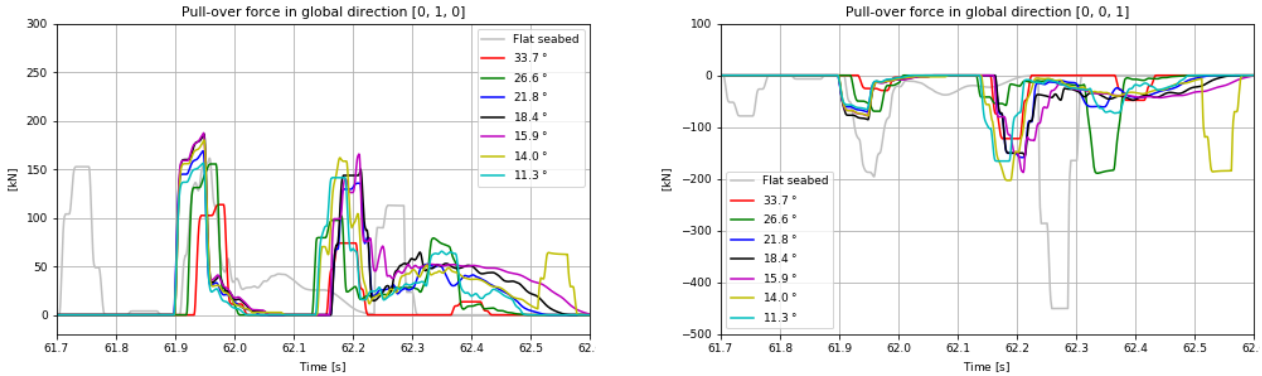

(a) Transverse pull-over load

(b) Upward pull-over load

Figure A.12: Clump weight pull-over loads for OD12W6H2

Appendix B

Results from pre-tests investigating the effect of extra nodes and increased rock dump stiffness

B.1 Results from extra nodes

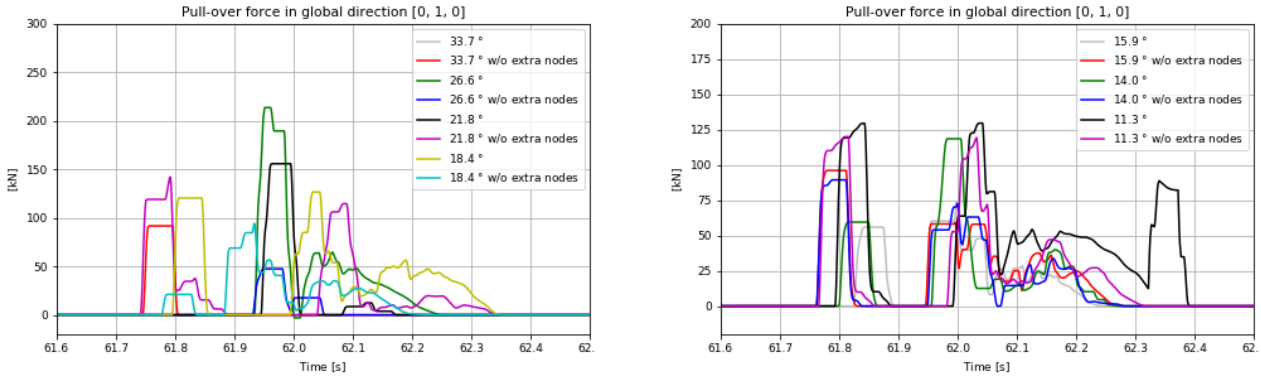

Figure B.1: Clump weight transverse pull-over loads for OD12W1.5H1 with and w/o extra nodes

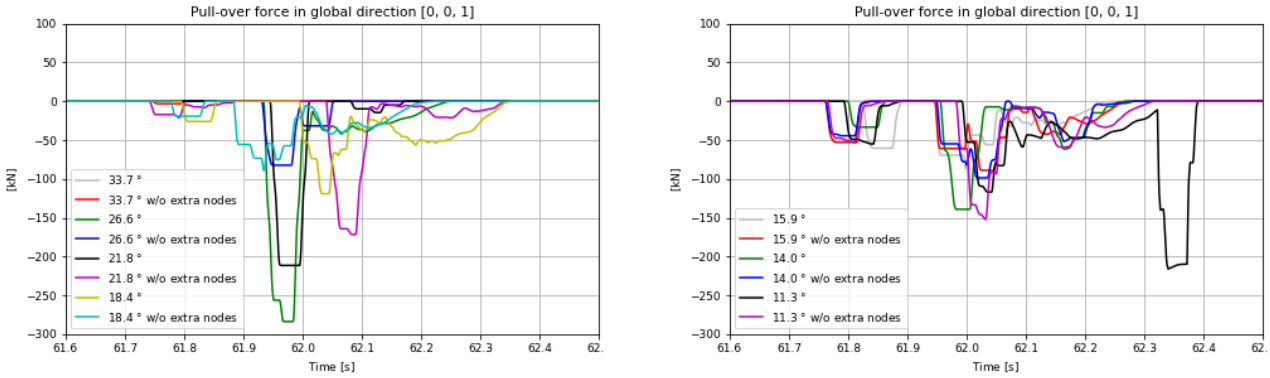

Figure B.2: Clump weight upward pull-over loads for OD12W1.5H1 with and w/o extra nodes

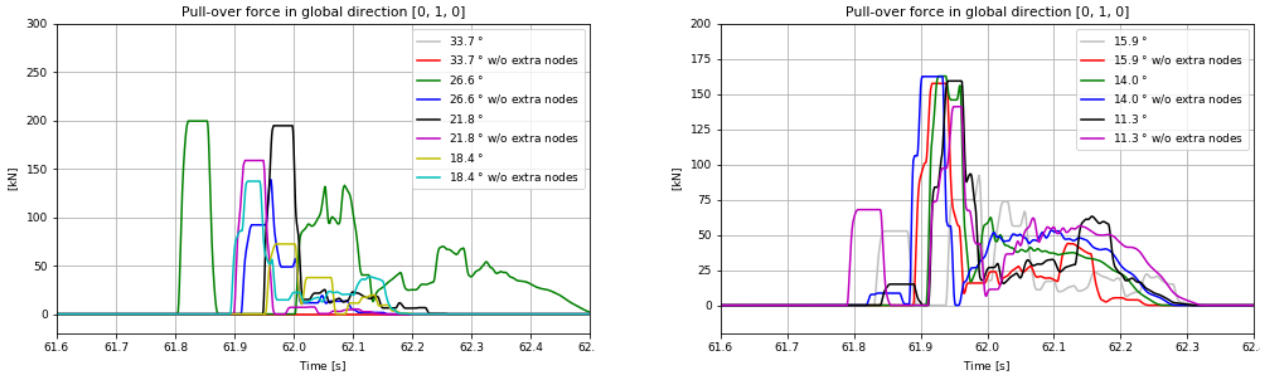

Figure B.3: Clump weight transverse pull-over loads for OD12W2H1 with and w/o extra nodes

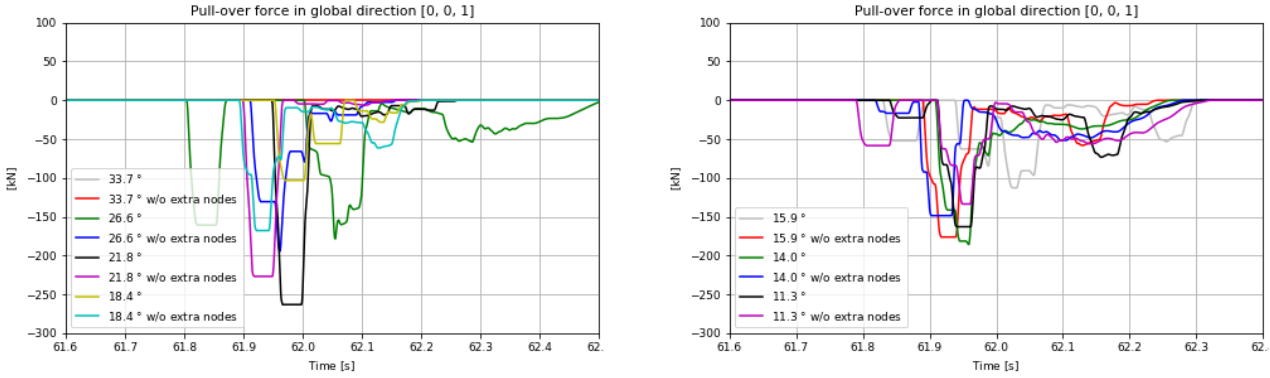

Figure B.4: Clump weight upward pull-over loads for OD12W2H1 with and w/o extra nodes

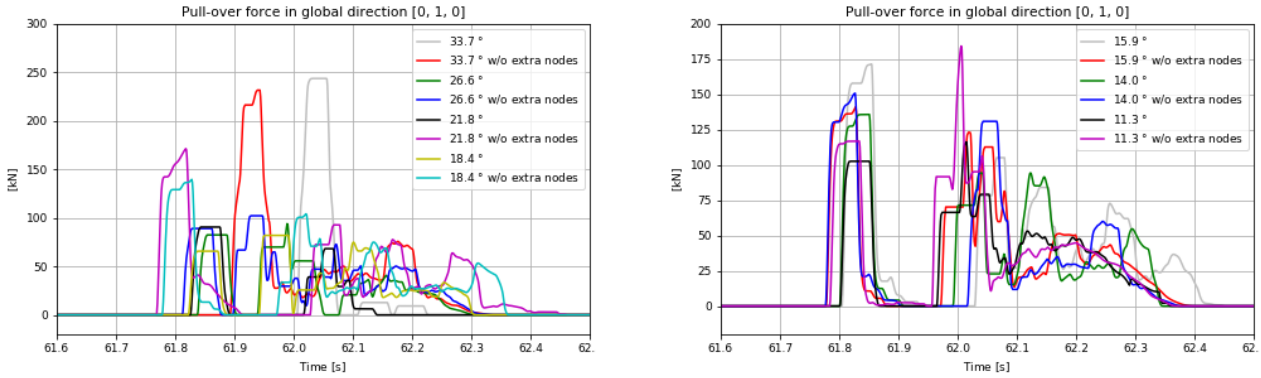

Figure B.5: Clump weight transverse pull-over loads for OD12W4H1 with and w/o extra nodes

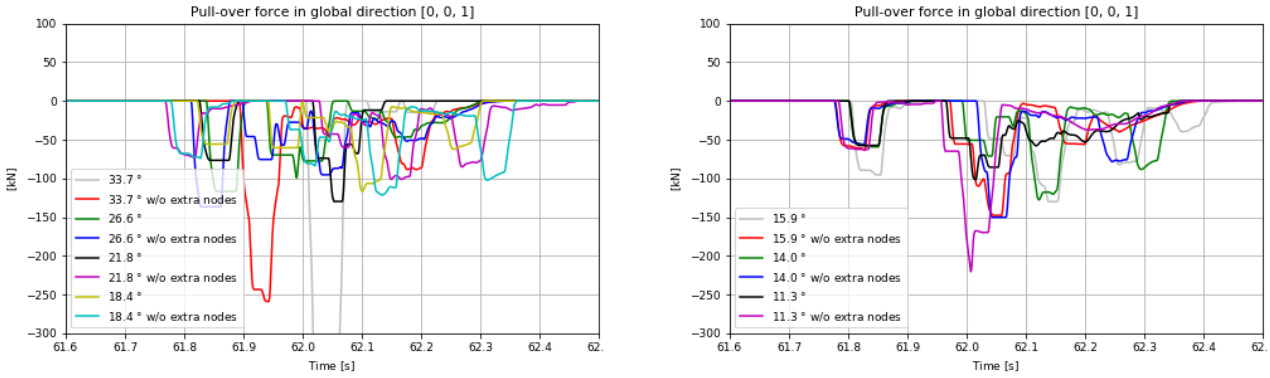

Figure B.6: Clump weight upward pull-over loads for OD12W4H1 with and w/o extra nodes

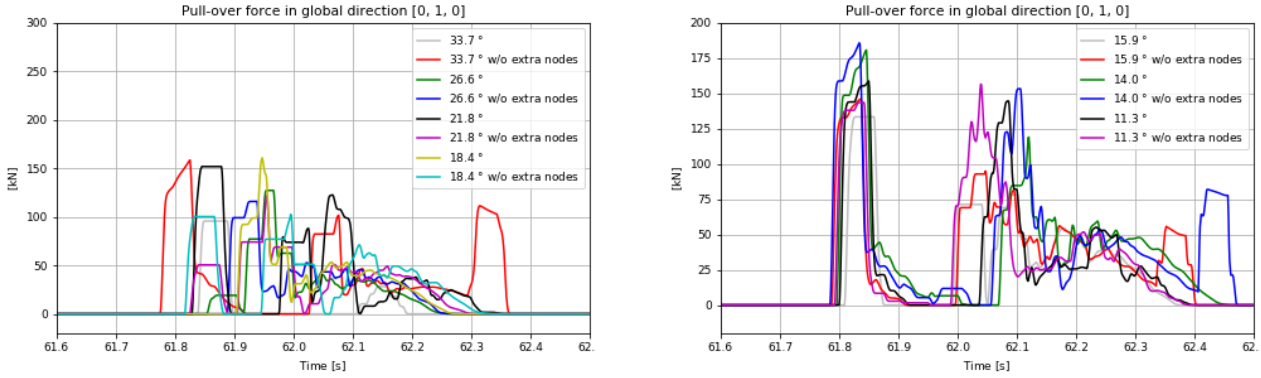

Figure B.7: Clump weight transverse pull-over loads for OD12W6H1 with and w/o extra nodes

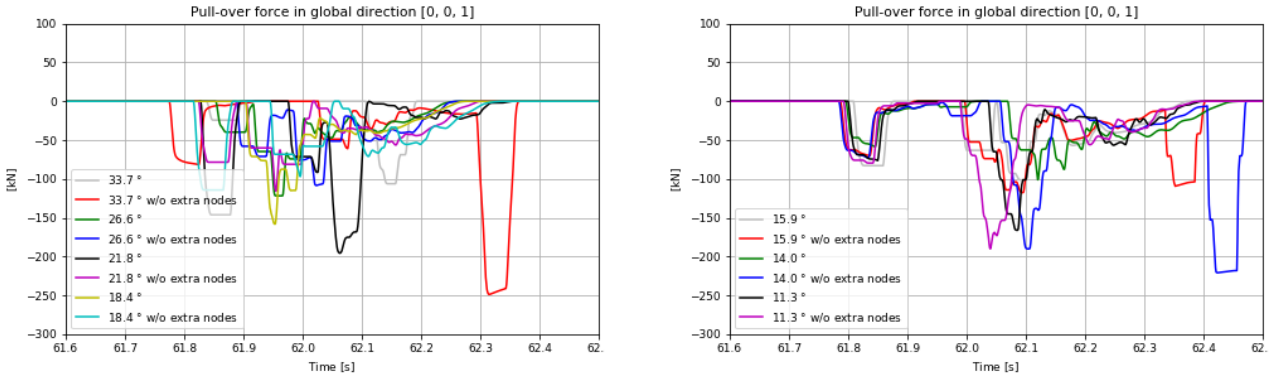

Figure B.8: Clump weight upward pull-over loads for OD12W6H1 with and w/o extra nodes

B.2 Results from extra nodes and increased stiffness

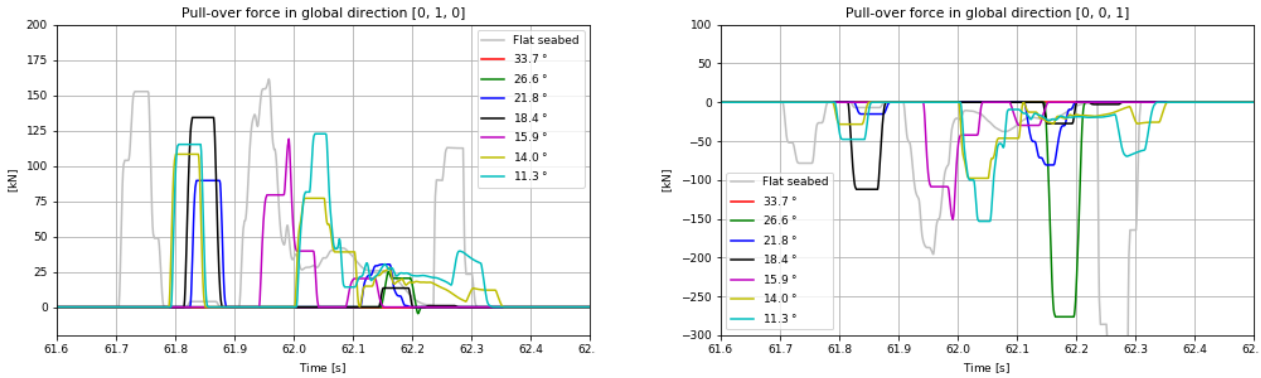

(a) Transverse pull-over load

(b) Upward pull-over load

Figure B.9: Clump weight pull-over loads for OD12W1.5H1 with 200 % increased rockdump stiffness

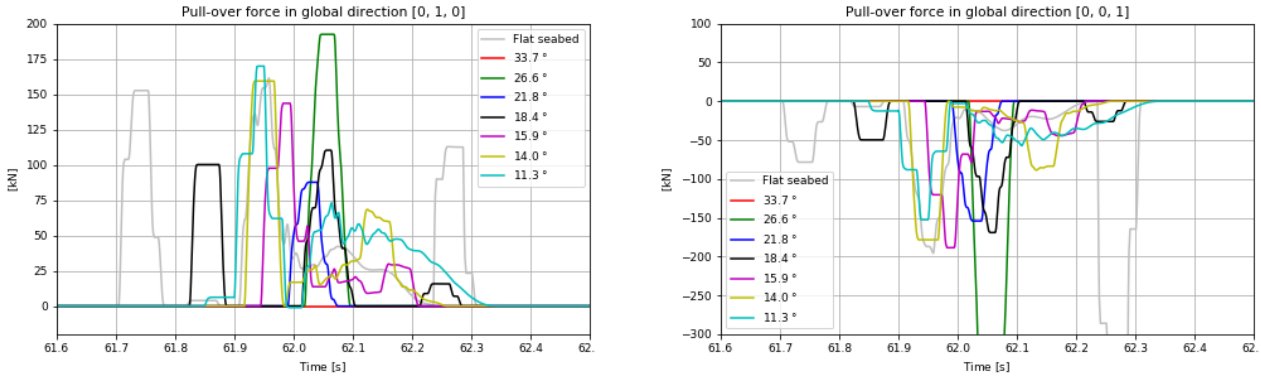

(a) Transverse pull-over load

(b) Upward pull-over load

Figure B.10: Clump weight pull-over loads for OD12W2H1 with 200 % increased rockdump stiffness

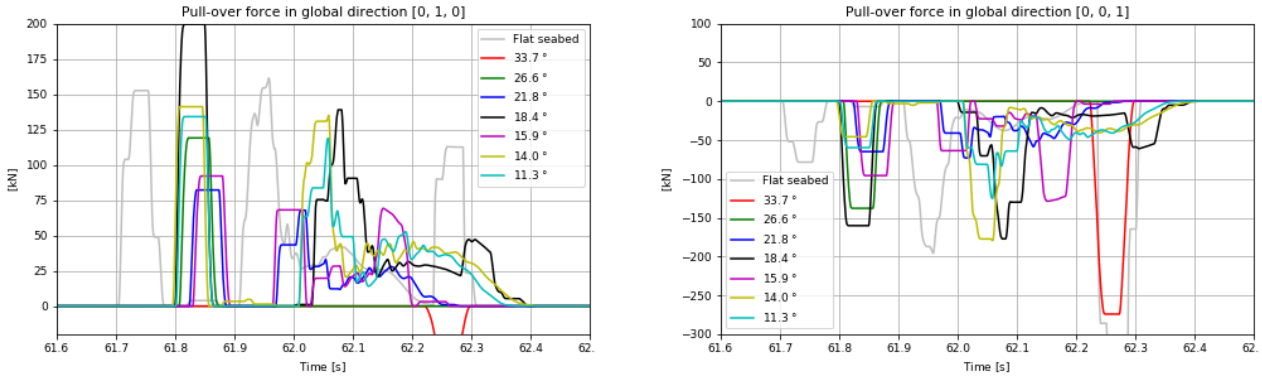

(a) Transverse pull-over load

(b) Upward pull-over load

Figure B.11: Clump weight pull-over loads for OD12W4H1 with 200 % increased rockdump stiffness

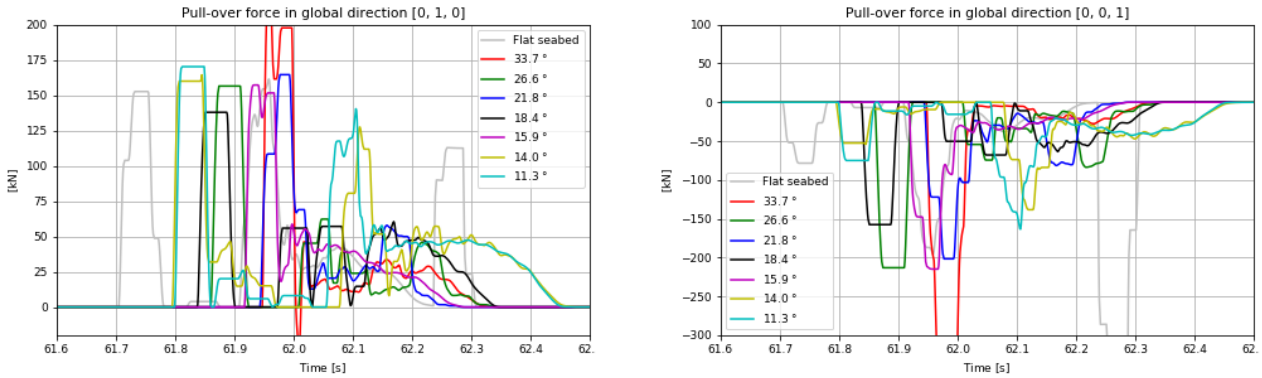

(a) Transverse pull-over load

(b) Upward pull-over load

Figure B.12: Clump weight pull-over loads for OD12W6H1 with 200 % increased rockdump stiffness

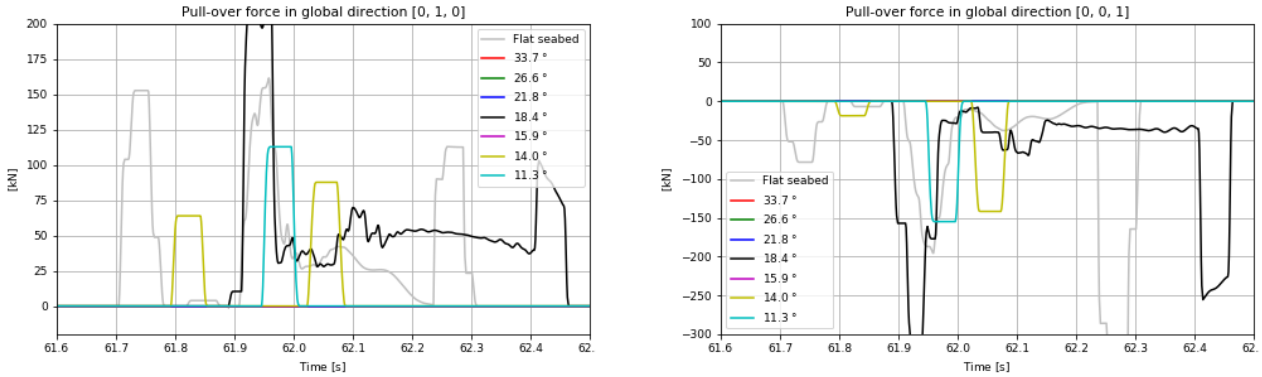

(a) Transverse pull-over load

(b) Upward pull-over load

Figure B.13: Clump weight pull-over loads for OD12W1.5H1 with 10 times increased rockdump stiffness

Truls Wanvik Krogstadmo

Reduction of trawl impact loads on pipelines resting exposed on the seabed

NTNU
Norwegian University of
Science and Technology